Design and Measurement Analysis of Hot Embossing System for High Aspect Ratio Microfluidics

by

Nicholas Ragosta
Sc.B. Mechanical Engineering (2012)
Brown University School of Engineering

Submitted to the Department of Mechanical Engineering in partial fulfillment of the requirements for the degree of

Masters of Engineering

at

MASSACHUSETTS INSTITUTE OF TECHNOLOGY

September 2013

Author.....

Department of Mechanical Engineering

August 9, 2013

Certified by: .....

Dr. Brian Anthony
Thesis Advisor

Accepted by:.....

Dr. David E. Hardt

Ralph E. & Eloise F. Cross Professor of Mechanical Engineering, Chairman, Department Committee on Graduate Students.

This page intentionally left blank.

Design and Measurement Analysis of Hot Embossing System for High Aspect Ratio Microfluidics

By

Nicholas Ragosta
Sc.B. Mechanical Engineering (2012)
Brown University School of Engineering

Submitted to the Department of Mechanical Engineering on August 9, 2013
In Partial Fulfillment of the Requirements for the Degree of
Master of Engineering in Manufacturing

Abstract

Microfluidics is a growing technology in the arena of medical diagnostics. Daktari Diagnostics is a startup located in Cambridge, MA that seeks to introduce a lab-on-a-chip device for monitoring HIV in patients. This work investigates hot embossing as a prototyping process for Daktari's microfluidic device. A hot embossing machine was designed and built for the purpose of prototyping a critical feature of their microfluidic network. The machine was designed for an embossing area of 6 square inches, and was found to have a maximum positional repeatability of 43 microns.

The microfluidic feature that was prototyped is known as the assay channel. This feature is a high aspect ratio channel with a depth of 50 microns and width of 4 mm. A 10-micron ridge is adjacent to the channel. Several measurement methods were evaluated with gage repeatability and reproducibility studies to determine the methods most capable of quantifying the quality of embossed parts. The end determination was that quality of parts should be defined by the completeness of formation of the ridge lining the channel. The height and width measurements of the ridge were used as quality metrics. The precision to tolerance ratio (P/T ratio) of the measurement method used for finding ridge height was found to be 0.44 and the P/T ratio of the ridge width measurement method was found to be 0.33.

Thesis Supervisor: Dr. Brian Anthony
Title: Research Scientist

This page intentionally left blank.

Acknowledgements

I would like to thank:

Everyone at Daktari Diagnostics for inviting us to be a part of their amazing company, and allowing us to partake in their culture of indulgent chocolate consumption.

Rob and Aaron, our advisors at Daktari Diagnostics, for their guidance, excitement and encouragement

My teammates, Khanh and Viren, for telling me when I was being an "idiot" (their words, not mine) and for their tireless work ethic and inspiring levels of motivation

Our thesis advisor, Dr. Brian Anthony, for his always-helpful insight and his willingness to share knowledge gleaned from many years of intimate study of our topic of research

Jennifer Craig, our writing advisor, who has helped transform this thesis from a pile of hand-scribbled notes into the elegant prose of a mid-century poet laureate

Finally, my parents for teaching me the value of hard work, friendship, and a home cooked meal

Table of Contents

List of Figures

List of Tables

1 Introduction

This thesis explores using hot embossing as a prototyping process of microfluidic channels for Daktari Diagnostics. The capabilities of the process were investigated with specific emphasis placed on reproducing a key feature of their current product.

1.1 Background and Research Motivation

Daktari Diagnostics is a startup company that is currently specializing in affordable and accurate Human Immunodeficiency Virus (HIV) diagnostics. HIV replicates in the human body by invading helper T cells (specifically the CD4+T cells). As the virus spreads, the patient's CD4 cell count declines and their ability to fight infection diminishes. Thus, CD4 cell count (cells/microliter of blood) correlates to the severity of the infection. A measurement of CD4 cells cannot be used to diagnose a patient as HIV positive; however, it is an effective and essential measurement for determining if a patient is responding to medication. Measurement of the CD4+ T lymphocytes is a critical part in the staging of the HIV-infected patients, determining need for antiretroviral medications and monitoring the course of their infection[1].

In developed countries, the CD4 count (CD4 cells per microliter of blood) is performed every three to six months using a method known as flow cytometry. This requires expensive ($30,000 to $150,000) equipment and trained operators. In resource poor countries, these assets are only available in the largest national hospitals. For many patients afflicted by HIV, this means that they must send blood out from a local clinic and wait days or even months for the results to return from the central hospital laboratory. These economic and technical limitations have made these instruments difficult to sustain in resource poor environments[2], where there are more than 35 million HIV-infected people, 6 million of which require urgent anti-retroviral treatment. The need for a low cost CD4 measurement technique is widely recognized[3].

Daktari is attempting to create a CD4 cell count system that is simple to operate, low cost and portable. Their product includes a microfluidic cartridge with a circuit of channels

for reagents and blood to flow. The CD4 cells are preferentially captured in a basin known as the assay channel, and then counted using impedance measurements[2]. CD4+ cell size is on average 8.5 microns in diameter, with 0.2% being above 12 microns[4]. The microfluidic device contains channels as shallow as 50microns and as deep as 1mm.

1.2 Problem Statement

To arrive at a functional design, it is necessary that Daktari Diagnostics take advantage of manufacturing methods that are capable of producing parts with features in this 10s of microns range. For commercial production, Daktari will use an injection molding process. However, for prototyping this method may not be the most efficient. Daktari is interested in other manufacturing processes that are capable of accurately and reliably creating aspects of their microfluidic card for prototyping purposes. This thesis evaluates hot embossing as a prototyping process.

1.3 Current Prototyping Processes

Currently, Daktari uses several processes in conjunction for the development stage of the product. These are: Photolithography and Polydimethylsiloxane (PDMS) molding, micromachining, and injection molding. Each of these processes has limitations that prevent them from being ideal prototyping processes. The processes and limitations are discussed in more detail in chapter 3; a brief description of each process is below.

1.3.1 Photolithography

Photolithography is a technique used to produce very precise (nm resolution) patterns on a substrate. The general principle of the process is that a photosensitive material is selectively exposed to a UV light source. This exposure cures portions of the resist in the desired pattern while the remaining material is etched away. The technique is commonly used to make integrated circuits, but has recently been used as a method for producing molds for microfluidic applications. One major limitation of this process is the cost and complexity associated with making the mold. Another limitation, and Daktari's biggest concern, is that this process does not produce parts that are representative of

production parts, meaning both the geometry of the parts produced and the material used differ from production specifications.

1.3.2 Micromachining

Micromachining directly into the substrate is another method that Daktari has used for prototyping microfluidic designs. Micromachining, either through micro milling, laser machining or micro-electrical discharge machining (micro-EDM) is a subtractive manufacturing process that affords great flexibility. This process is capable of producing complex micron scale features into almost any material desired. The major limitation here is the time required to produce a single part. It may take several hours to micromachine one microfluidic design, and Daktari may need up to 50 parts made of a single design to fully evaluate it.

1.3.3 Injection Molding

Injection molding is the method currently used by Daktari for commercial production of their microfluidic card. Injection molding is a method in which a mold cavity is filled with a molten thermoplastic. It allows for highly complex parts to be rapidly produced. The major limitation of this process is the time and cost required to make a mold. A single mold cavity may take up to six months to design and manufacture. While this manufacturing process is desirable for volume production, it is not ideal as a prototyping process.

1.4 Unmet Needs

The processes described previously do not meet all of the requirements of an effective development tool for microfluidic devices. They are either prohibitively slow, prohibitively expensive, or produce parts that are not characteristic of parts produced with the production process. Therefore, there is a need for a more effective prototyping process.

The process must produce parts that are representative of production grade parts. This means that the behavior of flow through the channels in the prototyped parts must be similar to the flow that will occur in production parts. If this is not true, then the process

cannot be realistically used as a development tool. The new development process must produce parts that have geometry representative of the final production parts. This includes tapers, surface roughness characteristics and material.

For the process to be an effective prototyping tool, it should take a relatively short amount of time to iterate on the design. This need translates to a requirement that has the entire process, from tooling to prototype production, be as short as possible.

1.5 The Hot Embossing Solution

Hot embossing is a viable solution for filling the prototyping gaps left by the previous processes[5]. It offers advantages in achievable feature replication[6], correct prototyping material, low process cycle time, and a variety of tooling options. Most features producible by injection molding and machining can be achieved by hot embossing, such as high aspect ratio features[7] and low surface roughness[8]. Mold tools for hot embossing can be produced through micromachining or lithography processes. The tools in hot embossing are used to transfer features over to substrate materials. The selection of substrate materials is very flexible and allows the correct material to be used for prototyping. The time in which it takes to make a single micro hot embossed part has been shown to be as low as 2min/part[9]. This bridges the gap between the fast process times of injection molding to the slow process time of micromachining. Hot embossing is able to bring prototype designs to production more quickly because the time required for tooling can be considerably less than that of injection molding where complicated features like ejection pins add to tooling time. Hot embossing also offers different materials for tooling that injection molding does not [8,10].

While there are many apparent benefits of using hot embossing, this technology is still an emerging manufacturing process that is not widely used commercially. The process exists primarily in academic and research settings and is still in the process of making a transition into commercial arenas. The true capabilities of the process will depend on the specific geometries of the parts being produced, and so this process must be evaluated for Daktari's particular needs.

1.6 Research Objectives

The focus of this work was to develop a hot embossing machine capable of prototyping the key aspects of Daktari's microfluidic card and to determine a method to assess the quality of embossed parts. Developing the hot embossing machine entailed designing a machine, building the machine, and finally characterizing its performance.

Following construction and testing of the hot embossing machine, a methodology was developed for inspecting hot embossed parts. The measurement methodology was developed by first cataloguing the critical dimensions of the features to be inspected. Next, methods were determined to measure each of these dimensions. These methods were evaluated with a series of gage repeatability and reproducibility studies that resulted in an estimate of the measurement error introduced by each method. Finally, a proposal was made for the singular dimension or group of dimensions that are most capable of being measured to evaluate the quality of an embossed part.

2 Background and Product Description

2.1 Microfluidics

The HIV diagnostic product developed at Daktari consists of a variety of parts but one of the most important and the critical part in the instrument is the microfluidic cartridge, which is manufactured using Poly methyl methacrylate (PMMA). The microfluidic cartridge is the component where the blood enters, mixes with different reagents in precise quantities and accurate measurements of the CD4 count of the blood are made. The important requirement for such a cartridge is having accurate quantities of the reagents and the blood flow at a precise rate through the channels. A microfluidic chip is suitable for this need.

Microfluidics has the potential to significantly change the way modern biology is performed. Using microfluidic devices we can work with smaller reagent volumes, shorter reaction times, and the possibility of parallel operation. They also hold the promise of integrating an entire laboratory onto a single chip (i.e. lab-on-a-chip)[11]. Apart from the traditional advantages of miniaturization, the greatest potential lies in the physics at the micro scale. By understanding and leveraging micro scale phenomena, microfluidics can be used to perform experiments which may not be possible on the macro scale which allows the introduction of new invention in functionality [12].

A microfluidic approach has been used for a wide range of applications which include analysis, diagnostics and synthesis [13]. Microfluidics is the analysis of accurate and precise flows through constrained routes or channels. Typically microfluidics is used to analyze fluids, which flow, mix, separate and are processed otherwise. Some of the applications include passive fluid control using capillary forces, rotary drives applying centrifugal forces for the fluid transport on passive chips. Microfluidic chips can also be used to enhance rare cell capture and fractionation using biochemical interactions. Many of the microfluidic devices take advantage of the 3D structure of channels to increase the surface area available to be coated with the antibody [4].

There are a variety of ways in which the microfluidic chip can be manufactured which include soft lithography, micromachining and micro-injection molding. Some of the important parameters to be considered as shown in Figure 1 while producing the microfluidics part are:

1. Surface Finish: The surface finish plays an important role in the flow characteristics of the fluid and it depends on the process used for manufacturing.
2. Dimensional Tolerances on Features: The sides of the channel are important for the flow characteristics as well as the capture of any cells if relevant. The tolerance on these features like the width and length of the channels determines the flow characteristics. Also, the linearity of the features is an important along with the parallelism of the planes of the features.
3. Positional Tolerance: Parallelism and Perpendicularity with the outside boundary of the microfluidics may play an important role. Also, the positional tolerance of the features with respect to the outside boundary may be a crucial parameter.

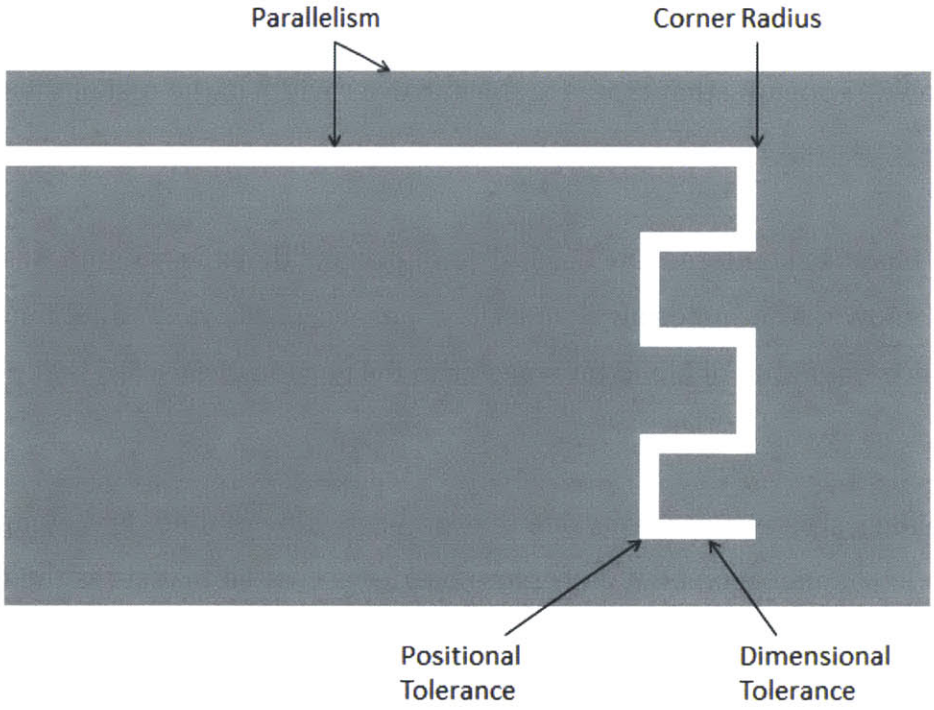

Figure 1: Critical parameters in microfluidics

Most of the crucial parameters can be further listed down according to the application of the microfluidic chip, which is in this case the microfluidic cartridge used at Daktari. The critical features and parameters which are important to the performance of the device are enlisted the following section. These features in addition to the parameters listed above will be the basis for evaluating hot embossing as an appropriate prototyping process for Daktari Diagnostics.

2.2 General Card Features

Several parts of Daktari's microfluidic network have unique aspects that make them difficult to prototype. These features are also parts of the microfluidic network that need to be thoroughly iterated upon to reach a functional design. Therefore, it is necessary to demonstrate that hot embossing is a suitable manufacturing method for these key features before it can be declared an effect prototyping tool.

Blood is first introduced to Daktari's product through a feature known as the fill port. This is an inlet that is designed to allow blood to be pulled into the microfluidic network of the card through capillary action. The inlet resides on an edge of the card. It will be a channel of uniform depth. The fill port may have uniform width, or it may have a design with a wide opening that tapers to the narrower width of the rest of the microfluidic network.

After blood has entered the card, it is important that the volume of blood to be analyzed be known. The metering channel is a portion of the microfluidic network that takes in a precise quantity of blood for transfer to the portion of the card that performs the analysis.

A capillary stop is a passive valve that prevents flow of fluid. By having an abrupt, large change in channel geometry, a pressure barrier is created that stops the flow of fluid [14]. Daktari uses capillary stops in their microfluidic network to direct the flow of blood. Figure 2 below shows an example of a capillary stop and how it operates. The fluid flows in

the main channel past the capillary stop. Some fluid enters the stop, but its motion is halted when it reaches the portion of the channel that has a sudden change in depth and width.

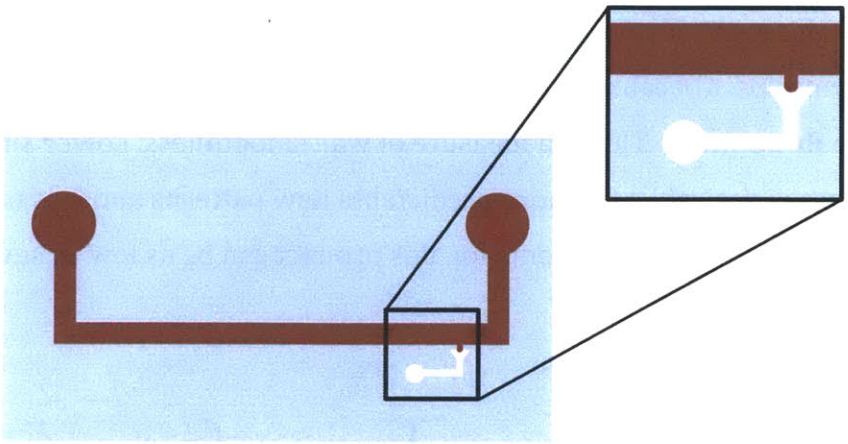

Figure 2: Schematic of a channel with a capillary stop

2.3 Targeted Feature: The Assay Channel

The most critical portion of the microfluidic system is a portion of the card known as the assay channel. This is the region in which a crucial analysis of the blood is performed. It contains a large collection of tight tolerances and dimensions that are both unique to this area and common to different features on the card. Therefore, prototyping of this feature will be a good indicator of hot embossing's capability to prototype various parts of Daktari's card.

2.4 General Channel Considerations

The microfluidic channels in Daktari's product are in general defined by six basic geometric parameters. These are:

1. **Depth**. Channel depth varies widely on Daktari's microfluidic network and can be as shallow as 50microns or as deep as 1 mm.
2. **Width**. Channels of widths at large as 2mm in span exist on Daktari's card.
3. **Draft Angle.** This is a measurement of the verticality of the channel's walls. Perfectly vertical walls are desirable, but not possible because of the molding process currently being used.

4. **Upper Radius**. This is the radius at the upper edge of the channel. In general this radius is governed by radius of the tool used to make the mold.
5. **Lower Radius**. This is the radius at the bottom edge of the channel. The tool can be made with essentially 0 radius at this point, however there may be a radius left on the polymer part because of the manufacturing process.
6. **Surface Roughness.** This is a measure of wall smoothness. Lower surface roughness is desirable, for more predictable flow patterns and less trapping of cells. Surface roughness requirements for this product can be as low as several tens of nanometers.

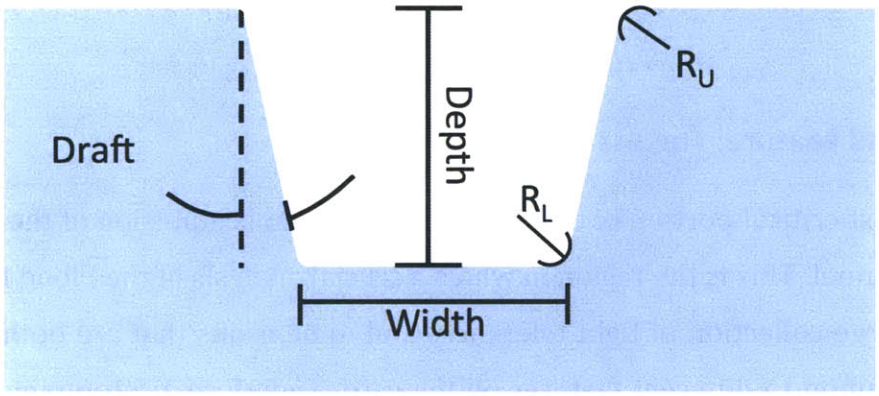

Figure 3: General channel dimensions

3 Review of Prototyping Processes

Many manufacturing processes can be used to produce parts with micro features. However, these micro features need to have a certain accuracy and fidelity. They need to satisfy the requirements of being biocompatible, corrosion-resistant and disposable etc. The manufacturing process needs to be viable with regards to the materials used and the feature size to be attained. Some of the potential manufacturing processes are discussed below based on the requirements listed above and manufacturing challenges. These processes are being currently used at Daktari for rapid prototyping the assay channel. Each of these processes has limitations that hot embossing will hopefully overcome.

3.1 Photolithography

Photolithography has been shown to be a cost effect and rapid way for producing micron scale features[15]. Additionally, photolithography in conjunction with Polydimethylsiloxane PDMS is commonly used as a means to prototype microfluidic channels[16].

3.1.1 Process

A positive mold containing the desired features is created using a photolithography process. The steps of the process are as follows and Figure 4 shows the differentiation of a positive and negative mold.

1. A photoresist resin is spin coated onto a silicon wafer
2. A mask is applied that covers some portions of the wafer and leaves other areas exposed
3. The wafer is exposed to UV light, this cures the resin not covered by the mask
4. The uncured resin is etched away leaving the completed silicon tool

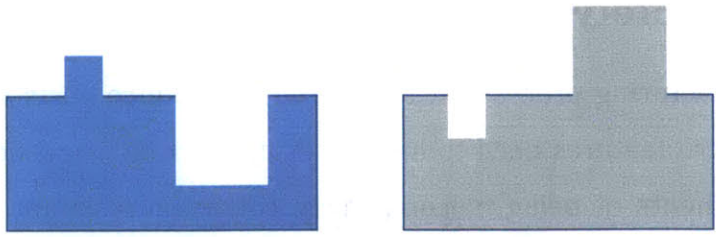

Figure 4 The positive mold (left) holds desired features and the negative mold (right) holds the opposite geometries of the features

Once this silicon positive mold is completed, PDMS parts can be produced from it. Liquid PDMS is poured onto the positive mold along with a hardener. Once the PDMS cures, it is removed from the silicon positive mold and creates a negative.

3.1.2 Limitations

This process can create parts quickly. It may take a couple weeks to receive the silicon positive mold from a semiconductor foundry. However, once the tool is made, PDMS copies can be produced rapidly and at low cost. The greatest problem with this process is that it produces parts that do not have geometry or properties that are entirely representative of the final production process. Photolithography results in parts that have nearly perfectly vertical walls and can produce corners with almost non-existent radii[17]. Conversely, injection molding (the production process) produces parts with tapered walls and corners with radii. Additionally, this process produces fluidic channels in PDMS, which is not the production material. Material certainly has an effect on flow characteristics and because of this results from testing PDMS parts may not be representative of how the design will perform with production material.

Another limitation of this process is that it is best suited for creating features with uniform height. Daktari's actual product is a microfluidic network with complex geometry with steps and ramping inclines. Therefore, this process is best for prototyping only portions of the design.

3.2 Micromachining

Micromachining can be used to produce parts with microfluidic applications because of the available working materials, machinable geometries, achievable feature sizes and surface roughness[18].

3.2.1 Process

Like traditional milling, a micro mill uses endmills with sizes as small as five microns that can cut into metals and softer materials. During the milling process, the endmill is moved relative to the work piece. This allows features to be cut directly into the thermoplastic substrate. In micromachining, the microfluidic channels are cut directly into the thermoplastic substrate. This process allows for complete control of the end part and is capable of producing many types of geometries.

3.2.2 Limitations

An advantage of micromachining is the flexibility afforded by the process. Once a micro mill is acquired, designs can be quickly iterated on. However, the benefit of not requiring custom tooling for each design is balanced by the relatively long cycle time of this process when compared to injection molding or producing PDMS parts from a silicon tool. Daktari anticipates needing 20-50 of any given prototype design for testing. This requirement makes the cycle time of micromachining each part undesirable.

A potential problem with micromachining is that tool marks left by the process may produce surface roughness characteristics that are undesirable. As mentioned previously, the cells of interest for Daktari are on the order of 1-10 microns. It is possible to achieve a surface roughness several orders of magnitude lower than this [18], however if the process is not carefully controlled then this characteristic might be problematic. Another artifact and problem with machining is the introduction of burrs, which could have an impact on the performance, or assembly of microfluidic devices. Burrs are introduced when material is not fully removed or becomes welded on the edges of a corner. Figure 5 depicts a cross sectional view of burrs and shows tool marks and potential burrs left by micro machining on aluminum.

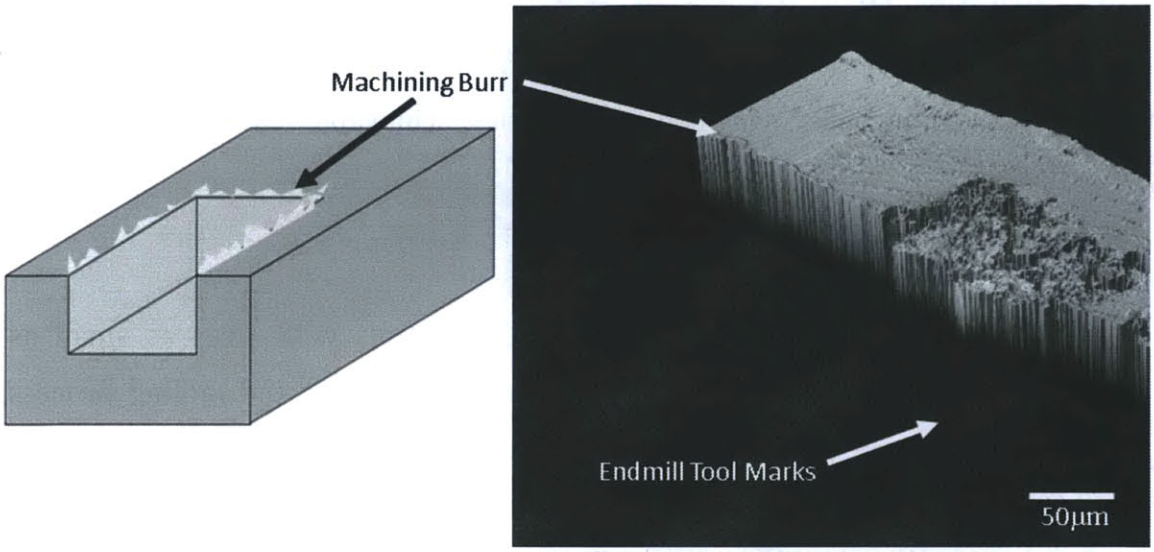

Figure 5 Cross sectional depiction of burrs on the edge of a possible machined channel (left). An interferometer image of a machined feature showing tool marks and possible burrs (right).

Micromachining also limits features such as sharp convex corners, which are sometimes used in microfluidic devices to control fluid flow. An example of this use of sharp corners is to control capillary action where the sharp corners can be used to stop fluid flow. The radius of the endmill usually dictates the achievable radius on the interior of a corner, but usually not the exterior. Control and prediction of the corner milling resolution has also been seen as an issue in automated machining for mass production [19]. Figure 6 shows the common process for milling a corner.

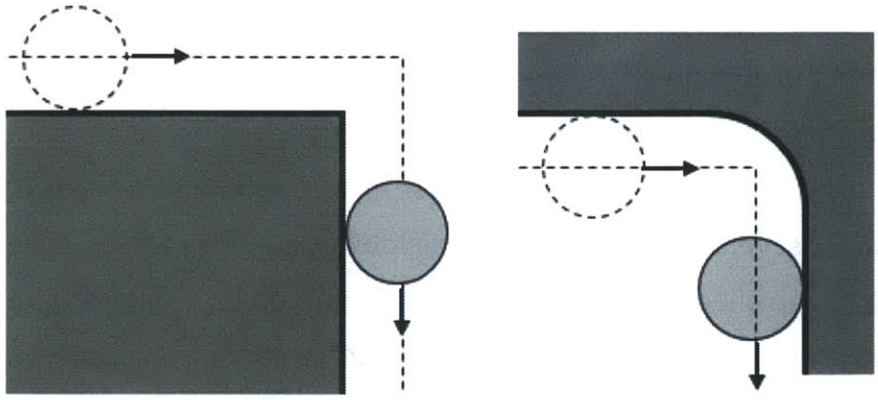

Figure 6 The standard process for milling the outside radius (left) and inside radius (right) of corners.

3.3 Injection Molding

Injection molding is a common process used to make parts containing micro-features. It offers the ability to use a wide variety of thermoplastic materials, many of which are biocompatible.

3.3.1 Process

Micro-injection molding is a process of transferring a thermoplastic material in the form of granules from a hopper into a heated barrel so that it becomes molten and soft. The material is then forced under pressure into a mold cavity where it is subjected to holding pressure for a specific time to compensate for material shrinkage as shown in Figure 7. The material solidifies as the mold temperature is decreased below the grass transition temperature of the polymer. After sufficient time, the material freezes into the mold shape and is ejected. This cycle continues to produce a number of parts. A typical cycle lasts between few seconds to few minutes [20]. The process has a set of advantages that make it commercially applicable. Advantages include the wide range of thermoplastics available and the scope for complete automation with short cycle times [21,22], cost effectiveness for mass-production process, especially for disposable products, very accurate replication and good dimension control, low maintenance cost of the capital equipment, when compared to the lithographic methods and applicability of the large amount of industrial information and technical know-how available for the traditional injection molding process. Also, because the working materials are injected into the cavities at a quasi-liquid state, the high mobility of the material makes making high aspect ratio, larger than 10, devices possible [23]. The process requires relatively inexpensive equipment and a metal mold to be produced. Additionally, the complexity of geometry possible is only limited by mold making capability. The dimensions of the injected parts fall into a region from 500 nm to several hundred micrometers.

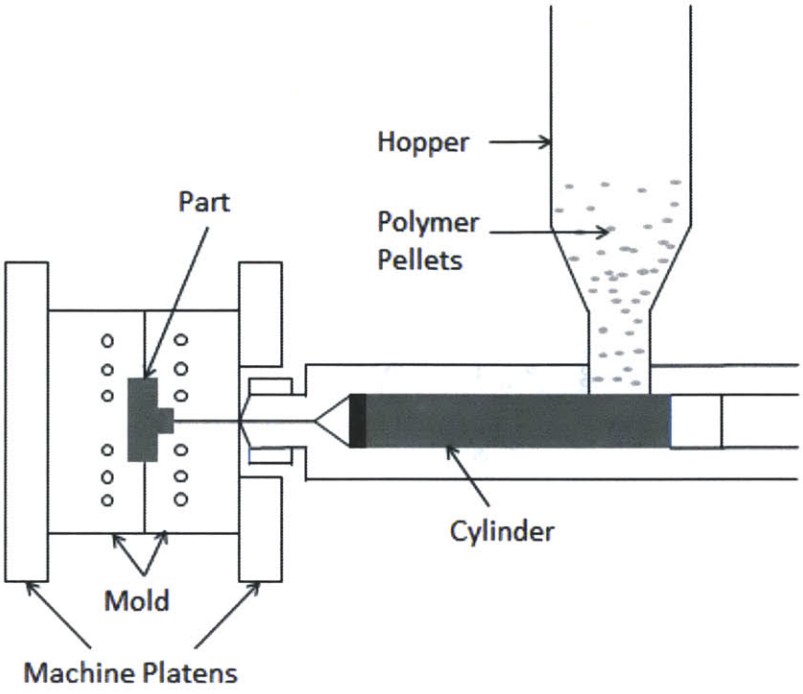

Figure 7: Injection Molding Process

3.3.2 Limitations

However, because the working materials are processed under wide temperature range, from the room temperature to 10 to 20 degrees above the polymer melting temperature, the shrinkage of the material is large, and hence good uniformity in the walls with different thickness is hard to achieve[24].

Daktari will finally use the injection molding process for the manufacturing of the device on a mass-level. Once tooling is completed, their contract manufacturer is able to produce their backbone (cartridge) in a high volume and at relatively low cost per unit. If Injection molding is used as a prototyping tool, then parts produced are completely representative of what the parts will be like from a production run.

The major limitation of this process is the monetary and time investment required to make the mold. Lead times for precision micro molds can be in excess of 6 months, and changes to the mold design can take weeks to complete. While the fidelity achievable

through injection molding is desirable, the time required to make tooling is too long for this process to be an effective development tool. Daktari needs a prototyping tool which gives them a part which has the same material properties as the final part, which is made out of PMMA, be robust and function like the final product in a short period of time. This will enable reiterations of the design at a faster rate with a prototype, which is actually similar to how the product will work.

4 Hot Embossing Process

Hot embossing is a promising technique for manufacturing micro-fluidic devices due to its excellent feature transfer capabilities from master molds, with high aspect ratios and low roughness, onto polymers[7,25]. This meets the requirement for prototyping microfluidic devices that have varying feature sizes, surface roughness and complex geometries. It has also been shown that hot embossing has the capability for producing Poly methyl methacrylate (PMMA) parts with microfluidic features and low cycle times[9,26].

The cost associated with creating the hot embossing master tool can be equal to or lower than injection molding in most cases [11]. On the other hand, the cost for the embossing equipment and materials are relatively low in comparison due to lesser heat and force requirements. Hot embossing requires much less force and heat in comparison to casting or injection molding. The working substrate is normally only heated to, or a little above, its glass transition temperature (Tg) and needs only a few MPa of pressure to transfer features from a master mold onto the substrate[27]. Hot embossing is a very flexible process that often only requires the change out of the master tool between prototype designs. The simplicity flexibility of the system drives engineering, material and energy costs down.

4.1 Selection of substrate

Daktari currently uses PMMA as the primary material for their diagnostic chip for many reasons. PMMA is used for the purpose of hot embossing and injection molding at Daktari because it is an economical alternative to polycarbonate, especially when extreme strength is not necessary. Also, PMMA does not contain the potentially harmful bisphenol-A subunits found in the polycarbonate. PMMA is often preferred as the polymer because of its material properties, easy handling and processing and low cost. The glass transition temperature (T_g) of atactic PMMA is 105 C (221 F). The forming temperature starts at the glass transition temperature and goes up from that point. PMMA is a strong and lightweight material with a density of 1.17-1.20 g/cm^3, which is less than half of that of glass and has an

ignition temperature of 460 C and burns forming carbon dioxide, water, carbon monoxide and low-molecular weight compounds including formaldehyde. PMMA is the least hydrophobic of all the common plastic materials. Moreover, its optical clarity is also a significant benefit for the testing purposes. PMMA will be the primary material used in this work since it is commonly used in hot embossing and is the material used for Daktari's diagnostic chip.

4.1.1 Basic Properties of Thermoplastics

A thermoplastic is a thermo-softening polymer that becomes pliable with an increase in the temperature and returns back to the original solid state with cooling. Most of the thermoplastics have a high molecular weight and its massive molecular chains have high intermolecular forces binding them together. These forces help in the binding of the material once the temperature cools down and hence the polymer can set back into its solid state. Above its glass transition temperature T_g and below its melting point T_m the physical properties of a thermoplastic change drastically without an associated phase change. Within this range, the thermoplastic is a rubbery mass due to alternating rigid crystalline and elastic amorphous regions approximating random coils. This makes hot embossing of these thermoplastics possible without working in a broad temperature range like in case of injection molding. Brittleness might be a deterring factor for the hot embossing process and this can be reduced with the addition of plasticizers, which interfere with the crystallization to effectively lower the T_g. Modification of the polymer through co-polymerization or with the addition of non-reactive side chains to monomers before polymerization can also reduce the T_g.

4.2 The Hot Embossing Process

Hot embossing is the process in which a substrate is impressed with features from a master tool. The master tool holds the negative of the desired features so that the positive of the features may be transferred. It is also very common to heat up the master mold and usually results in better feature transfers and lower cycle times[25]. Figure 8 depicts the process overview with the master tool and substrate.

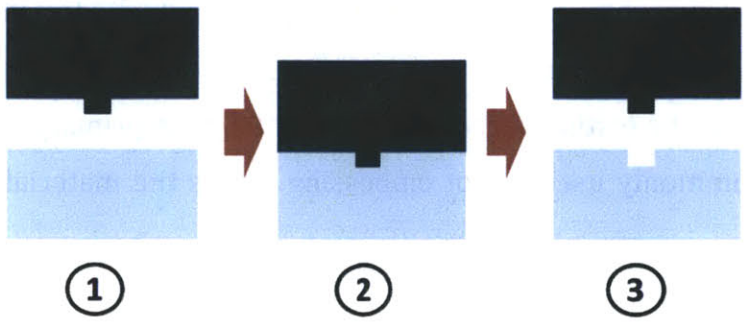

Figure 8: The master tool (top) and substrate (bottom) are heated up (1), then pressed together (2) and finally released (3)

Figure 9 shows the force and temperature cycle of the hot embossing process. The process cycle starts when the substrate begins heating up to or past its glass transition temperature, T_g, from T_0 to T_1. At T_1, the master tool is pressed into the substrate and held for a period of time at a constant molding force. The holding time lasts until T_2, at which time the substrate is set to cool. At T_3 the substrate temperature reaches below its T_g to a desired de-molding temperature and the molding force is released, ending the process cycle.

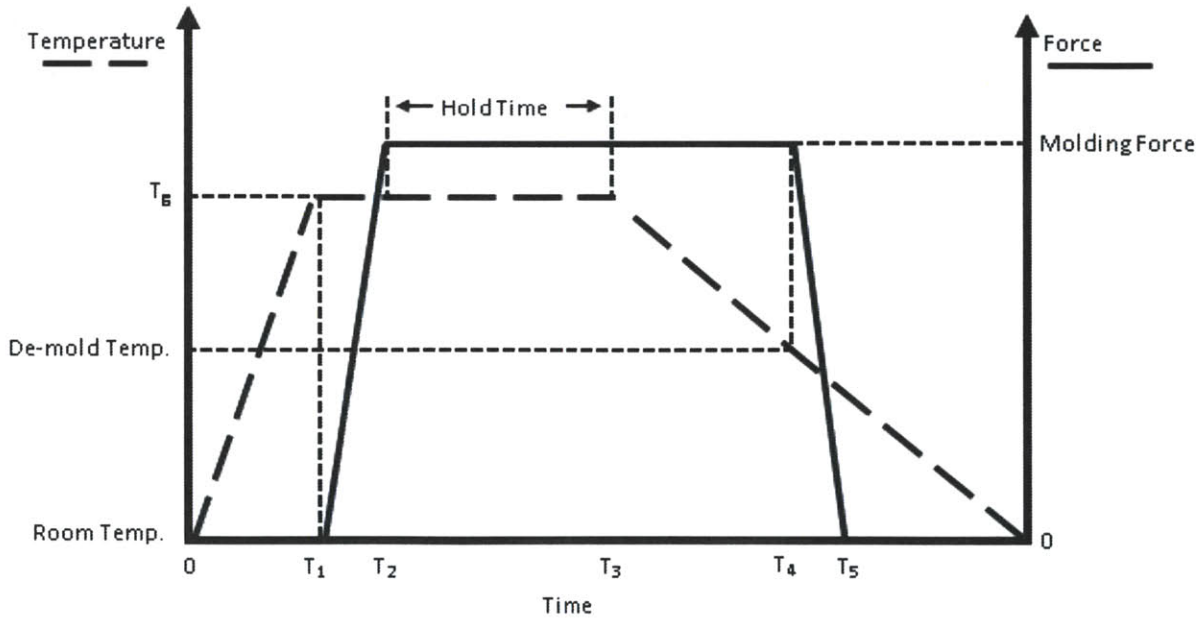

Figure 9: General hot embossing temperature and force cycles. The process cycle begins from T = 0 to T = T3

4.2.1 Initial Heating Stage

Referring to Figure 9, the heating stage occurs between T_0 to T_1. During the initial heating stage, the substrate is heated up to or a little past its T_g. It is also very common to heat the tool up at this time to the same temperature of the substrate or a bit cooler[28]. This initial heating prepares the substrate to be malleable and less viscous for the embossing stage. The higher the substrate temperature is, the less force is required. Also, a higher replication accuracy is correlated with better material flow[29]. Uniform heat distribution is preferable because it can dictate the quality of the part and complexity of process control and analysis. Control and repeatability of the temperature during this stage is desired for quality and process control purposes.

4.2.2 Embossing Stage

The embossing stage spans from T_1, the time in which the master tool and substrate come into contact, to T_4, when the tool and substrate start to separate. The embossing stage initiates from T_1 to T_2, during which time the tool and substrate come into contact and force begins to be applied and ramped up to a desired load. Once a desired force is reached, it is kept constant from T_2 to T_4. Constant force as well as constant position can be kept during this time, depending on the types of features required. For example, a part may have to be made to a certain thickness. This would only be achieved under constant position holding and not force. The holding time occurs between T_2 to T_3 and defines the amount of time that the substrate is placed under constant force and heat, or position and heat.

4.2.3 Cooling Stage

Cooling happens after T_3 and is the stage that brings the substrate below its T_g. De-molding temperature plays a large role in the final shape of the embossed part and is usually set well below the substrates T_g. Releasing the molding force at too high of a temperature may cause the substrate material to flow and fill in the features that were created[29]. Cooling rates also has an effect on thermal stresses, which would affect part quality[30,31]. For the purposes of this work, the cooling rate does not have to be rapid and can be kept such that the best quality parts are produced. A long cooling time (~10mins) would be acceptable.

4.2.4 De-Molding Stage

De-molding begins at T_4, at which point the substrate has been cooled below its T_g to a desired de-molding temperature. Force application is released at this point and the tool and substrate are pulled apart until there is no longer contact, at T_5. De-molding can require a considerable amount of force depending on the size of the part, features, and amount of friction between the tool and substrate[32]. Materials such as mold release may be used in order to facilitate the de-molding process, but could potentially yield undesirable part quality, especially for a feature that requires tight tolerances. The de-molding process has been shown to contribute greatly to the quality of the part, especially when friction and substrate shrinkage are considered. Parts have been seen to have poor quality because of high friction and shrinkage[33]. Control of how the tool and substrate separate can also have an effect on the part quality. It has been recommended that the tool and substrate be separated initially at a single location or edge, then "peeled" away from one another[32].

4.3 Consideration of Process Capabilities

To consider hot embossing as a viable rapid prototyping process for Daktari, it must have capabilities in replicating a wide range of features. This section will provide an overview of some of the features that may be challenging for hot embossing to accurately and precisely produce. These features include many of the channel parameters introduced in chapter 2, as well as features that are specific to the assay channel.

4.3.1 Sharp Radii

Many features such as the assay channel require a sharp radius on raised edges. During the hot embossing process, the substrate exhibits a "dragging" behavior where the sidewalls, near the tip of the tool feature, "drags" the substrate as pressure is applied between the tool and substrate. This dragging process can wear the tip of the tool out while creating air gaps. Figure 10 shows a cross section of a channel and how air gaps can increase the radius on the raised edge. These air gaps can be reduced by increasing forming temperature so that the substrate can more easily flow and fill the gaps[34]. Increasing pressure and embossing hold time can also help reduce these gaps.

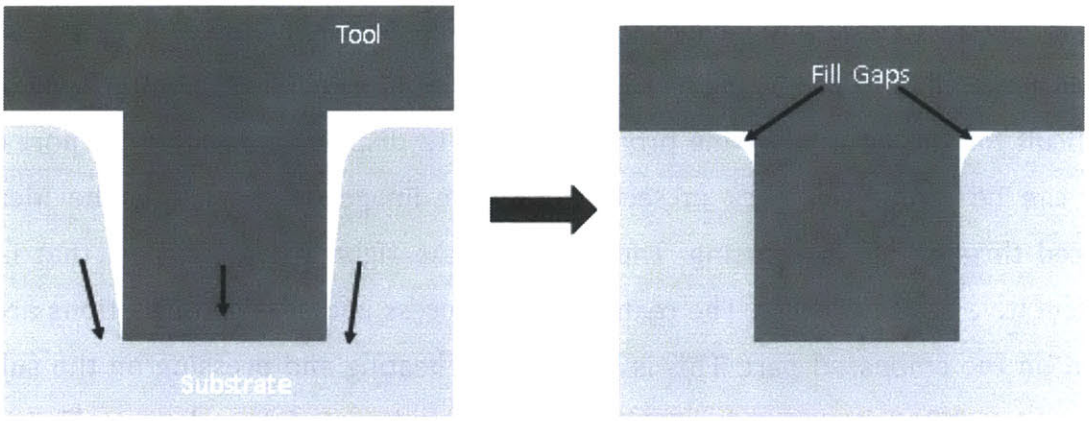

Figure 10 The left image shows the dragging effect where the arrows indicate the direction of the tool and material movement. The right image shows air gaps that can reduce feature radius.

4.3.2 Unfilled Extruded Features

The filling of high aspect ratio cavities can be difficult and can depend on the temperature, pressure, and hold time. The effects that cause incomplete filling in corners may also contribute to this incomplete filling of extruded features. Figure 11 shows an unfilled cavity during the embossing process. The substrate is pushed into the cavity, but if the hold time, pressure and temperature are not adequate, then the substrate may not be able to flow and fill the cavity.

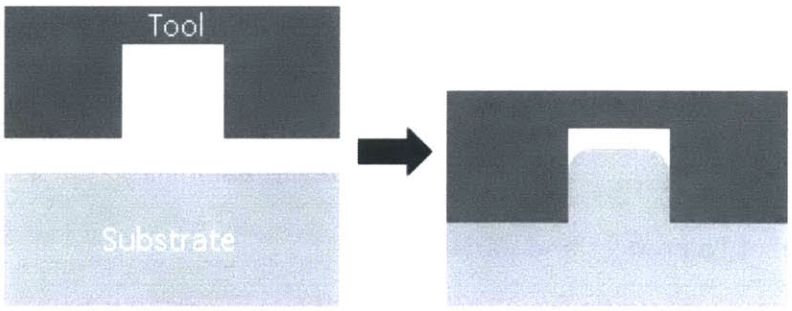

Figure 11 Cavities in the mold can be unfilled during the embossing process if temperature, pressure, and holding time are not adequate.

4.3.3 Features Ending on Edges

It may be necessary to have features that reside directly on the edge of an embossed card, such as a fill port. Producing features that reside on the edge of an embossed part may be difficult for the hot embossing process. Figure 12 displays a possible fill port design, which can be referenced back in section 2.2. The image on the left is the ideal part produced through hot embossing. The image on the right displays a part that is more representative of the process. The reality of the process is that edge distortions are often present on the embossed part. This is because the heating and pressing on the substrate causes material flow that is unconstrained at the boundaries of the substrate. This may be problematic when producing features that must reside on the edge of a part. Boundary bowing may also occur if the tool is smaller or of the same size as the substrate. Material that is not under constant pressure from the tool will deform with random warping during cooling.

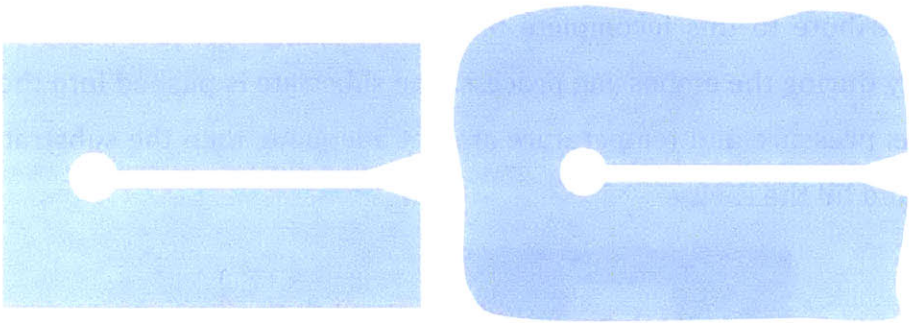

Figure 12: Substrate edge distortion

4.3.4 Control of Tolerances and Variability

It will be necessary to demonstrate the capability of hot embossing to produce features with tightly controlled dimensional tolerances. Referring to the assay channel in section 2.3, it is important that this feature maintains very low variability in the dimensions of the channel card to card and that the dimensions are precise as possible. The assay channel is a straight rectangular channel with a defined ridge around its perimeter. Figure

13 below shows what the assay channel may look like. The two holes represent inlet and outlets for a fluid.

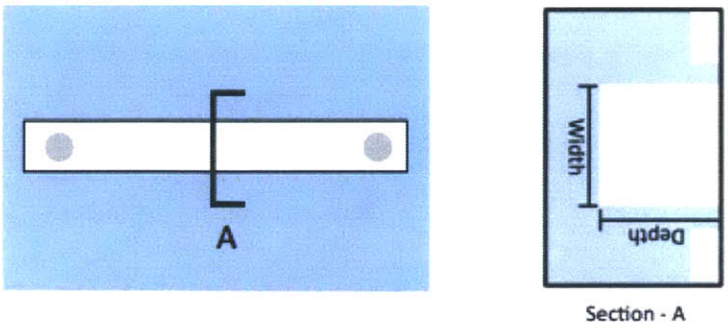

Figure 13 Schematic of a general cuvette feature

For hot embossing to be an effective method of producing this channel it is necessary that the variability of the process be well understood. This feature will also test the capability of hot embossing to fully transfer the mold onto the substrate. It will be critical to know what percentage of the mold geometry is transferred into the substrate. For example, if the mold has a feature with a cross section that is 10 microns deep and 10 microns wide, it will be important to know how closely the corresponding feature on the embossed part matches these dimensions.

4.3.5 Abrupt and Variable Geometries

Another common feature for this microfluidic network are areas where multiple channels come together at a junction. These junctions may bring channels together that have different depths and different widths. The hot embossing process must be capable of producing features of variable depth, either with a gradual incline at the bottom of the channel or with a step. The process must also be capable of producing features with variable width. Figure 14 below displays one possible design for a junction of multiple channels. Notice the change in channel width from the left to the right. This sudden change in width may be a necessary aspect of Daktari's product. It will be necessary to investigate the capability of the hot embossing process for producing channels with sharp corners, like those seen at the junction. Another variable dimensional control would be in the depth of

channels. The channels should be a constant depth along the length and width so that their functionality can be more predictable.

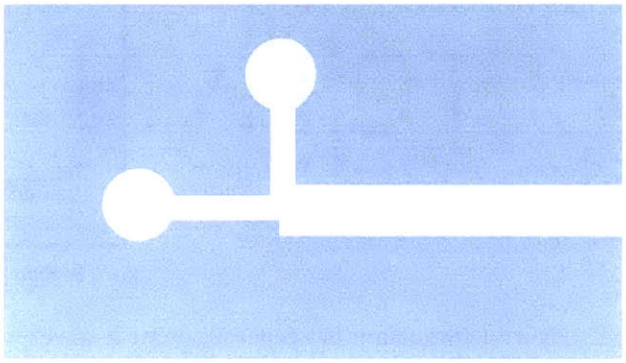

Figure 14: Schematic of 3-way junction

4.3.6 Surface Roughness

The cuvette feature requires not only tight tolerances, but also a low surface roughness. This feature is a wide and very shallow basin (roughly 50 microns in depth). Therefore, tight dimensional tolerance of the channel depth and width are critical. Additionally, surface roughness of the bottom surface is of paramount importance in the assay channel. The CD4 cell counting is occurring in this channel; therefore surface roughness must be maintained at a level that does not cause unwanted trapping of cells. The assay channel will also challenge the capability of hot embossing to produce large and smooth surface area features.

5 Machine Design Approach

This chapter will outline the design requirements needed for an embossing machine that is capable of making Daktari's assay channel. The general effects of different operating parameters will be described so that a basic idea of how different components and their operating ranges can work together to make parts. Design requirements will then be discussed. Current design practices that are in-line with this study will then be highlighted to help with the design.

5.1 General Effects of Operating Parameters

Hot embossing feature replication is largely dependent upon three factors; embossing temperature, pressure, and embossing time. The combination of values of the three settings effects not only the cycle time of the embossing process, but the achievable quality of the embossed substrate. For example, low embossing temperatures would require high pressures in order to achieve the same results as high embossing temperature and low pressures (Hale, 2008). The lower embossing temperature would decrease the heating and cooling time resulting in a possible decreased cycle time. This assumes that the embossing time is equal for both settings.

The tradeoff between these different settings would be in equipment size, cost, process cycle time, and achievable feature resolution. It is important for this design to be flexible with embossing temperature and pressure in order to accommodate future tool designs. Embossing and cycle time is not as important because it has been decided that low volume (20-50) production is required for prototyping.

5.2 Design Requirements

The following design requirements help guide machine design so that it may be able to hot emboss Daktari's microfluidic feature.

5.2.1 Tool and Substrate Fixture Requirements

It was decided that the embossing system should be able to accommodate the master tool and substrate material with surface sizes ranging from 25mm x 90mm to 65mm x 100mm. All sub features of the microfluidic device are able to fit on a 25mm x 90mm area, which provides flexibility in designing and testing of such features. The microfluidic device is able to fit into the 65mm x 100mm area, allowing for prototyping of the entire device. The substrate normally has the same surface size as the master tool, so the fixture holding the substrate should be positioned and orientated in the same manner as the tool. Repeatable placement of the substrate is not critical as long as the tool is able to emboss all features onto the substrate without deformation. The substrate can be reworked after embossing so that deformed edges can be taken off, so long as features do not reside on them. The fixture should also be able to hold down the substrate during the de-embossing phase so that the tool and part can be separated.

5.2.2 Force Requirement

Daktari has chosen PMMA to be the working material for the microfluidic device. Forming pressures as low as 1MPa can be used for high temperatures and long embossing times, but on average, 2MPa is used for embossing micro features on PMMA, and 4MPa being a rare case (Wang, 2006). 2MPa is used as the standard requirement, hence with the entire microfluidic chip measuring 63mm x 100mm, a working force of 12.60kN would be required. It should be noted that the working force could be lower than 12.60kN since increasing embossing temperature or time could achieve the same results as working with this load. Also, pressure is the least sensitive variable in the embossing process because it normally only needs to be above a certain threshold (David Hardt, 2005). The machine should also be able to meet de-molding forces, which could be high for large parts. It was determined that the machine did not have to initially meet 12.60kN of force since the largest embossing area that would be tested initially would be 22.50cm^2. For a 2MPa application pressure, a working force of 4.5kN would have to be met.

5.2.3 Heating Requirements

Commercially available PMMA has a T_g of between 85 to 165^{0}C, thus the embossing temperature must be able to reach above this temperature. The specified maximum operating temperature was chosen to be 200^{0}C in order to accommodate any future changes in plastic selection for prototyping. Popular plastics such as polycarbonate, polystyrene, and Zeonex have, on average, T_gs below 200^{0}C. It should be noted that hot embossing can tolerate embossing temperature tolerances of +/- 3^{0}C, so the accuracy of temperature control is defined by this tolerance (Wang, 2006). Heating rate is not as important because the entire process is not aimed to be rapid and is allowed to take up to half an hour. The substrate only needs to be brought to a desired temperature and kept there. Uniform heating should be considered in order to increase process control and part quality.

5.2.4 Cooling Requirements

It has been shown that the de-embossing temperature has an effect on not only the cycle time, but also on the quality of the embossed substrate (Matthew E Dirckx, 2011). The cycle time, in the case of prototyping 20-50 microfluidic parts, is not as important as the quality of the part itself. A cycle time of up to 30 minutes is acceptable in this case. Although cooling rate has an effect on part quality, the system does not require precision control of this parameter as long as it is consistent with every embossing run and fits within the 30min process window. As noted earlier, cooling over a longer period of time typically provides for better parts that suffer less from thermal stresses.

5.2.5 Alignment Requirements

Alignment of the heating platens is important because part planar uniformity is dependent upon this. Figure 15 shows how platen alignment can affect a part.

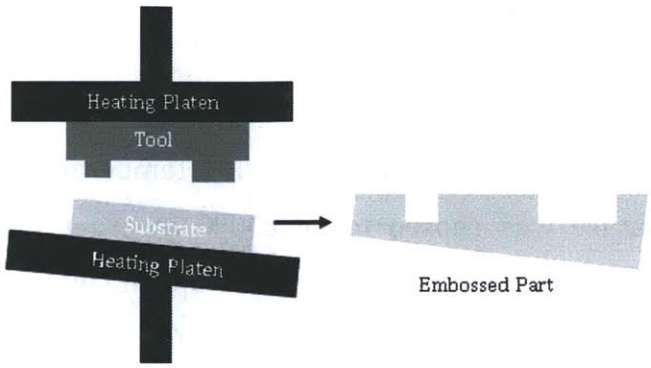

Figure 15: Depiction of misalignment

Alignment requirements, defined primarily by Daktari's microfluidic chip, concern planar x and y travel, angular rotation and vertical parallelism. Daktari has expressed interest in possibly embossing features on both the top and bottom surfaces of a substrate. This double embossing would require features from one side to line up with features on the opposite side. Unfortunately, there is currently no specified high precision x, y and angular alignment requirements because of a lack of understanding on how top and bottom features will perform together under misalignment. However, planar alignment and vertical parallelism should be designed to as high tolerance as possible while considering costs and time.

5.3 Common Design Practices

Simple thermocouples and liquid cooling systems have been shown to be an effective way to measure and facilitate in temperature control[9]. Effective cooling and heating systems help to drastically reduce the process cycle time. The cost associated with this system is associated with the desired cooling rate, accuracy, and thermal mass to be cooled. Temperature control has been shown to be an important parameter in reducing embossed part defects[32].

Force application and control can be achieved using different motors or hydraulics/pneumatics. Servomotors allow for great position control, but can be limited to the amount of force they can apply. Hydraulics and pneumatics offer much greater forces, but can be challenging in position controlling. Constant force application is generally more

common and important than constant position, so pneumatics and hydraulics are generally used. It should also be noted that in most embossing cases there is a force threshold, that once achieved, most embossed features do not change drastically in quality, from process to process, beyond this threshold [9].

In most cases, two heated platens are used for heating up and controlling the temperature of the substrate and master tool. The cost and effectiveness of the platens are related to the size and material used. Platens are normally not sized much larger than the master mold and would only require the increase in size to accommodate a heating source. Aluminum and brass are common materials used due to their low cost, machinability, and effective thermal conductivities.

6 Machine Design and Evaluation

This chapter will provide an over view of the machine design and describe its operating parameters and procedures [35]. Important operations performed by subcomponents and the characteristics of the machine will then be discussed.

6.1 Full Assembly

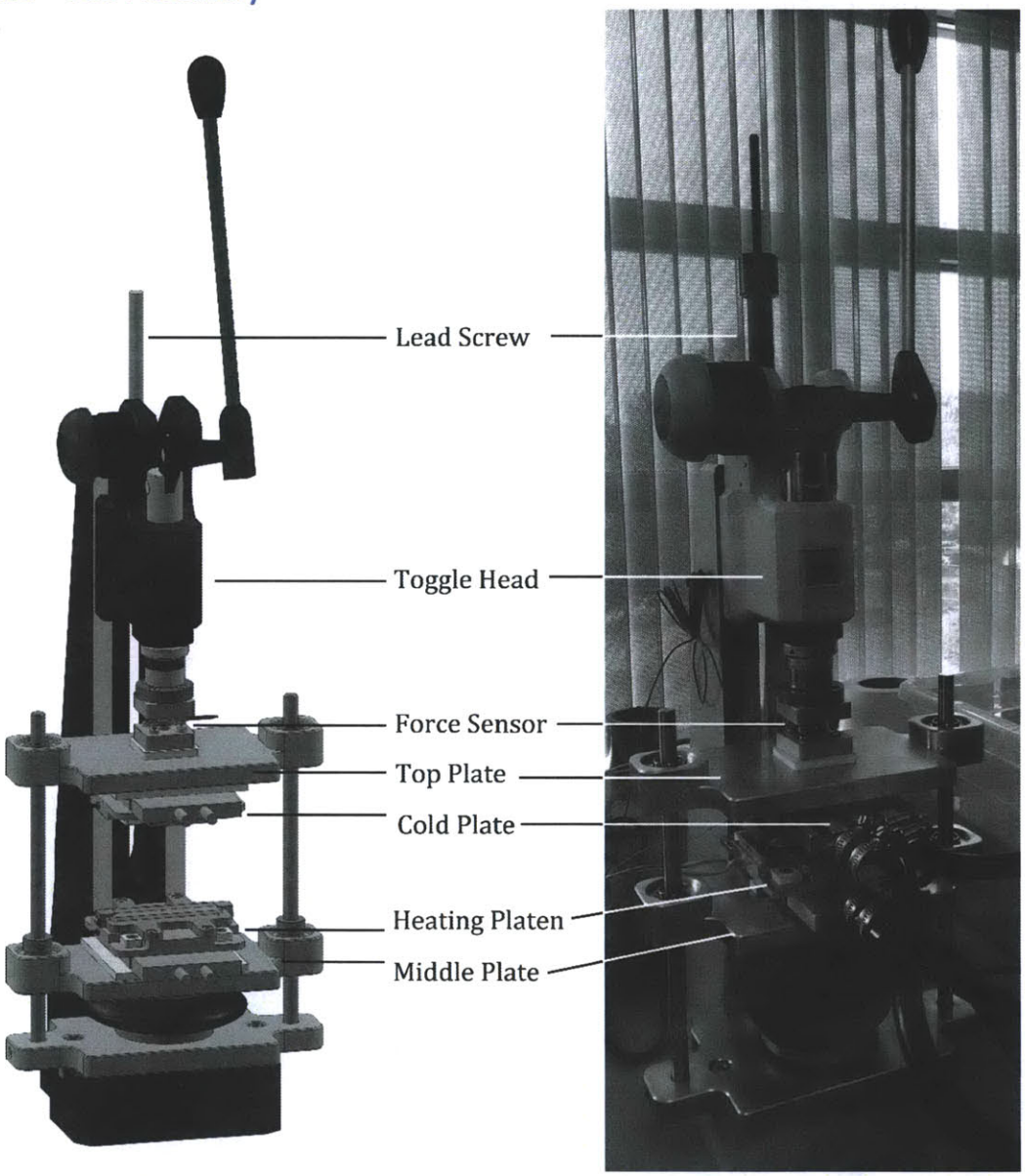

Figure 16: Full assembly view

6.1.1 Operating Parameters

A design of experiments was performed in order to determine optimal operating parameters [35]. Parameters may change according to changes in tool features. Parameters that produced the best parts are listed in the table below.

Table 1 Machine Operating Parameters[36]

Tool Temp	140 C
Substrate Temp	130 C
De-Embossing Temp	70 C
Pressure	3500 N
Holding Time	12 min

6.1.2 Operational Procedure

a. The toggle is not engaged
b. The top and middle stacks are set to their starting positions by rotating the linear traveling lead screw that moves the toggle head
c. The master tool and substrate are loaded onto the top and middle fixtures, respectively
d. The heating platens are then raised to their desired temperatures
e. Once the desired temperature of both platens are reached, the embossing head is moved down using the lead screw
f. The force sensor indicates when contact is made by the output voltage reading begins to change
g. The lead screw is turned until the desired force is indicated by the sensor
h. The hold time begins and the temperature and force are kept constant (the force can be allowed to decrease slightly because of substrate flow)
i. After the holding period, heating is shut off and the liquid cooling system is turned on
j. The toggle head can be raised using the lead screw once the platens reach a temperature below the substrates T_g

6.2 Load Bearing and Tilt Compensation

The embossing system frame handles the loading application as well as the alignment between the tool and substrate. The definition of what the frame consists of can be seen in Figure 17. This system uses a Schmidt model 15F toggle head and frame capable of applying 12.00kN of force. The tool and substrate can be brought into contact using either the toggle action, which has a working stroke of 34.8mm, or the linear traveling lead screw, with a working range from 80mm-325mm.

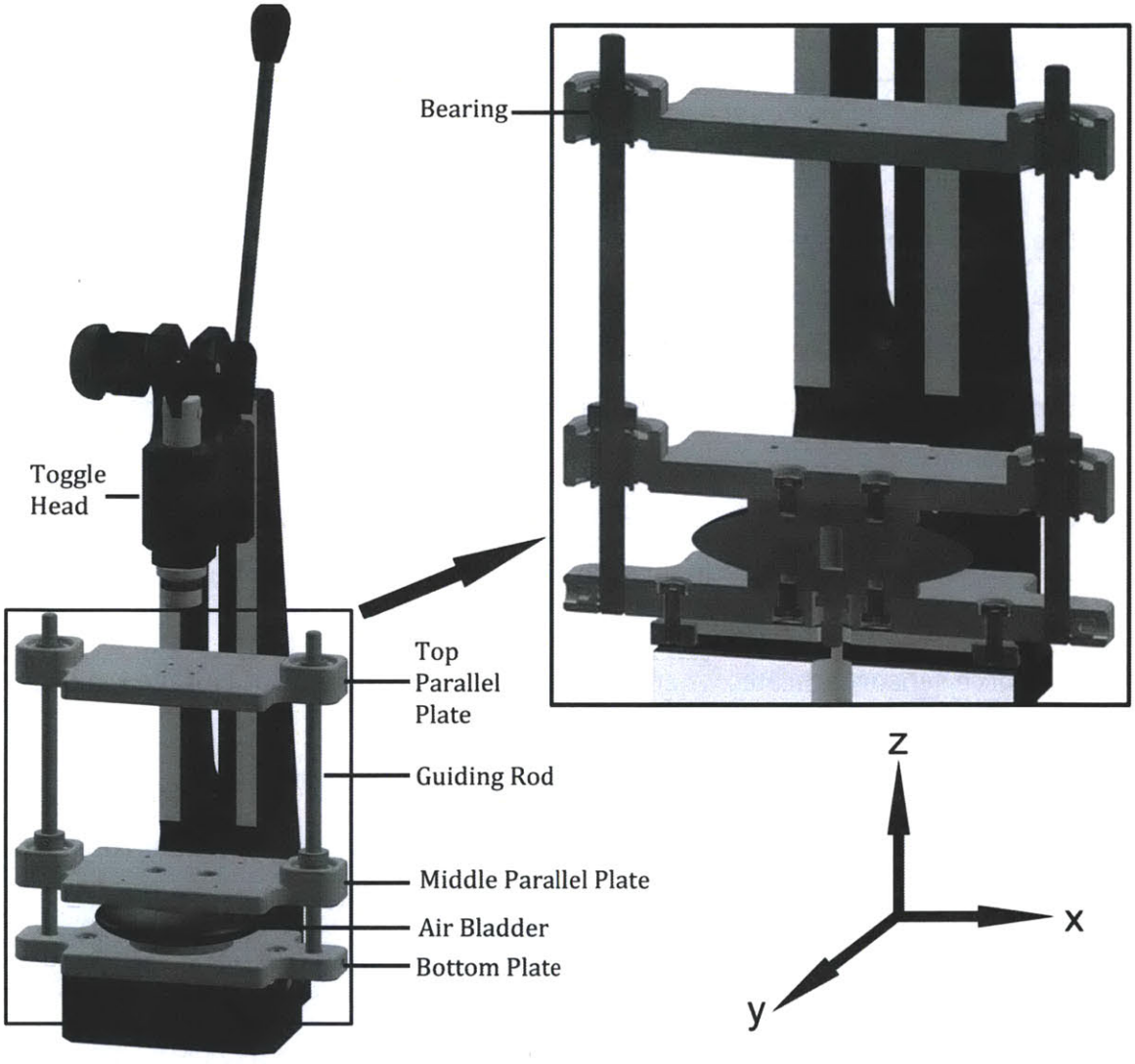

Figure 17 Frame assembly and cross section views.

Referring to Figure 17, the top and middle plates ride on guide rods using linear roller bearings. The bearings have individual inner bore diameter tolerances of 12.7mm+0.0/-6.35μm and tilt allowances of 15 minutes. The guiding rods have a diameter of 12.7mm+0.0000/-5.08μm. Maximum tilts of the stacks are dictated by the allowable tilt of the bearings. The frame also consists of an air bladder, rated for 6.67kN at 100psi, which couples the bottom plate to the middle plate, allowing for tilt compensation and equal pressure distribution between the tool and substrate. When the tool and substrate contact, the air spring distributes pressure evenly, theoretically making the top and middle plates parallel. Tilt may have an effect on feature quality by introducing gaps into the substrate during the initial stages of embossing. Figure 18 shows how such gaps may form. The figure also shows how repeatability of feature location, relative to a locating point, could be affected by tilt. During the tilting process, the top and middle plates may be misaligned since they can move relative to one another.

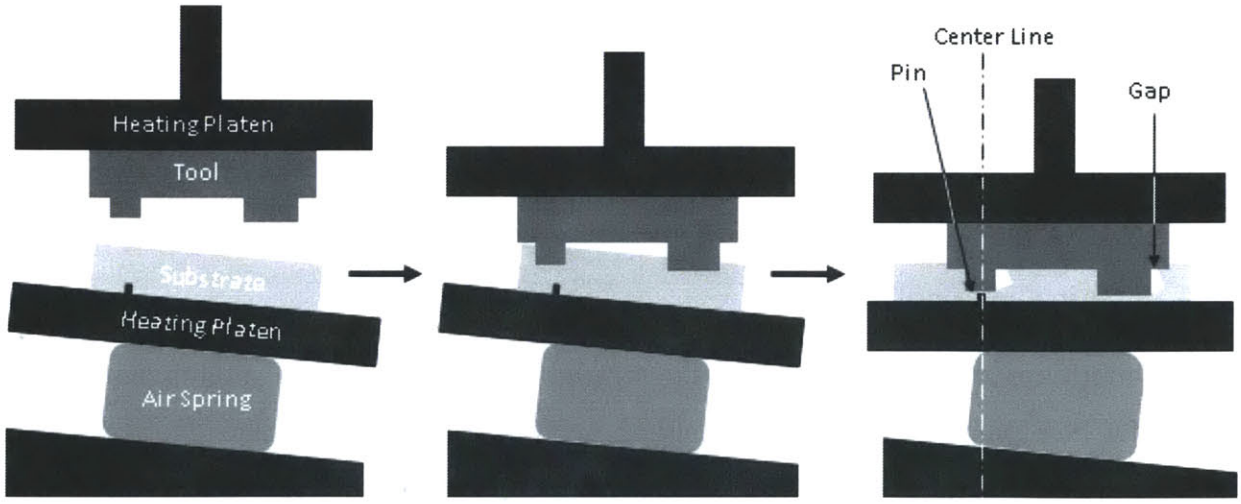

Figure 18 Visualization of misalignment air gaps.

6.3 Tool and Substrate Fixturing

The embossing tool was mounted directly to the heating platen and did not require a fixture because it was not removed in between experiments. The tool and substrate were positioned in line and orientated with one another. A fixture was designed so that the general placement of the substrate could be somewhat repeatable. The substrate fixture

has three outer locating pins that rest on the perimeter of the PMMA. This fixture also has three secondary inner pins that are embossed onto the backside of the PMMA. These embossed pin features were used to assess the machines x, y and angular repeatability, and as locating features for attachment to a measurement fixture. The PMMA is held down using side clamps, which in the event of substrate shrinkage onto the tool, helps to hold down the PMMA as the tool is lifted upwards and de-embossed. This fixture is mounted directly to the heating platen through four bolt patterns. Figure 19 shows how the substrate was fixtured.

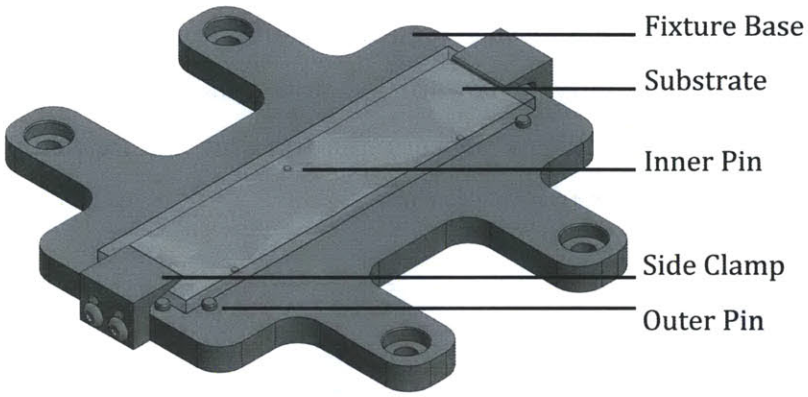

Figure 19 Substrate fixture

6.4 Heating and Cooling

Both the tool and substrate had dedicated heating platens and cooling plates. Figure 20 shows the tool and substrate assemblies. A single 150W-heating cartridge was inserted into each platen and was oriented in the direction of the tool and substrate lengths. These cartridges were used because of their rated heating temperature of 538°C and low cost. They are aligned in the same direction as the tool and substrate to provide uniform heating from the mid line. An Omega CN7500 series temperature controller capable of maintaining 2°C accuracy and a 200°C rated adhesive thermocouple were used to control the heating of each platen. The thermocouples were placed on the surface of the heating platen. Precise control of heating rate was not considered to be an important aspect of the machine because of the allowable 30-minute embossing process time window. Ceramic Macor

insulation was used to reduce thermal transfer to the frame components through conduction. Convection and radiation heating were assumed to be negligible in comparison to conduction. Figure 20 shows the conduction path blocked by the insulation at the top of the bolt heads and bottom of the cold plates.

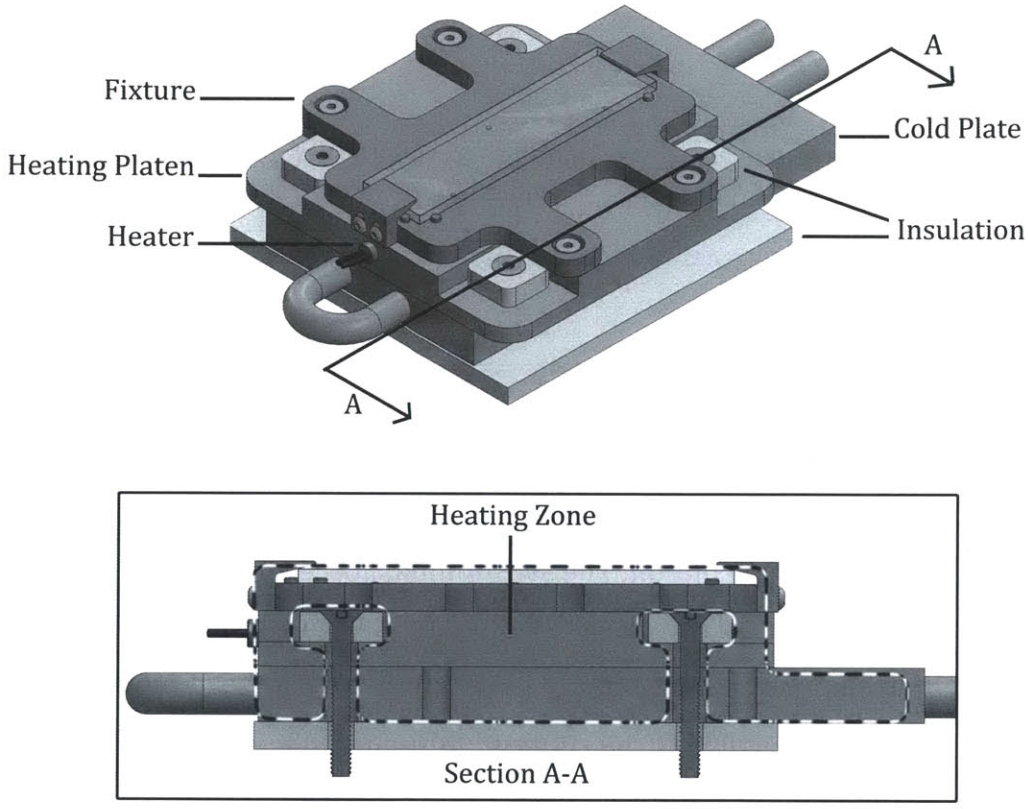

Figure 20 Substrate heating assembly and cross section

Cooling was achieved by using cold plates placed directly in contact with the heating platens. The cold plates ran a double loop, with 11L of recirculating room temperature water as the acting fluid. A pump provided flow of 38L/min over 1.83m of head (47L/min at 1.5m of head). This system was able to cool each platen from 140C to 40C in 2 minutes. Figure 21 shows experimental cooling data. The top plate was designed with the same configuration setup, minus the substrate fixture, and was bolted directly onto the heating platen.

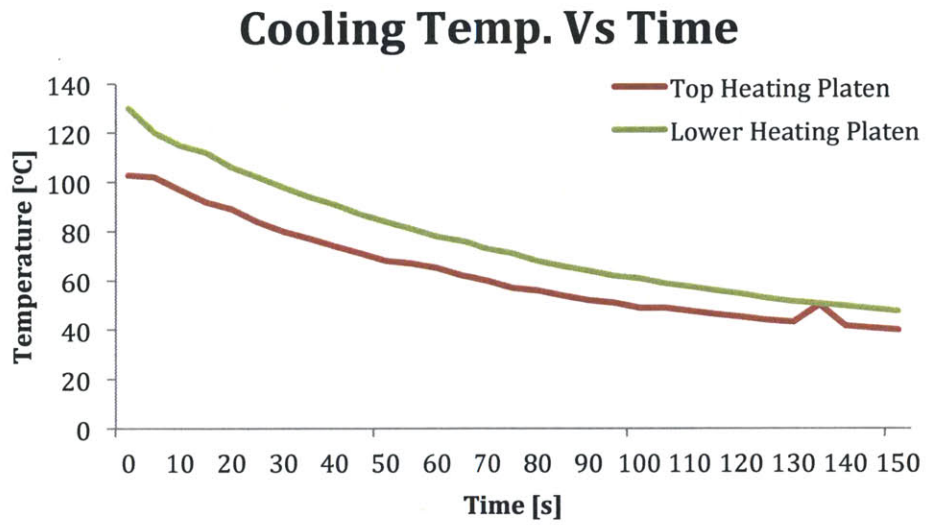

Figure 21 The cooling profile of the top and lower heating platens over a period of 2.5 mins.

6.5 Load Sensing

The load sensor was used to determine the amount of force applied between the substrate and tool. A Futek LCM200 sensor was chosen based on its size, 4.45 kN sensing capacity and in line mounting option. The sensor limits force application to 2MPa since the embossing area is 22.50cm^2. The sensor is bolted to the top parallel plate and de-coupled from the toggle head. De-coupling the sensor from the toggle head allows for the frame assembly to be unconstrained from top to bottom. This allowing for any vertical misalignment at the point of the toggle head to be resolved after the toggle head applies pressure on the force sensor. The alignment correct was thought to help reduce any errors that could occur in constraining the frame assembly and having the load sensor pick up stresses such as shearing. Figure 22 shows the placement and mounting of the sensor. De-coupling was achieved by providing a gap between the flange that connects the toggle head to the force sensor and the top aluminum block that the sensor was screwed into.

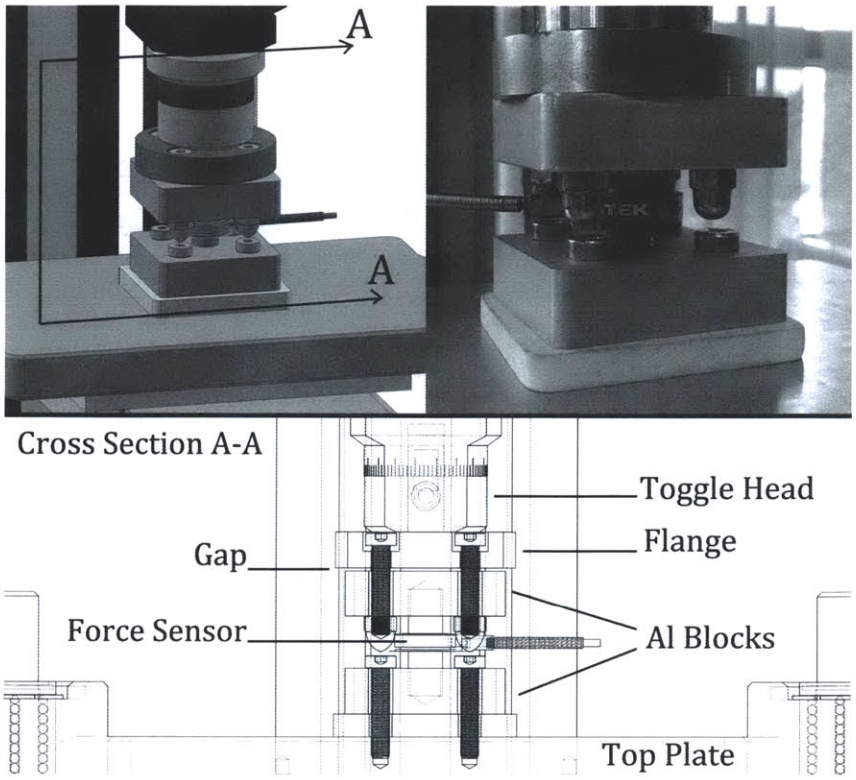

Figure 22 De-coupling of force sensor

6.6 X & Y Repeatability

Referring to Figure 17, the alignment system consists of the top and middle plates, air spring, guiding rods and bearing. To evaluate the x and y positional repeatability of the embossing system, the distance between fiducials that resided on the back and front of embossed parts were measured. By measuring the variability of these distance measurements over 10 parts, an estimate of the positional repeatability could be calculated. This positional repeatability was then decomposed into purely x and y planar slip, and rotational error.

The fiducials used were marks left by the 3 locating pins embossed onto the back of parts and surface features on the fronts of these parts left by the embossing tool. Figure 23 shows the three embossed pin fiducials, on the top images, with their corresponding embossing tool fiducials, directly below. The planar distance between corresponding fiducials were taken for the three locations and used to estimate planar misalignment.

Figure 24 shows a sample of how the planar distance between corresponding fiducials was measured.

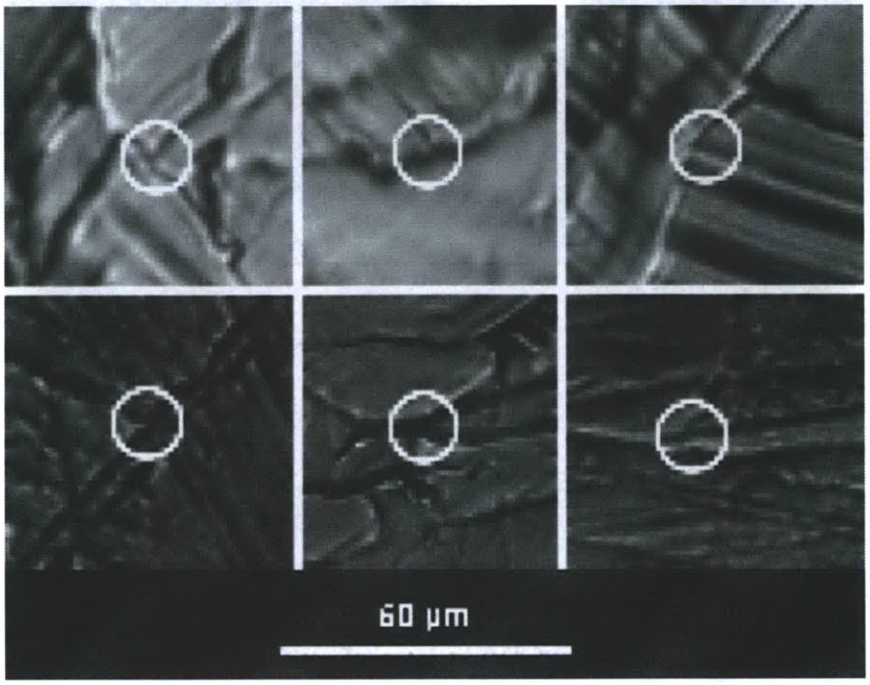

Figure 23 Fiducials used for x, y repeatability measurements

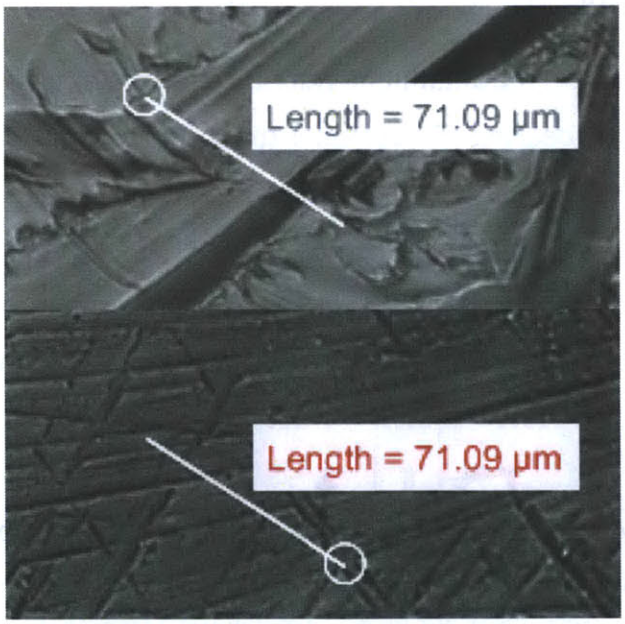

Figure 24 Distance between fiducials

Table 2 shows the measurements taken at the three locations for the 10 samples. All the parts had the same set of parameters with the tool temperature being at 140 C, the substrate temperature at 120 C, pressure of 600 lbs, holding time of 10 minutes and the de-embossing temperature of 30 C. The measurements were taken on a Nikon Eclipse Ti-SR optical microscope with a magnification of 10X.

Table 2: Measurement Data for XY Repeatability Analysis

	L1_M1	L1_M2	L1_M3	L1 Avg	L2_M1	L2_M2	L2_M3	L2 Avg	L3_M1	L3_M2	L3_M3	L3 Avg
R1	139.30	139.58	139.30	139.39	79.00	78.86	79.23	79.03	71.09	71.42	70.42	70.98
R2	129.77	129.77	128.33	129.29	98.37	97.21	96.93	97.50	78.01	76.49	76.58	77.03
R3	126.83	128.81	128.25	127.96	81.52	81.66	83.33	82.17	58.30	58.84	58.10	58.41
R4	138.64	140.40	138.79	139.28	93.57	95.08	96.48	95.04	73.24	72.90	74.32	73.49
R5	144.61	143.15	143.69	143.82	66.06	65.17	67.82	66.35	39.27	39.69	40.29	39.75
R6	127.91	128.32	128.59	128.27	76.49	77.28	75.69	76.49	53.66	52.92	53.80	53.46
R7	138.70	139.51	139.00	139.07	73.94	74.80	72.95	73.90	76.71	76.72	76.71	76.71
R8	153.38	152.53	152.54	152.82	58.09	57.29	57.95	57.78	80.40	80.30	80.29	80.33
R9	151.12	152.52	151.68	151.77	58.93	59.29	58.21	58.81	79.23	78.67	78.36	78.75
R10	148.06	147.50	146.70	147.42	56.62	56.96	58.58	57.39	76.74	77.79	77.07	77.20

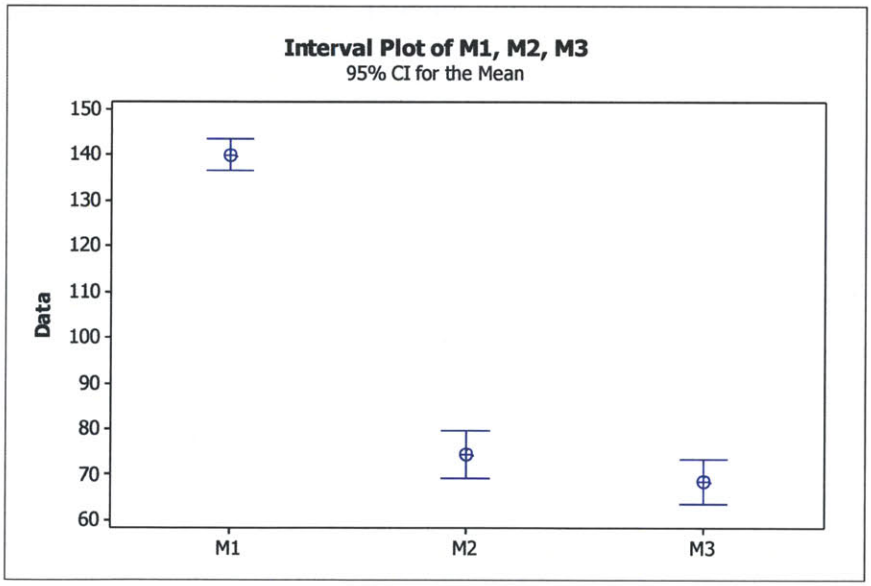

Figure 25: Error Band for the three Locations

Figure 25 depicts a plot of the 95% confidence interval on these fiducial measurements. The width of this confidence interval is what was used to estimate positional repeatability. If there was no angular component to this repeatability, then all three measurement positions should have confidence intervals of similar widths. However,

the confidence interval on the measurements taken at position 1 is visibly narrower than the intervals for positions 2 and 3. This difference is attributable to angular misalignment, and indicates that location 1 is located closer to the central axis of the press than the other two locations.

A summary of these error bands (95% confidence intervals on measurement) is seen in Table 3. Calculated error band for the three locations and the distances of these locations from the central axis are as follows:

Table 3: Error Relation to Distance

(All values in microns)	*Location 1*	*Location 2*	*Location 3*
Error Band	26.55	41.75	41.13
Center Distance	8690	33448.559	33448.559

To decompose the measurements summarized in the above table into errors attributable to pure x and y planar slip and angular error, the below equation was used.

$$E = e + \alpha l \tag{1}$$

E is the total positional error, e is the static x and y error component, and the αl term is angular error. Angular error is a function of distance from the central axis of the press, α is a constant describing the severity of this error, and l is the radial distance from the central axis. The axis that l is measured from can be seen in Figure 26 and Figure 27. The axis runs down the toggle head, along the center of force application.

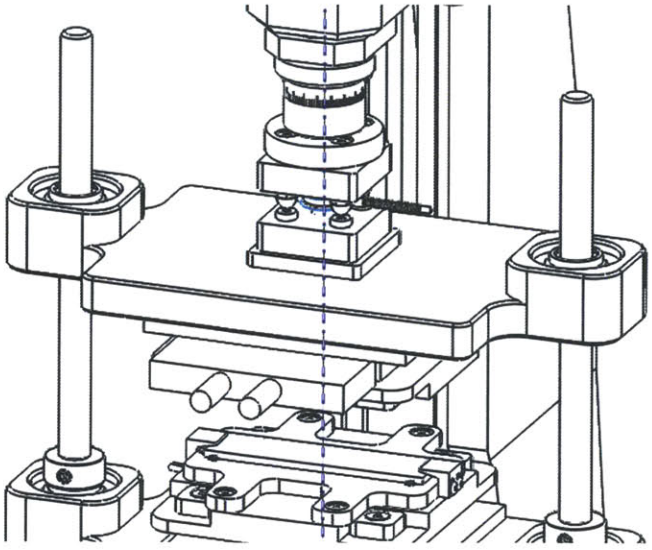

Figure 26: Central axis: ISO view

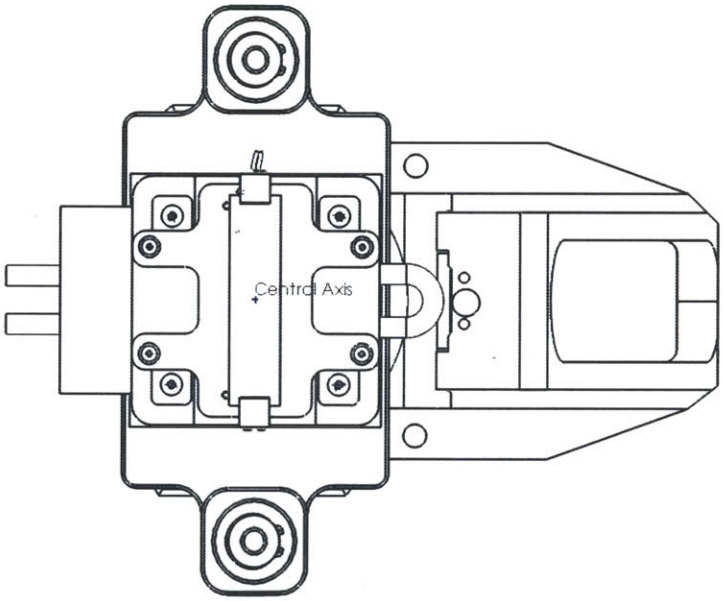

Figure 27: Central axis: top view

The x and y planar slip (e) was found to be 21 microns. The constant describing angular error was found to have a value of 0.000614. Using this data, the maximum positional error for embossing with our tool was calculated. With the spatial error remaining constant at 21 micron, the angular error at a distance of 3.6 mm (maximum distance of a feature embossed from the center for the cuvette) is equivalent to 22 microns.

Hence, the total XY repeatability is equivalent to 43 microns. This is the positional error located at the via furthest from the center of the tool.

6.7 Parallelism

As shown in Figure 17 the setup includes the three plates, with the guiding rods and the air bladder as a subsystem for the purpose of alignment. The bearings used are linear roller bearings with re-circulating stainless steel balls and a ceramic cage. For attaining greater accuracy in the parallelism between the plates, the plates were precision manufactured with 12.5 micron (0.0005 inch) tolerance for parallelism.

The guiding rods are used with linear roller bearings (AISI 52100 Steel balls and DURACON M90 cage), which allow an angular misalignment of 0.25^0 that incorporates a 43 micron clearance (allowable wiggle room for the air bladder) across the width of the cuvette at a distance of 10 mm from the center. The air bladder (*Single-Tire Style Air Spring rated @1500lbs*) is used to absorb the inaccuracy in parallelism to make the plates parallel. For analysis of the capability of the system to provide absolute parallelism, two methods were shortlisted as options:

- Use of the Nikon Eclipse Ti-SR optical microscope to focus on one fiducial on one side of the part produced and then recording the z direction travel to focus on a different fiducial on the other side of the part.
- Use of a Vernier Callipers with a precision of 10 microns to measure the 4 corners of the part to find out the parallelism accuracy across the length and the width of the part.

The Nikon Eclipse Ti - SR optical microscope was tested for repeatability for the z travel measurement and it was repeatable with a precision of 25 micron. The Vernier Callipers instrument with precision of 10 micron was the better of the two options.

To analyze the parallelism of the parts the method used was the measurement of the thickness at four locations on the part. The positions of these measurements are shown in

the Figure 28. These measurements were used to find the parallelism across the length of the part and across the width of the part. Ten parts were measured at these 4 locations to find out the tolerance of the system for parallelism. Table 4 shows the results of the analysis.

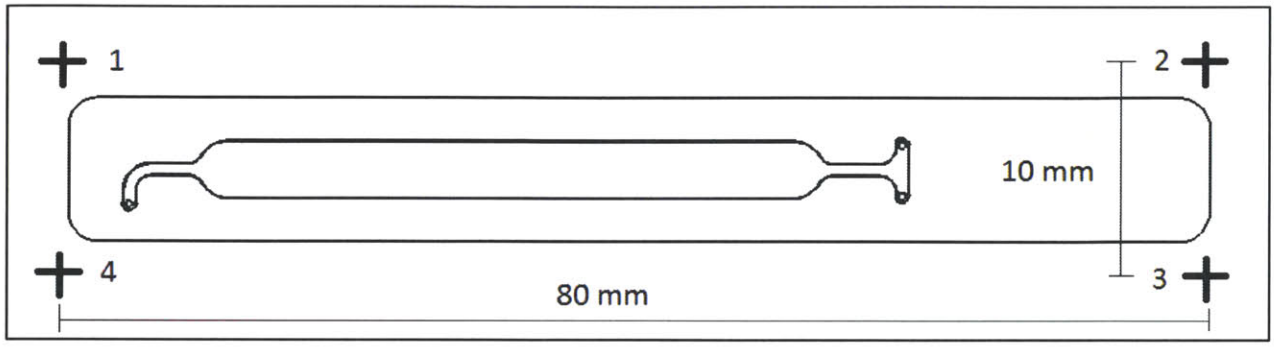

Figure 28: Measurement Locations for Estimating Platen Parallelism

Table 4 Parallelism Measurements

(all values in mm)	*M1*		*M2*		*M3*		*M4*		*Along the length*	*Across Width*
R1	3.05	3.04	3.04	3.05	3.07	3.07	3.08	3.08	0.00	0.03
R2	3.02	3.01	2.99	2.99	3.01	3.01	3.04	3.05	0.03	0.02
R3	3.01	3.01	3.04	3.05	3.05	3.06	3.04	3.04	0.03	0.02
R4	2.95	2.94	2.93	2.92	2.96	2.98	2.99	3	0.02	0.05
R5	2.97	2.97	2.99	2.99	2.99	2.98	2.96	2.98	0.02	0.00
R6	2.93	2.93	2.95	2.95	2.96	2.95	2.96	2.95	0.01	0.01
R7	2.97	2.95	2.97	2.98	2.98	2.99	2.98	2.97	0.01	0.01
R8	2.9	2.89	2.89	2.88	2.94	2.92	2.95	2.95	0.02	0.05
R9	2.95	2.95	2.93	2.93	2.95	2.94	2.95	2.98	0.02	0.02
R10	2.94	2.95	2.93	2.93	2.98	2.98	2.98	2.98	0.01	0.04
R11	2.98	2.98	3	3	3.01	3.01	3.02	3.02	0.00	0.02
									0.02	0.03

The parallelism achievable with this system was found to be 30 microns across the width of the part and 20 microns across the length.

7 Critical Dimensions

7.1 Description of the part

To evaluate the capability of hot embossing as a prototyping process for Daktari, the assay channel of their microfluidic network was chosen for replication. This specific feature was selected because it represents a location that has undergone extensive iterative design, and therefore would likely benefit from the ability to be prototyped with greater speed and fidelity. Additionally, this feature contains some of the tightest tolerances and smallest dimensions on the microfluidic product and so represents one of the most difficult features to replicate.

The assay channel is a rectangular channel that has a high aspect ratio. The depth of this channel is 50 microns, while its width is 4 mm. A microscope image of the complete channel cross section can be seen in Figure 29. Immediately adjacent to the channel, is a 10-micron ridge. A microscopic image of this feature is seen in Figure 30. This feature poses one of the largest challenges for the embossing process. It is a tightly toleranced feature with small dimensions, which is adjacent to a zone of high material displacement.

This chapter will detail the critical to function dimensions of the assay channel. These dimensions include cross-sectional measurements of the channel as well as measurements of channel uniformity, surface roughness and bow. One or more of these dimensions was chosen as a metric to describe embossed part quality. This quality metric was used as a response variable for a DOE optimization of the embossing process.

Figure 29: Microscope Image of Channel Cross-Section

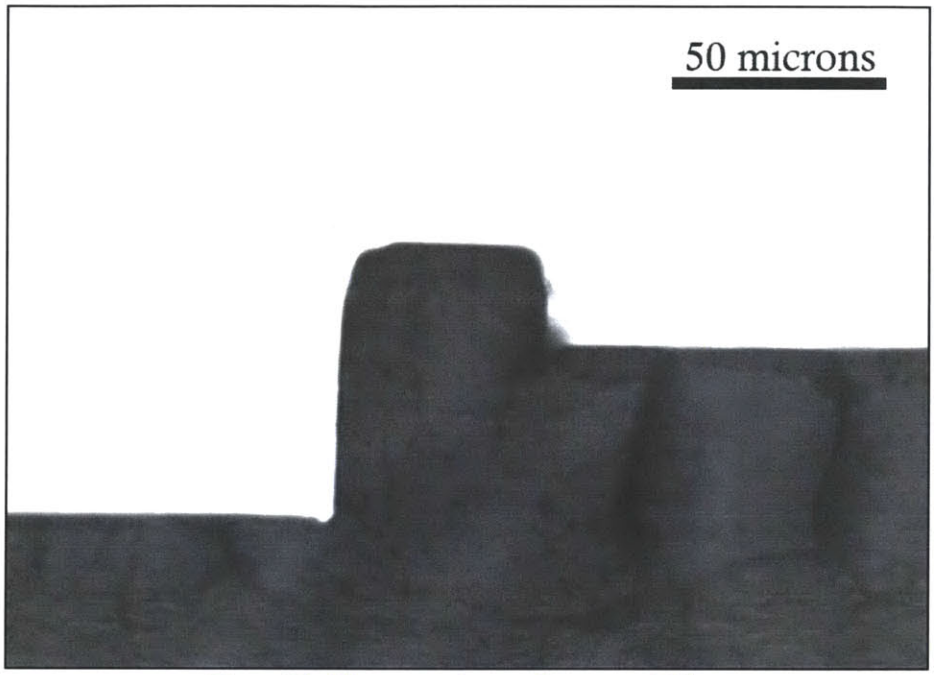

Figure 30: Microscope Image Close-up of Ridge

7.2 Cross-Sectional Dimensions

Several critical dimensions of this channel can be described as 2-dimensional measurements taken from a cross-section of the channel. These dimensions are the depth and width of the channel, the height and width of the ridge, the draft on the channel walls, and the radius of the inner edges of the ridge. This section will detail the relative importance of each of these dimensions.

7.2.1 Width and Depth

Correct depth and width of the channel are critical for proper performance of this device. As mentioned previously, the specification for the width of this channel is 4mm and the depth is 50 microns. The tolerances for these two dimensions are 10 microns and 1 micron respectively. Figure 31 displays the definition of channel width and depth.

The height and width of the ridge, as seen in Figure 32 are also dimensions of critical importance. The specification for this ridge height is 10 microns and its width is 50 microns. This ridge feature presents a difficult challenge for replication with hot

embossing, and its dimensions will likely be a clear indicator of the quality of finished parts.

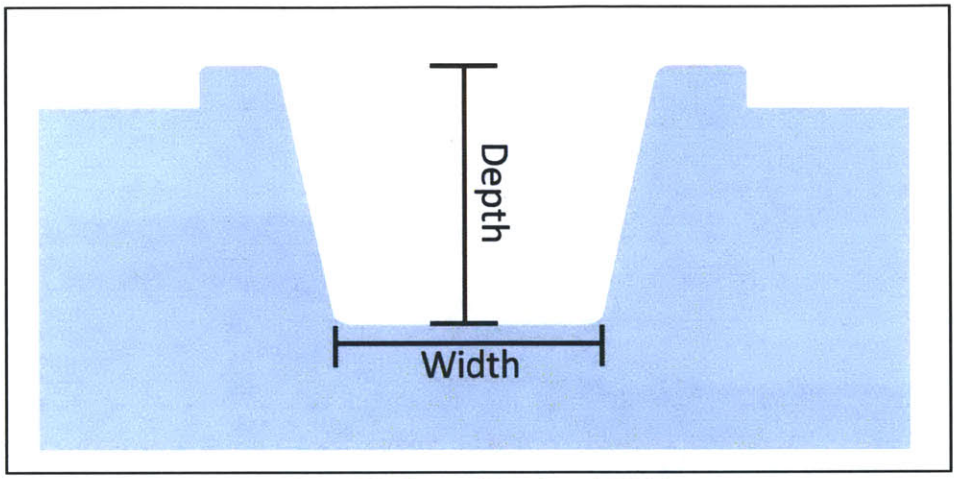

Figure 31: Channel Depth and Width

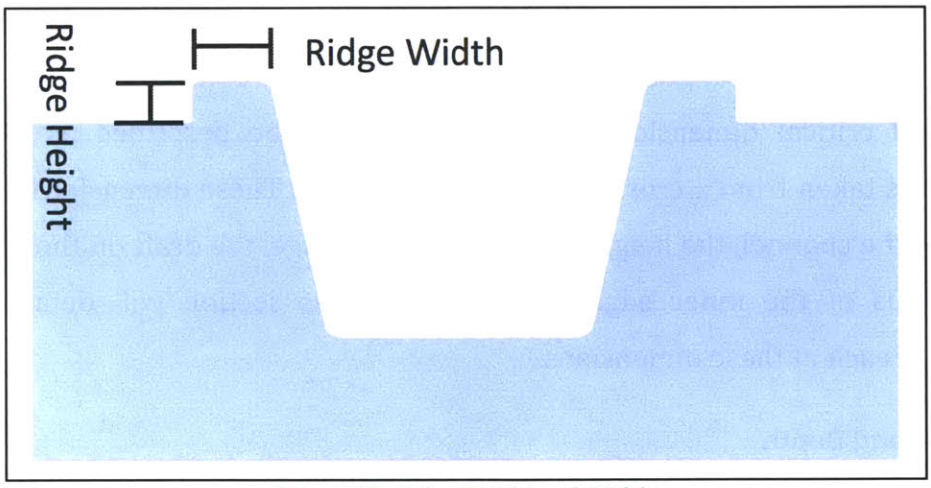

Figure 32: Ridge Height and Width

7.2.2 Edge Radius and Draft

A cover will be attached over the top of the channel. Therefore pinch points exist at the location of the upper edges of the channel. The radius of these edges must be minimized in order to limit the possibility that cells are trapped in these pinch points. A smaller radius at this edge is also indicative of more complete filling of the mold cavity. Figure 33 shows the location of this upper edge. Ideally, this radius would be non-existent.

Draft of the channel wall is another dimensional quality of the channel that can affect the performance of the embossed part. The production parts are injection molded and therefore have a designed-in draft. The parts produced with hot embossing are being made with a tool that has vertical walls. Draft should be essentially absent from fully formed parts. In the future, Daktari may design embossing tools that have a designed-in draft. If this were the case, measuring this draft angle would be critical to examining the quality of embossed parts.

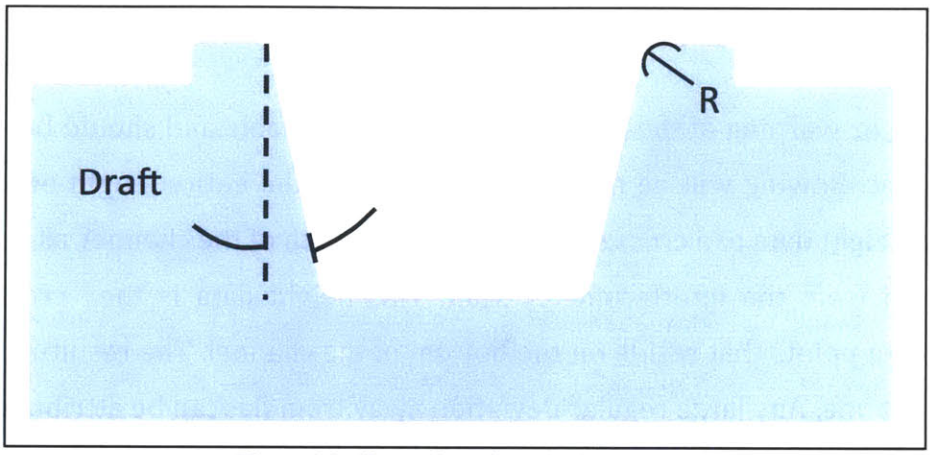

Figure 33: Channel Draft and Edge Radius

7.3 Overall part dimensions

In addition to cross-sectional measures, there are several measures of embossed part quality that must be obtained through measurements across the part as a whole. Channel uniformity, warping of the part, and surface roughness are all critical metrics that could have a significant effect on the performance of a finished part.

7.3.1 Channel Uniformity

Channel uniformity is a measure of within part variability. This metric will be used to measure how constant the cross sectional dimensions of a channel are along the length of a channel. The uniformity of channel width and depth are important for the performance of this product, as variations in these dimensions can cause anomalous flow of fluid through the assay channel. Taking cross-sectional measurements at several locations along the length of the channel and reporting the standard deviation of this sample of measurements will measure uniformity of these dimensions. An ideal channel, with perfect

uniformity would have identical width and depth measurements at all points along the channel.

7.3.2 Warping

Card bow is a measure of warping that occurs during the hot embossing process. After the load applied during the embossing process has been relaxed, it is possible for uneven cooling rates to cause the part to warp. Allowing the part to cool more thoroughly before removing the embossing load can reduce warping. However, this will lock residual stresses into the part and could make the part more difficult to de-emboss from the tool.

Bowing or warping of the embossed part is undesirable and should be measured as a quality metric. Bowing will be measured by scanning the entire length of an embossed channel. The height data of a cross section along the length of the channel, as seen in Figure 34 is obtained from the interferometer scan. This height data is then cropped to only include the data points that reside on the bottom of the channel. The resulting data should ideally be a flat line. Any large regular deviation away from flat can be attributed to general warping of the part. Figure 35 depicts measurement data of a channel that exhibits warping. The warping metric will be measured in microns and will be calculated as the maximum difference in height data from a set that should represent a flat plane.

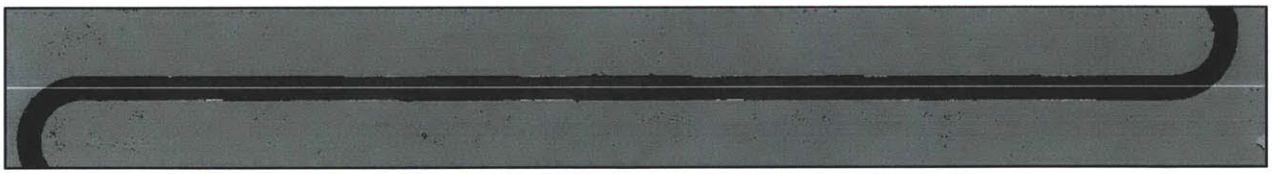

Figure 34: Scan of the Entire Length of an Embossed Channel

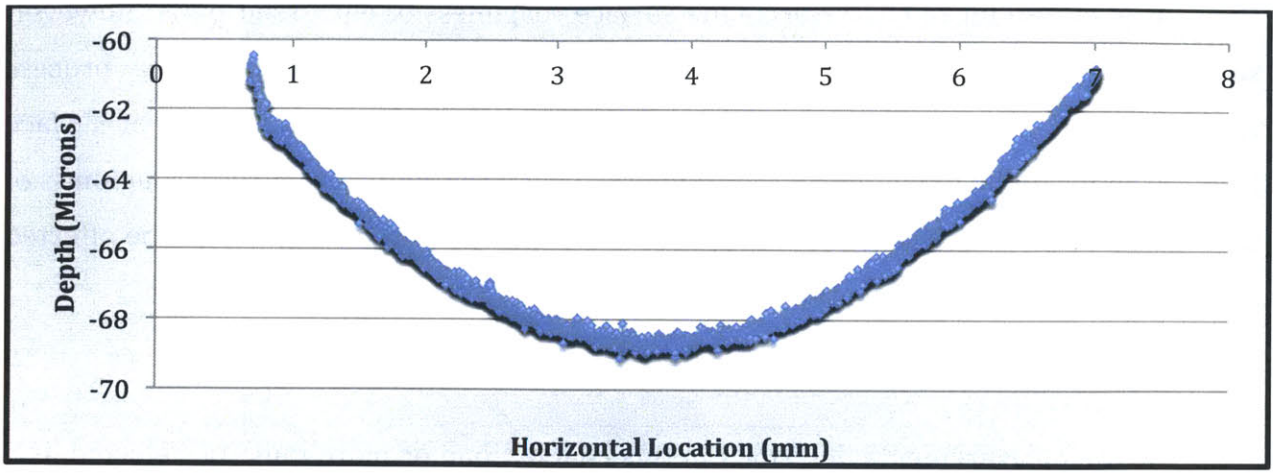

Figure 35: Along Channel Cross-Sectional Data Exhibiting Warping

7.3.3 Surface Roughness

As mentioned previously, achieving low surface roughness in microfluidic channels is important for proper performance of the device. Surface roughness must be minimized in order to reduce wall drag, ensure smooth flow and limit cell capture on channel walls. Surface roughness will be measured by scanning the bottom of an embossed channel using the procedure described previously. Figure 36 shows an image obtained from scanning the flat surface of a micro-machined hot embossing mold with an interferometer. The tool marks produced by the machining operation can be clearly seen.

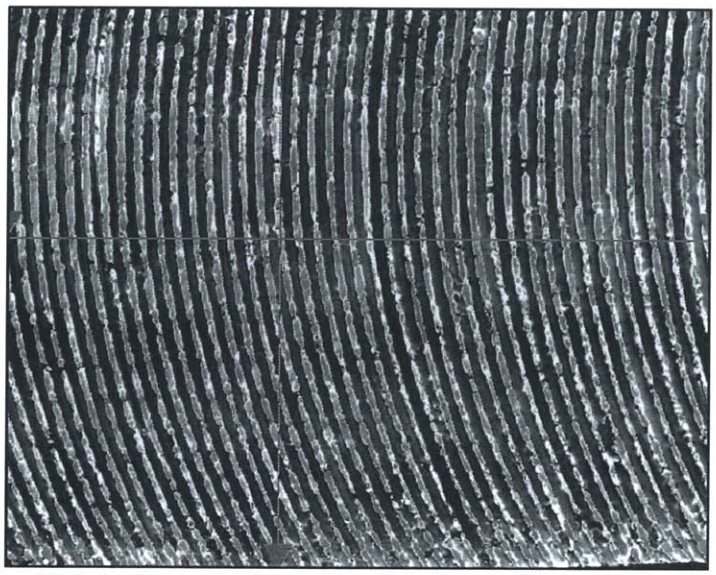

Figure 36: Interferometer Scan of Tool Marks on a Micro machined Tool

It is important to characterize the surface roughness of embossed parts; however, surface roughness will likely not be chosen as the response variable for process optimization. The hot embossing process accomplishes high fidelity transfer of surface features between the mold tool and the embossed part. Therefore, the surface roughness of the embossed part will likely match the surface roughness of the tool, and not be affected much by the process parameters.

7.4 Requirements of a Quality Metric

Of the measurements described in this chapter, one or more must be selected as a descriptor of part quality. Selecting the correct quality metric is necessary before performing a DOE optimization. This metric must be an accurate indicator of the effect of process parameters on embossed parts. It must be able to be precisely and accurately measured. The following chapter will describe the methods used to choose this quality metric.

8 Measurement Methodology

8.1 Overview of Motivation

After a part has been made with the hot embossing system, it is necessary to assess the quality of the embossed part. This chapter will detail both the measurement methods used to measure the critical to function dimensions described in the previous chapter (channel depth, channel width, ridge width, ridge height, surface roughness, channel bow, and channel uniformity), and describe the methods used to evaluate the effectiveness of these measurement techniques.

Quality of embossed parts will be determined by taking geometric measurements of the critical to function dimensions of an embossed part. The exact measurement technique used will depend on the dimension being measured. The effectiveness of each measurement method will be assessed with a Gage R&R study. This study will produce in a precision to tolerance ratio (P/T ratio) for each measurement method, which will be the end metric describing the effectiveness of the method. Once this P/T ratio has been computed for each measurement method, the best method for determining part quality will be selected.

8.2 Measurement Equipment and Methods

Two pieces of measurement equipment were used to inspect embossed parts. These were a traditional optical microscope and a surface scanning interferometer. The interferometer was used for depth, width and surface roughness measurements and the microscope was used to inspect the radius and draft of channel cross-sections. The merits of each piece of equipment and the methods used for each will be discussed in this section.

To take depth, width and height measurements, a piece of equipment capable of measuring features as small as 10 microns in height and as large as several millimeters was needed. Additionally, surface roughness will be taken as a measure of quality and thus the measurement instrument had to be able to resolve nanometer variations in a surface. A Bruker Interferometer (*ContourGT Inmotion 3D optical microscope)* was chosen to take

surface measurements of both the molding tool and the embossed parts. This instrument is specified by the manufacturer to be capable of measuring features from 0.1nm to 10mm in height, with sub nanometer vertical resolution.

Interferometry is limited in its ability to make measurements around vertical sidewalls. Because of this limitation, it is not an ideal measurement process for determining wall draft or edge radius. To take these measurements, PDMS replication of the part to be measured combined with traditional optical microscopy were used. The basic procedure being to make a cast of the part of interest with a soft silicone that can be easily be cut into cross-sections. These silicone cross-sections were then be imaged and measured with a calibrated optical microscope.

8.2.1 Interferometry Background

Interferometry is a measurement technique that takes advantage of interference patterns to superimposed light waves to produce information about these two waves. The general process of an interferometry measurement is first to divide a source beam into two beams using a partially reflective mirror. One of these beams is used as a reference beam; the other is used for measurement. The two beams travel along different paths before being recombined. The recombination of the beam creates an interference pattern that is a result of the two beams now being out of phase. By measuring the interference pattern, the phase shift of the measurement beam can be determined. This phase shift is a result of the measurement beam traveling along a longer path than the reference beam, and thus is indicative of how much further the measurement beam traveled than the reference beam. This difference in path distance is the measurement of the distance the measured surface is from the focal plane of the microscope.

The Interferometer used outputs a contour plot of everything in the measurement window. The time taken to perform this measurement depends on the total area to be measured as well as the range of depths to be scanned. Generally, this instrument performs a rapid quantitative measurement of the object of interest and is thus an effective tool for this application.

This measurement instrument does have some limitations. There are occasionally black regions on the finished scan that represent areas where data was lost. This occurs when the measurement beam is reflected from the object of interest such that it is not directed back at the lens of the instrument. Vertical sidewalls and highly varied topography commonly cause this loss of information. This limitation of interferometry means that the instrument is not ideal for measuring draft on a wall, or edge radii. Another point to note is that frequently parts measured produce a contour with a constant tilt. Tilt is compensated for within the measurement software.

8.2.2 PDMS Casting and Optical Microscopy

In order to view the cross section of an embossed channel and take edge radius and draft measurements, a casting technique combined with optical microscopy was used. The first step in taking this measurement was to take a PDMS casting of the part to be measured.

The PDMS used was a commercially available silicone produced by Dow Corning (184 Slygard Silicone). This PDMS was chosen because it has been shown as a suitable method to accurately replicate micro and nano-scale features down to 50nm [37]. It comes as a two-part resin and hardener set. The resin was mixed 10 parts to 1 by weight with the hardener and stirred in a weigh boat for 90 seconds. The fully mixed PDMS was then poured over the part to be replicated and both were then placed in a vacuum chamber for degassing. The vacuum chamber was set to 25inHg of vacuum. After 3 hours of degassing, the PDMS was cured in an oven set to 50 C for 2 hours. This curing temperature was chosen as it minimizes the shrinkage of the final PDMS part to roughly 1% [38]. Once the PDMS is cured, it was removed from the part and cut into cross sections. The PDMS cross-sections were measured with a Nikon Eclipse Ti - SR optical microscope.

It is also possible to inspect the cross-sections of embossed parts by breaking them across the channel. Parts inspected this way were first scored and then chilled prior to

breaking to ensure a clean fracture. This technique destroys the inspected part, and is not suitable for inspection of the molding tool's geometry.

8.3 Measurement Procedure and Data Processing

8.3.1 Interferometer Measurement Procedure

The first step in evaluation was a qualitative visual inspection of the tool and embossed parts. This inspection was for any obvious defects or damage. Figure 37 below shows an example of such a defect. This is damage on a micro machined aluminum tool. If such a defect were observed on a tool, the tool was retired. Defects like this on a part would cause the part to be rejected outright.

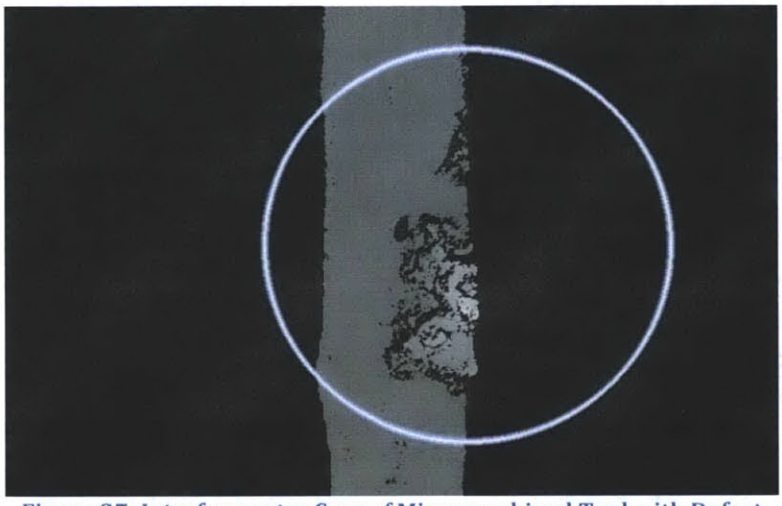

Figure 37: Interferometer Scan of Micro machined Tool with Defect

Following visual inspection, the part or tool was placed on the interferometer stage and the area to be inspected was scanned. All parts had 3 locating holes embossed into the back of the part. These three holes are aligned with pins on a fixture attached to the interferometer stage. These alignment pins are seen in Figure 38. A part loaded onto the measurement fixture is seen in Figure 39.

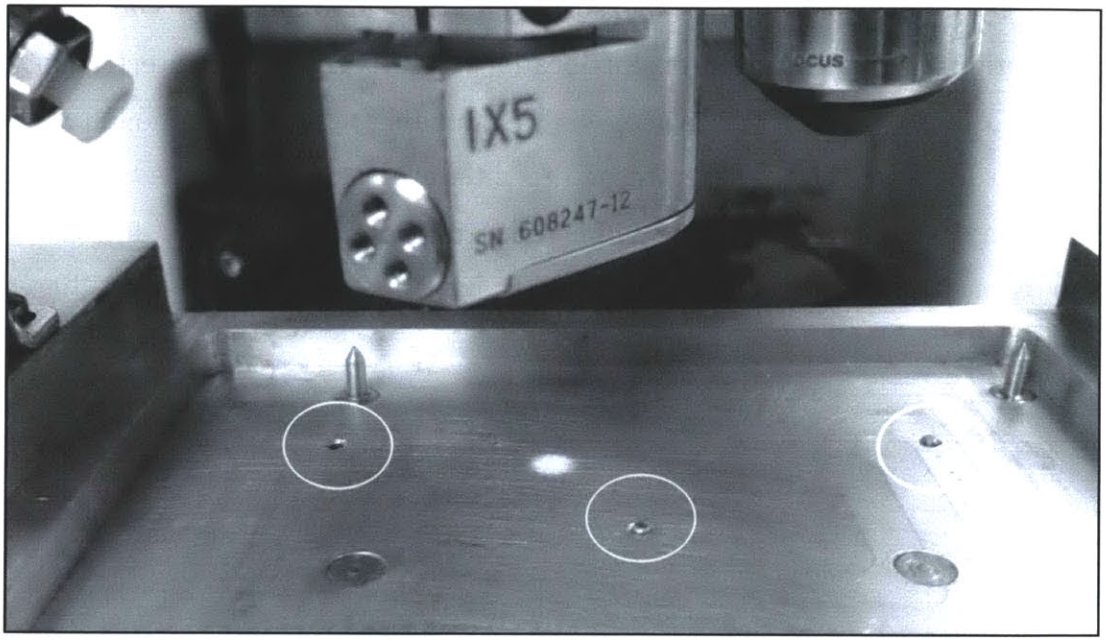

Figure 38: Fixture on Interferometer Bed. Alignment Pins are circled

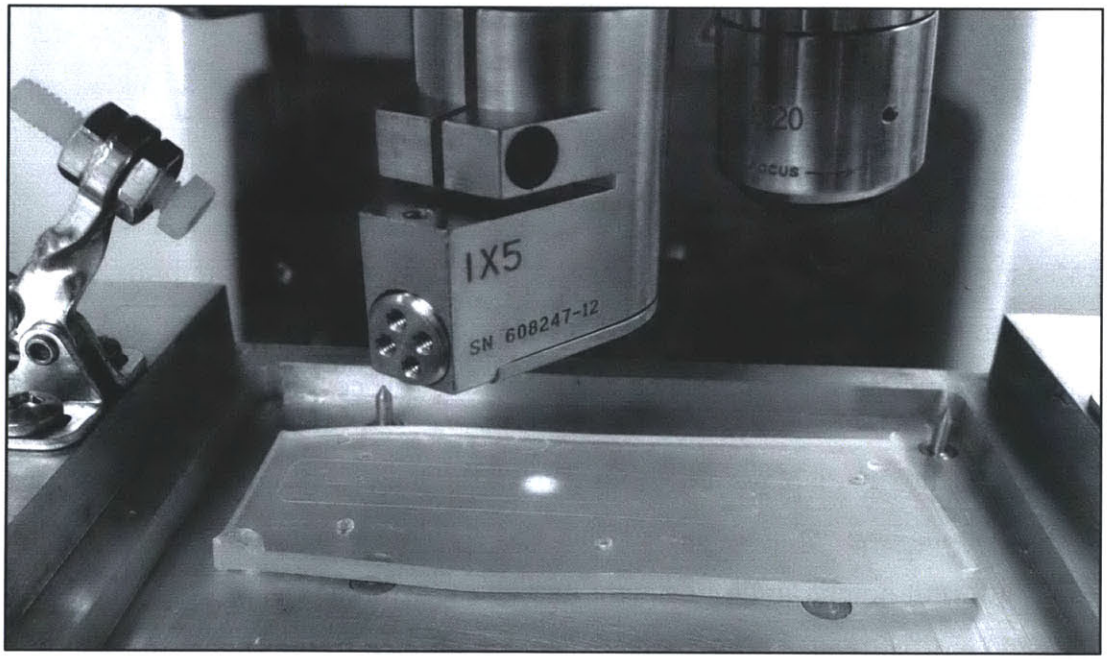

Figure 39: Measurement Fixture with Part Loaded

Scanning location was constant between parts and tools. Consistency of measurement location ensured that when the measurements of parts were compared any differences observed were attributable to differences in part geometry and not variation

introduced by differing location of measurement. The embossing tool was scratched at several locations to mark measurement locations. The stage of the interferometer was aligned with these reference marks as seen in Figure 40. The image on the left is the view seen by the operator. The crosshairs of the interferometer are aligned such that the horizontal line is collinear with the upper edge of the channel ridge, and the vertical crosshair is on the left edge of the alignment mark. The image on the right displays the resultant scan.

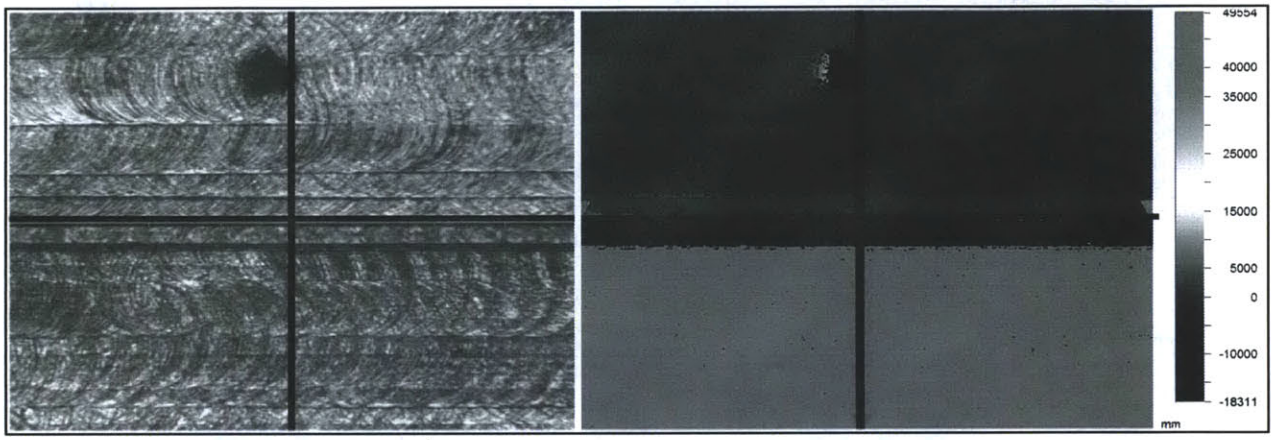

Figure 40: Alignment of Interferometer for Scan

8.3.2 Interferometer Data Processing

Measurements were obtained from the surface scan by two methods. One method was to use the built in data processing features of the Interferometer software, Vision-64. The second method was to export raw data for external processing.

Figure 41 below displays a contour plot of the height data produced from a scan at one location along the channel edge. The three colored regions correspond to three features of different height. Average height data of these 3 regions is obtained directly from the interferometer software. First, three masks are applied to the raw data to separate the height data of these three regions. Figure 42 displays the raw data in Figure 41 separated into three sets of data. Once separated, the heights of all the points in each region are averaged together to obtain a singular height value for the region.

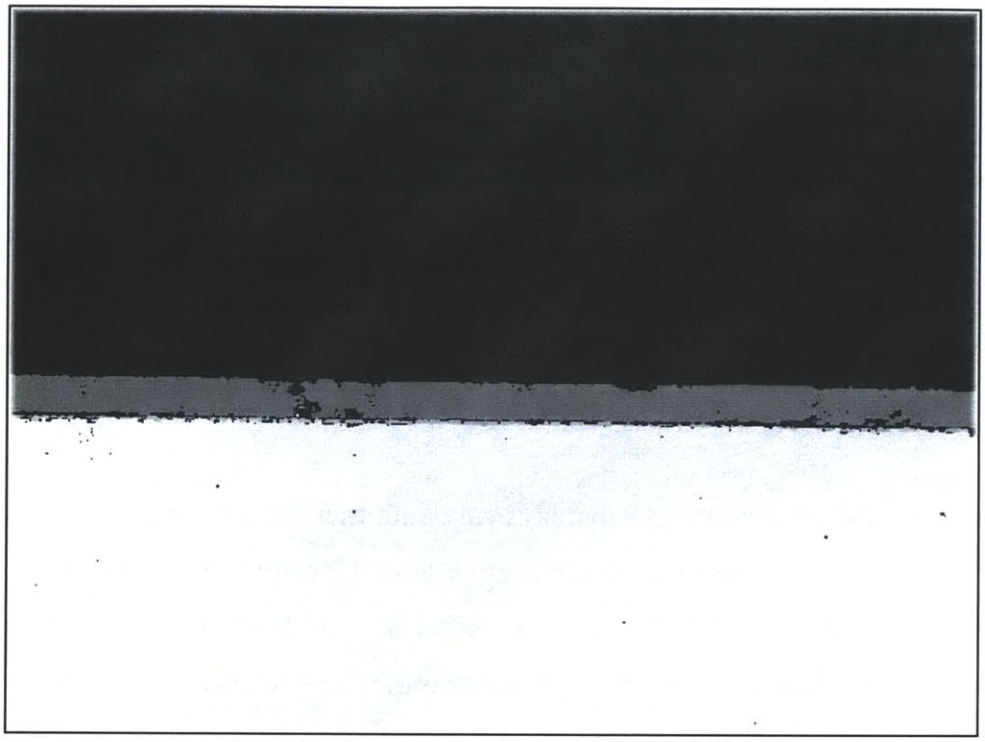

Figure 41: Contour plot of scanned channel edge

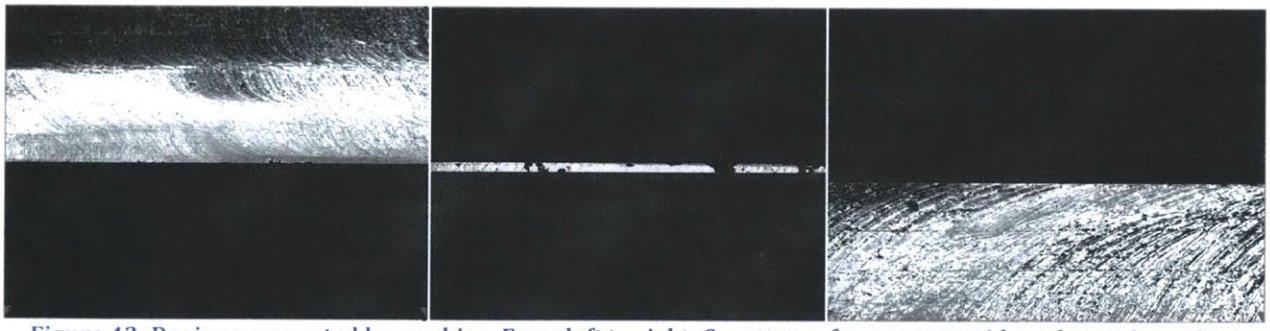

Figure 42: Regions separated by masking. From left to right: Cuvette surface, cuvette ridge, electrode surface

To calculate surface roughness, first the raw data must be filtered to include only height variation due to surface roughness. Figure 43 below displays 3-dimensional scan data of the bottom of an embossed channel. This raw data has not been corrected for "waviness" and thus a surface roughness calculation taken from this raw data would over-estimate the value. Figure 44 below shows cross-sectional data taken from the raw scan data. Curvature is visible in this data. To get an accurate measurement of surface roughness, this raw data must be flattened to remove height variation caused by this gross surface distortion.

The raw data is filtered using a Gaussian regression filter that is built in to the Vision 64 software. When using this filter two cut-off frequencies must be specified, a high and low frequency. Filtering low frequencies removes data that is attributed to large-scale variation in part geometry, such as warping. The wavelength of the low cut-off frequency is dictated by ISO standard 4288 [39]. This standard gives a cut off wavelength to be used for different ranges of expected surface roughness. In Daktari's case, they are expecting a surface roughness between 100 nm and 2 microns; therefore a cut off wavelength of 800 microns will be used.

The right image in Figure 43 displays raw data that has been filtered to only include the surface roughness component of the scan. Figure 45 shows cross sectional data taken from this filtered data. Notice that the data is now flat and fluctuates around a value close to 0. The mean for this data is calculated to determine the true location of the surface. This mean height is denoted by $\bar{y}$ in the below equation. Surface roughness, R_a, is then calculated by averaging the deviations of each height measurement from the mean height. The below equation was used to perform this calculation.

$$R_a = \frac{1}{N}\sum_{i=1}^{N}|y_i - \bar{y}| \tag{2}$$

This calculation was done within the interferometer software and uses all data points in the scan window to calculate surface roughness.

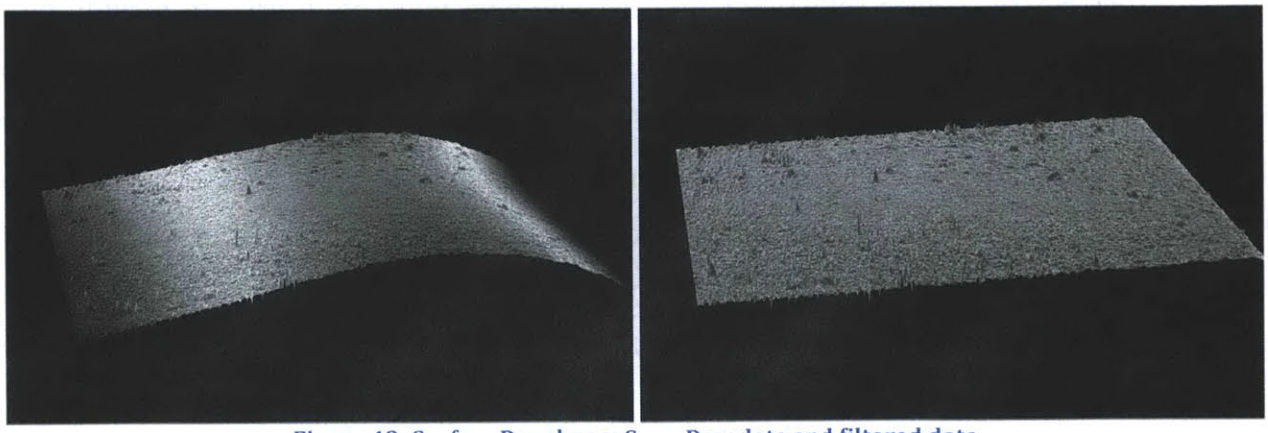

Figure 43: Surface Roughness Scan. Raw data and filtered data

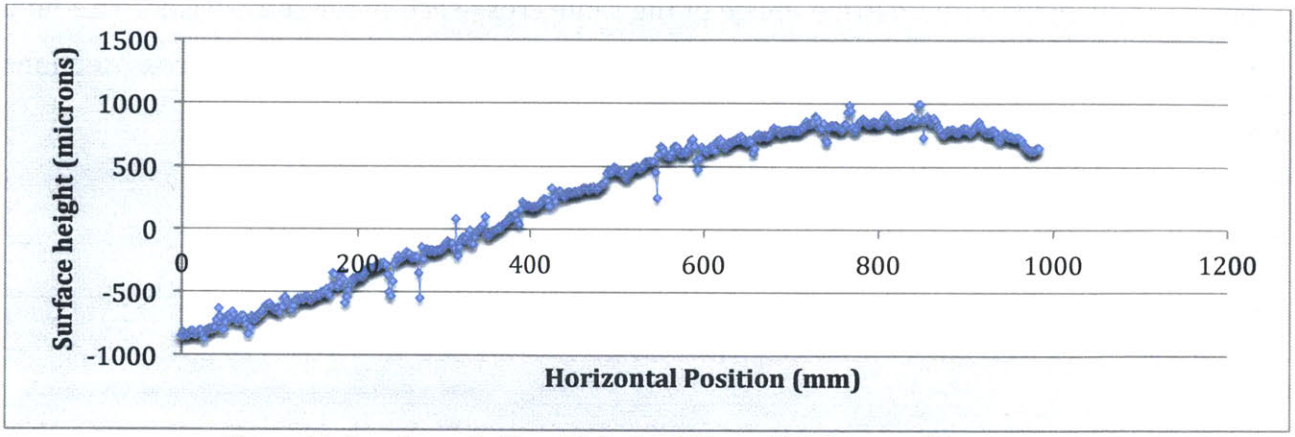

Figure 44: Raw Cross-Sectional Data Exhibiting a High Degree of Curvature

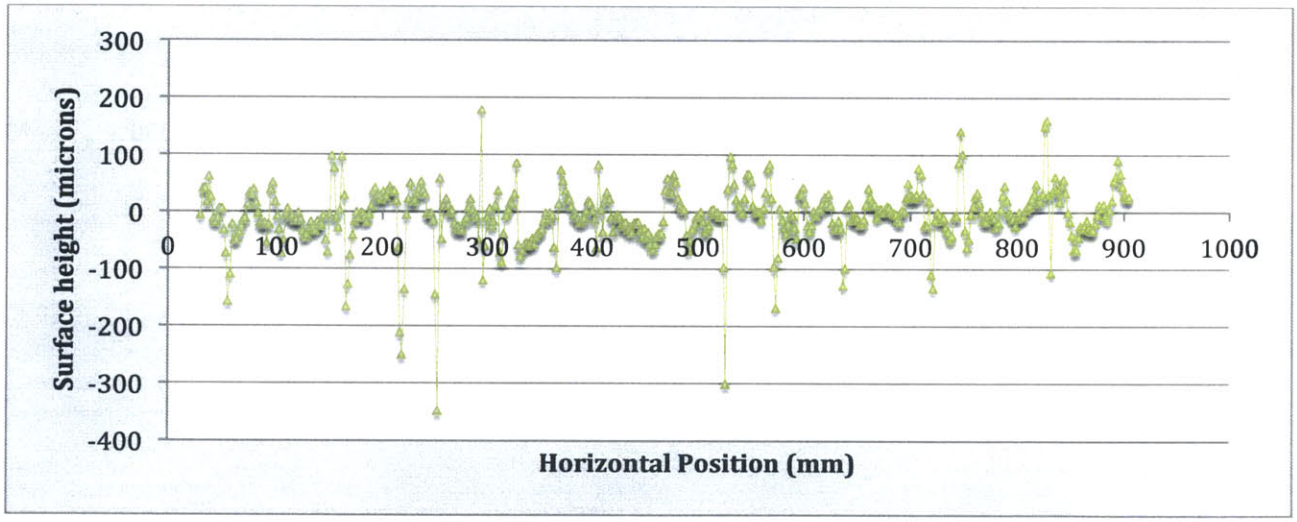

Figure 45: Filtered Surface Roughness Data

8.3.3 Processing Cross-sectional Interferometer Data

An alternative measurement method is to export the cross sectional data from the instrument software for processing. Figure 46 below displays a plot of the output point data along a scanned channel cross section. A Matlab script was developed to process this raw cross-sectional data (See Appendix B: Matlab). The script first identifies the location of the two edges. These are the transition from the bottom of the channel to the top of the ridge, and the transition from the top of the ridge to the surrounding area. The width of the ridge is estimated as the distance between the first and last data points on the top of the ridge. The heights of the three regions (the channel bottom, the top of the ridge, and the

exterior surface) are calculated by averaging all the data points that reside in these three regions. A plot of a channel represented by the averaging of this data is seen in Figure 47. Figure 48 displays a microscope image of the same cross-section for comparison. The final values for ridge width, ridge height and channel depth are averages of 5 cross sections taken from the same scan data.

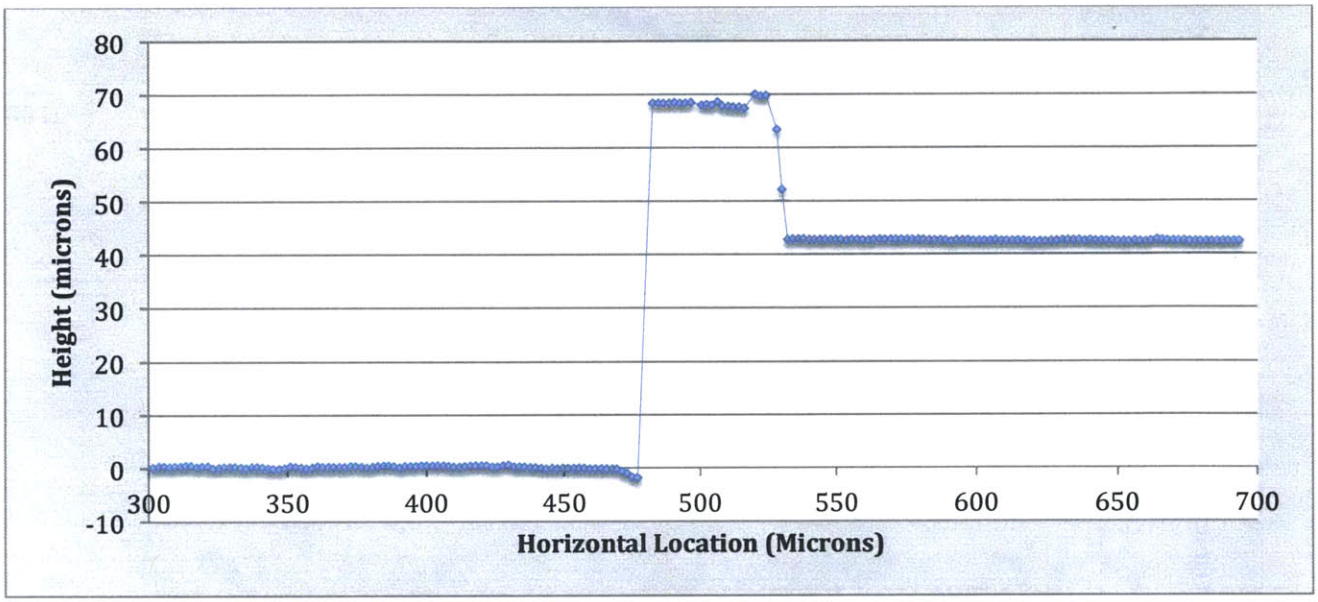

Figure 46: Channel Cross-Section Output Data

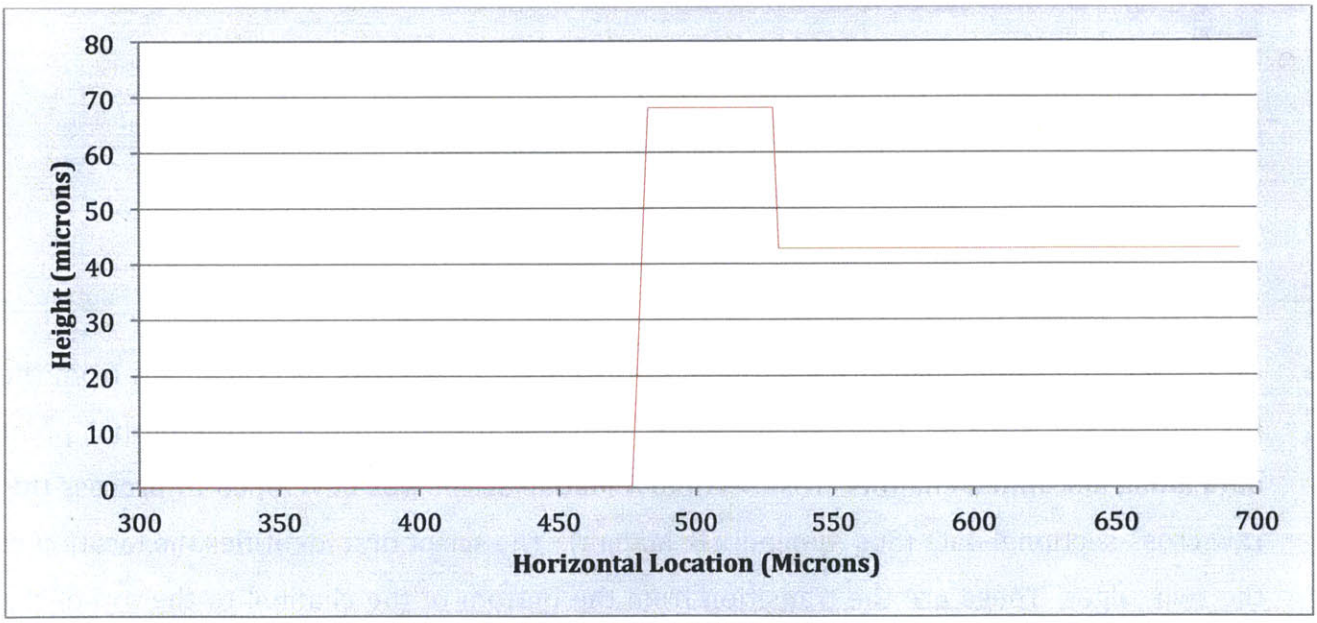

Figure 47: Channel Cross-Section Averaged

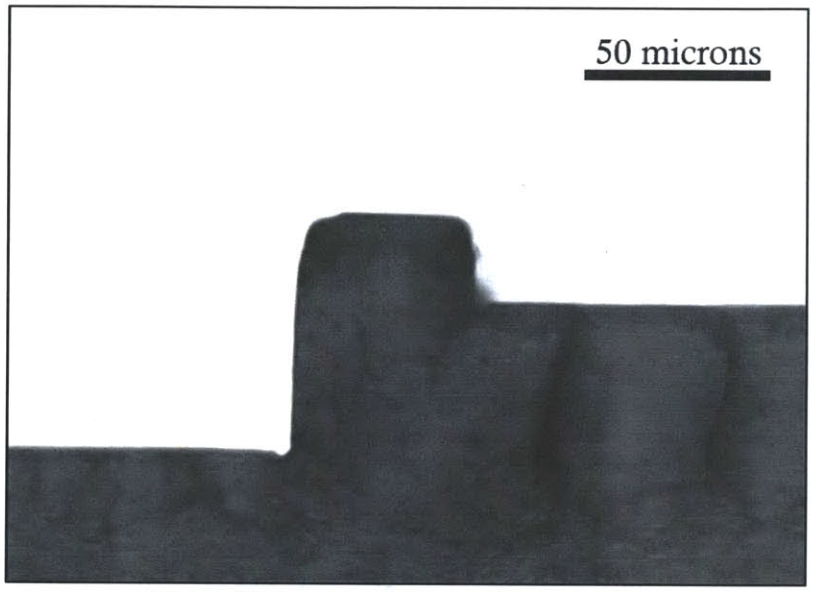

Figure 48: Microscope Image of Cross section

8.3.4 Microscope Measurement Procedure

Cross-sectioned PDMS casts of parts or broken embossed parts were photographed with a 40X optic to inspect the edges of the channels. Figure 50 below displays an image of the edge of the channel profile. The microscope software, NIS – Elements BR, allows for direct measurement after proper calibration. The resolution of this measurement software is 320nm per pixel.

Several measurement tools were utilized in the software. For measuring distance, a point-to-point measurement tool was used. This tool requires the operator to click the bottom and top edges of a channel to take a depth measurement. To measure the radius of the edge at a channel bottom, a circle must be placed at the corner of interest such that it is tangent to the bottom surface of the channel and the channel's sidewall. The software then outputs the radius of this circle. Figure 49 shows a pair of radius measurements taken from an embossed part.

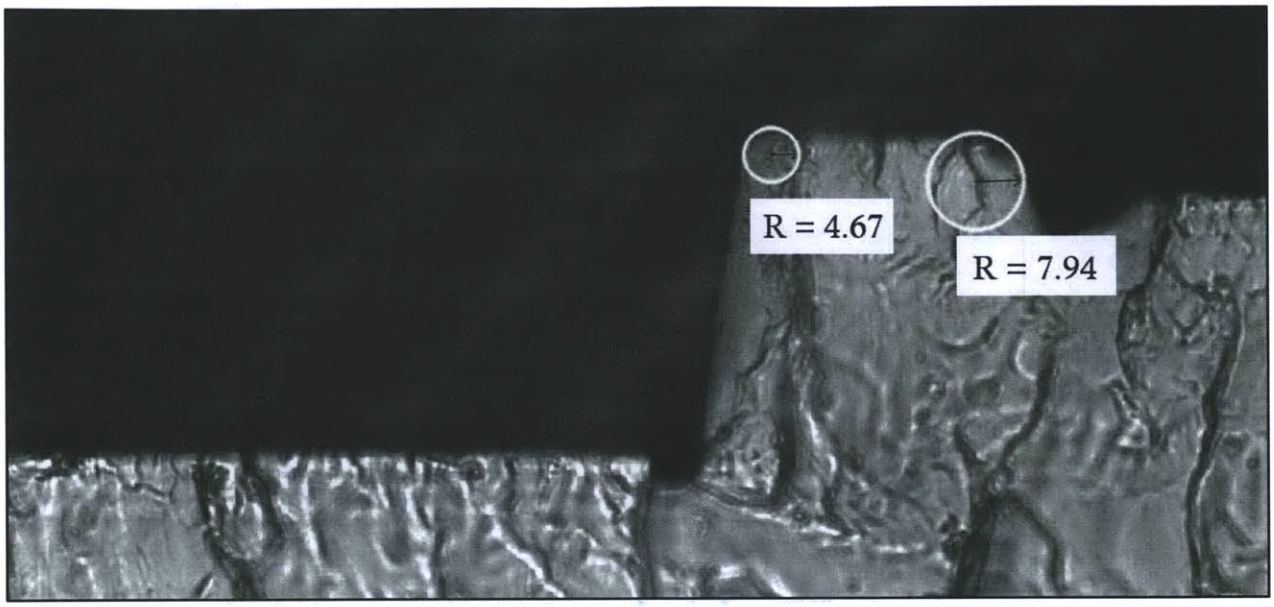

Figure 49: Measuring Radius of an Embossed Part (Magnification is 40X)

To measure taper two lines must be drawn, one collinear with the wall of interest and another that is parallel with the plane that would represent a perfectly vertical wall. The angle between these two lines is then taken as the draft of the wall. Each of these measurement tools requires the operator to choose the start point and end point of the measurement; therefore the major limitation of this method is that it introduces a lot of user error. This measurement method was reserved for dimensions that could not be reliably measured on the interferometer.

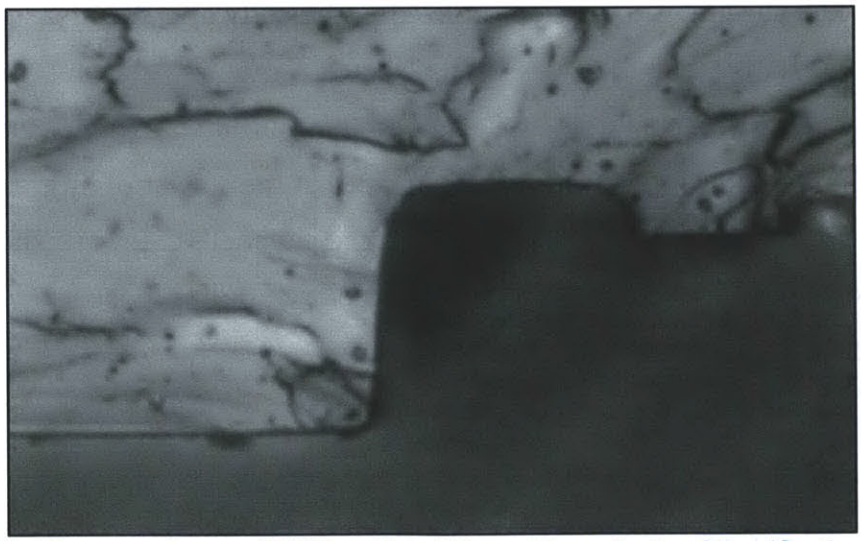

Figure 50: Microscope Image of PDMS casting of Channel Cross-Section (Magnification is 40X)

8.4 Evaluation of Measurement Methods

A gage R&R study is commonly used to evaluate the capability of a measurement system. Total variability of a measured part can be broken down into variability introduced by measurement and part-to-part variability, as seen in equation 3.

$$\sigma_{Total}^2 = \sigma_{part}^2 + \sigma_{Gage}^2 \tag{3}$$

The goal of a gage R&R study is to determine how much of the observed variability is attributable to measurement error. This determination is necessary to assess the capability of the measurement system to make the measurement of interest. This section will detail the statistical procedure employed to perform this study.

8.4.1 Gage R&R

The precision of the measurement method can be decomposed into two terms. These are repeatability and reproducibility, as seen below.

$$\sigma_{Gage}^2 = \sigma_{Repeatability}^2 + \sigma_{Reproducibility}^2 \tag{4}$$

Repeatability is defined as the measurement variability that is present during subsequent measurements of the same sample under the same measurement conditions. The measurement conditions include having the same operator perform a measurement of the same sample at the same location using the same measurement equipment with the same procedure as the previous measurement. Reproducibility is the measurement variability that is introduced when a measurement is performed under differing conditions. These conditions may include different operators or different measurement equipment.

Performing an experiment that contains multiple operators taking multiple measurements of a set of sample parts, and then performing a random effects model analysis of variance can obtain estimates of the repeatability and reproducibility variance. For this study, 10 parts will be measured for each dimension of interest. These samples will

be produced with the same operating parameters and will be selected so that the full range of the measured dimension's variability is seen in the study. Each sample will have its dimensions measured by two operators two times. The order of these measurements will be randomized in order to minimize the effect of any noise factors on the study. See Appendix B: Order of Measurements for the run order. The decomposition of total variability was calculated using Minitab following data acquisition.

8.4.2 Precision to Tolerance Ratio

The precision to tolerance ratio is a measure of the overall capability of the measurement system. This ratio is calculated by dividing the estimate of variability introduced by the gage to the tolerance band of the measurement. The equation below displays the equation used to calculate the precision to tolerance ratio. K is commonly set to 5.15 to represent a confidence interval for 99% of all measurements.

$$P/T = \frac{k\hat{\sigma}_{Guage}}{USL - LSL} \tag{5}$$

The lower the precision to tolerance ratio, the more capable the measurement system is for measuring the dimension of interest. Generally, a P/T ratio of less than 0.1 is desirable and a P/T ratio of up to 0.3 is acceptable. This ratio will be calculated for the measurement methods used for each critical dimension of the hot embossed part to determine the effectiveness of the method.

9 Measurement Results

9.1 Overview

This chapter will summarize the results of the gage repeatability and reproducibility studies performed for each measurement method described in the previous chapter. For each measurement method, the width of the tolerance band for the specification of this feature is listed along with the estimate of gage variance, the components of gage variance attributable to repeatability error and reproducibility error, the precision of the measurement method and the precision to tolerance ratio. Precision here is defined as 5.15 times the square root of total gage variance. This value is the 99% confidence interval for measurements taken. Recall that a P/T ratio of 0.10 is preferable, while values of up to 0.30 are acceptable. Table 5 contains the findings for all the studies.

In summary, the measurement methods utilizing PDMS casting and optical microscopy were too imprecise to be useful quantitative metrics of quality. The two measurement methods that are most capable are the ridge height and width measurements. The results for each measurement will be discussed in detail in the subsequent sections. Following discussion of each measurement method, a proposal will be made for the best metric to be used as a response variable for the DOE study.

Table 5: Summary of Gage RR Results

	Channel Depth	Ridge Height	Ridge Width	Cuvette Width	Surface Roughness	Radius	Channel Draft
Tolerance Band	2.00	2.00	10.00	20.00	N/A	6.00	2.00
Units	Micron	Micron	Micron	Micron	Nanometer	Micron	Degree
Gage Variance							
Total	0.1228	0.0292	0.4187	8.9237	57.7034	1.6850	4.2344
Repeatability	0.1106	0.0162	0.4187	5.4495	13.6782	0.3417	0.6242
Reproducibility	0.0121	0.0130	0.0000	3.4742	44.0252	1.3433	3.6102
Precision	1.80	0.88	3.33	15.38	39.12	6.69	10.60
Precision/ Tolerance	0.9022	0.4399	0.3333	0.7692	N/A	1.1142	5.2988

9.2 Measuring Channel Depth and Ridge Height

Both channel depth and ridge height measurements were taken on the Bruker interferometer using methods described in the previous chapter. These two measurement methods were found to have gage variances that are higher than ideal. However, the ridge height measurement method has a precision to tolerance ratio that is close to acceptable. Table 6 summarizes the results of the gage RR study for these two dimensions.

Table 6: Gage RR results for the Channel Depth Measurement and Ridge Height Measurement

	Channel Depth	Ridge Height
Tolerance Band	2.00	2.00
Units	Microns	Microns
Gage Variance		
Total	0.1228	0.0292
Repeatability	0.1106	0.0162
Reproducibility	0.0121	0.0130
Precision	1.80	0.88
Precision/Tolerance	0.90	0.44

Both of these methods have a small portion of error contributed by reproducibility variability. This means that the method is somewhat immune to changes in operator, and that the main source of variation in measurement is the equipment used. Figure 51 and Figure 52 plot the average measurements of each operator for the ridge height and channel depth measurements over the 10 sample parts. These plots show the consistency of measurements between operators.

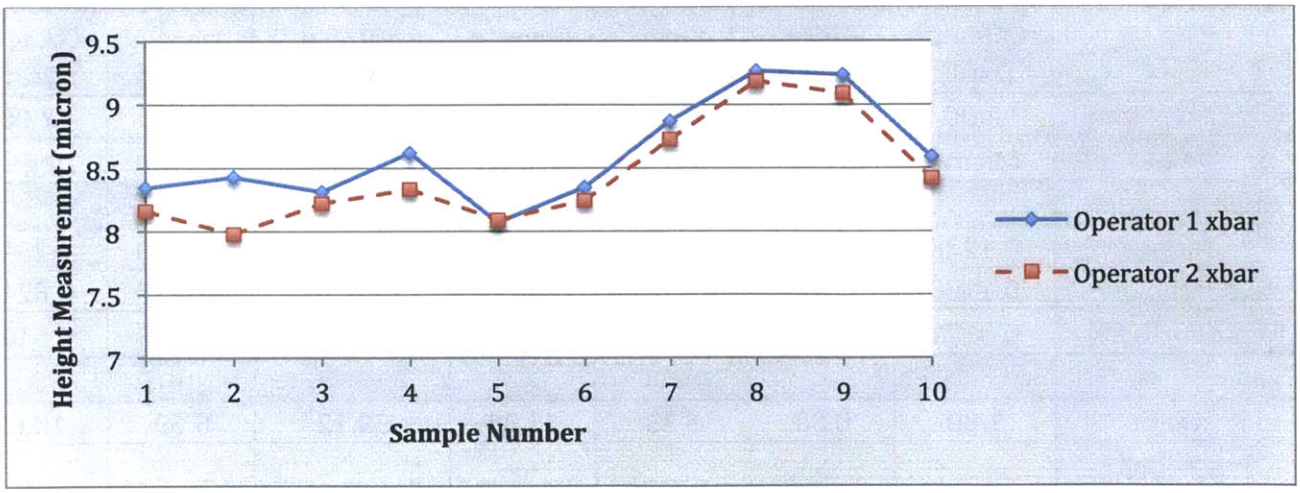

Figure 51: Averages of Ridge Height Measurements for Operators 1 and 2

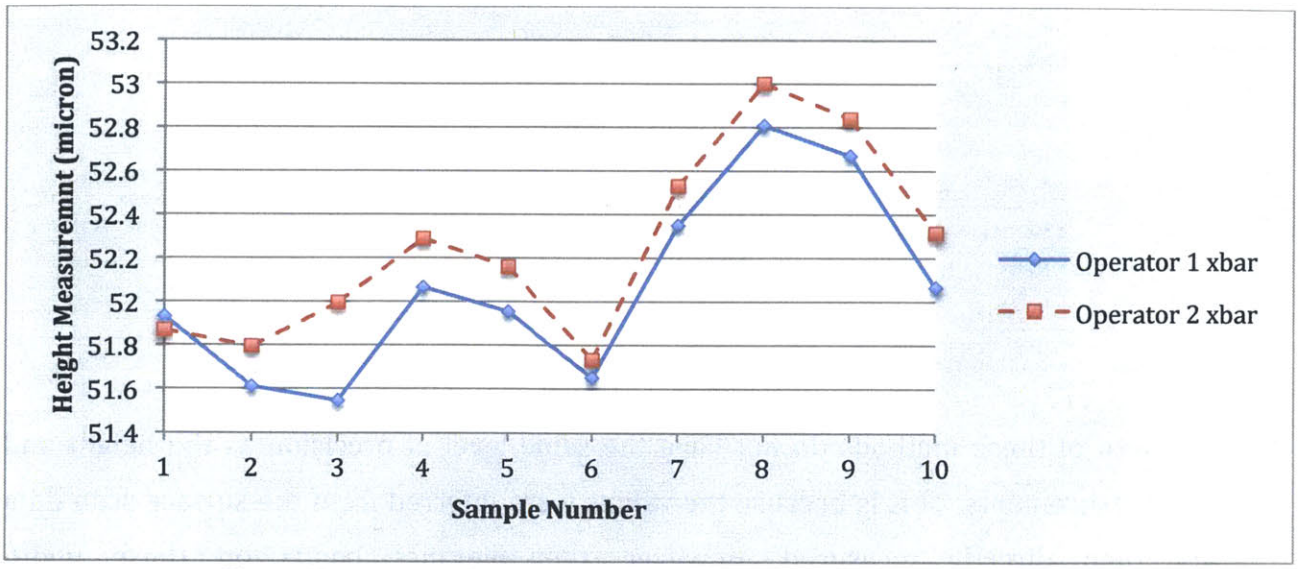

Figure 52: Averages of Channel Depth Measurements for Operators 1 and 2

The precision of the channel depth measurement method was 1.80 microns and the precision of the ridge height measurement method was 0.88 microns. When compared to the tight tolerance bands of 2 microns for both dimensions, these methods are not ideal for discriminating small variations between embossed parts. The small variance component attributed to reproducibility shows that the measurement equipment being used may be limiting the measurement precision found for the channel depth and ridge height measurement methods. Ideally, a more precision piece of measurement equipment would be used to inspect parts with such tight tolerances.

9.3 Measuring Ridge and Channel Width

The width of the ridge was not directly measured on the Interferometer, but was instead estimated from cross sectional scan data as the horizontal distance between the first and last data points of the top of the ridge. Similarly, channel width was estimated as a distance between the first and last points scanned on the bottom of the channel. A summary of the results of the two gage RR studies for these width measurements is presented in Table 7.

Table 7: Gage RR Results for the Ridge Width and Channel Width Measurements

	Ridge Width	Channel Width
Tolerance Band	10.00	20.00
Units	Microns	Microns
Gage Variance		
Total	0.4187	8.9237
Repeatability	0.4187	5.4495
Reproducibility	0.0000	3.4742
Precision	3.33	15.38
Precision/Tolerance	0.33	0.77

Both of these methods do not have the same level of precision as the height and depth measurements. This is because the values were inferred from the surface scan data rather than directly measured. However, the tolerance bands on these width measurements are considerably wider than the tolerance bands on the height and depth measurements. The tolerance band on the ridge width is 10 microns wide, and the tolerance band on the channel width measurement is 20 microns. The precision of the ridge width measurement is 3.33 microns, resulting in a precision to tolerance ratio of 0.33. This ratio is just over the acceptable limit. The ridge width measurement procedure is not ideal for discriminating between conforming and non-conforming parts, but is almost at an acceptable level of capability. The precision of the channel width measurement was found to be 15.38 microns. This measurement method has a precision to tolerance ratio of 0.77.

Higher precision for both of these measurements is desirable. It may be possible to increase the repeatability of these measurements by averaging a greater number of cross sections together when calculating width. This would make the measurement procedure less sensitive to variations introduced by cross section selection.

9.4 Measuring Radius and Draft

The measurement methods for channel radius and draft both were found to have a high amount of gage variance. A summary of the gage RR study results is presented in Table 8. It is important to note that for both dimensions, most of the variability in measurement is a result of operator-to-operator variation. The error in repeatability only accounts for

about 20% of the total gage variance when measuring radius, and about 14 % for the draft measurement.

Table 8: Gage RR results for the Radius Measurement and Draft Measurement

	Radius	Draft
Tolerance Band	6.00	2.00
Units	Microns	Degrees
Gage Variance		
Total	1.6850	4.2344
Repeatability	0.3417	0.6242
Reproducibility	1.3433	3.6102
Precision	6.69	10.60
Precision/Tolerance	1.11	5.30

The consistency of measurement for a single operator can be seen in Figure 53 and Figure 54. These two plots display the replicate measurements for radius of parts 1 through 10 for operators 1 and 2 respectively. Notice that sample-to-sample, both operators tend to make a pair of measurements that are of similar values.

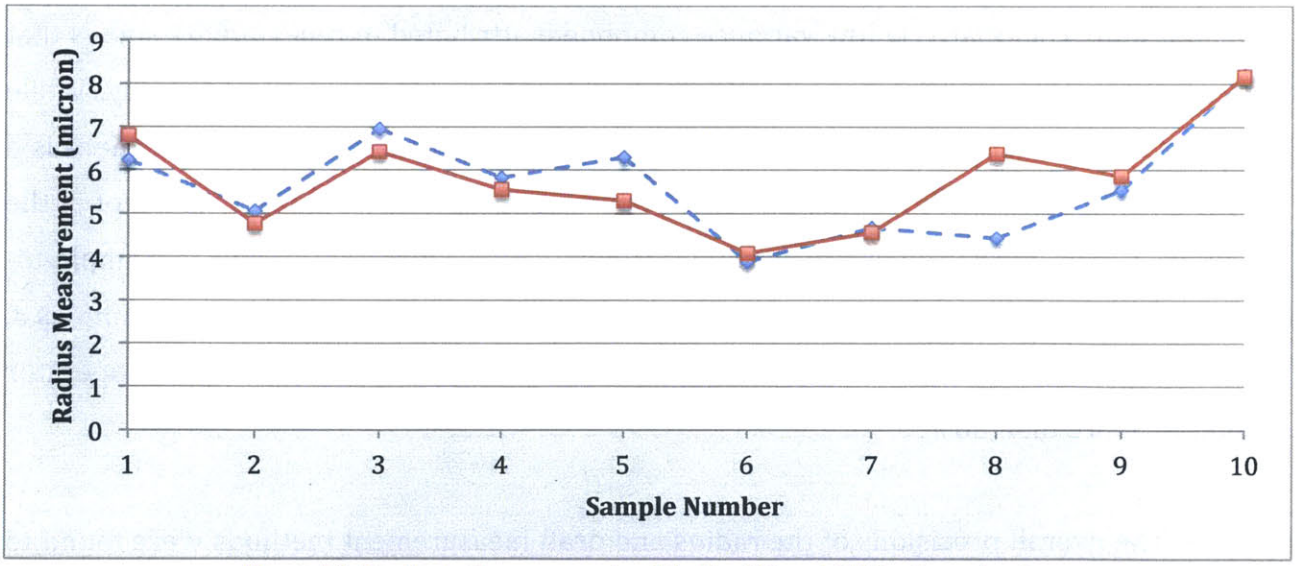

Figure 53: Replicate Measurements of Radius M1 and M2 for Operator 1

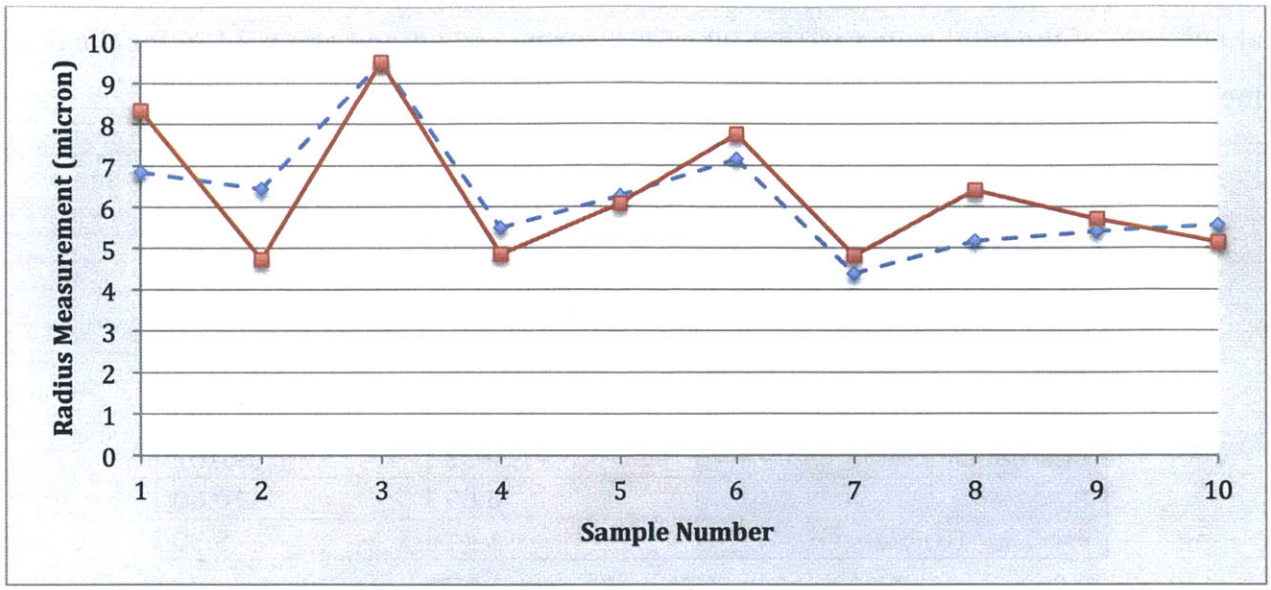

Figure 54: Replicate Measurements of Radius M1 and M2 for Operator 2

Both radius and draft measurements were taken on the Nikon Eclipse Ti - SR optical microscope with the NIS – Elements BR software package. This measurement procedure required operators to define the radius on a cross sectioned part by a circle drawn on a captured image. Similarly draft was measured as the angle between two edges identified by the operator. The relatively low variance component attributed to repeatability shows that operators have a tendency to make these two measurements in a consistent way. While there is some consistency of measurements part-to-part for the same operator, there is a large amount of variability in measurement operator-to-operator. Figure 55 is a plot of the average radius measurement of parts 1 through 10 for operators 1 and 2. Sample-to-sample there is not a lot of measurement agreement between the two operators. Samples 3, 6 and 10 are examples of measured samples where the reported values of each operator differ by more than 30%.

The overall precisions of the radius and draft measurement methods were found to be 6.69 microns and 10.60 degrees respectively. Compared to the tolerance band on the radius value of 6 microns, and the tolerance band on draft of 2 degrees, both of these measurement methods are too imprecise to be effective, having P/T ratios above 1. Neither of these dimensions will be chosen as the response variable for the DOE. However, they will still be used as qualitative tools to inspect embossed parts, and understand how the

process is affecting part formation. If necessary to take radius measurements for comparative analysis between parts, it is recommended that only one operator be used to take the measurements. By eliminating operator induced variability, the precision of this measurement method can be increased roughly two-fold.

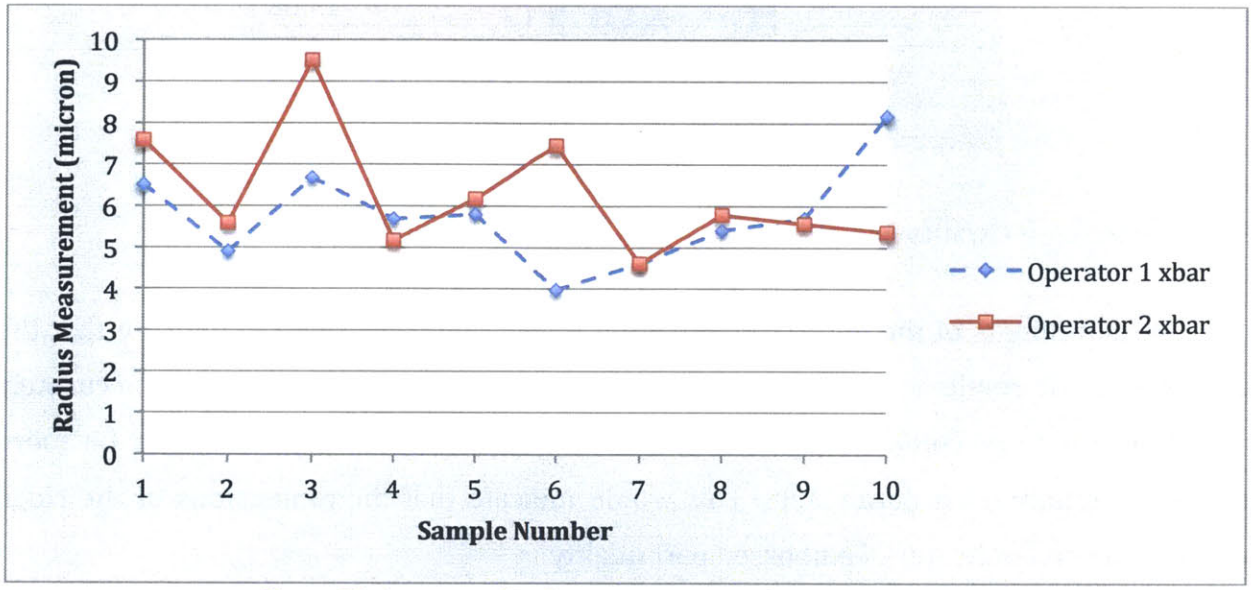

Figure 55: Averages of Radius Measurements for Operators 1 and 2

9.5 Measuring Surface Roughness

Daktari does not currently have a specified tolerance on the surface roughness of the bottom surface of the channel. Therefore no precision to tolerance ratio is reported for this measurement method. Additionally, this measurement will not be selected as a response variable for DOE optimization. The embossed parts tend to replicate the surface roughness of the embossing tool regardless of embossing parameters selected, and so it is not a good indicator of the effect of parameter variation on part quality.

Despite these facts, it is necessary to be able to characterize the surface roughness of embossed parts. Table 9 summarizes the results of the gage RR study performed for surface roughness measurements. The precision of this measurement method was found to be 39 nanometers.

Table 9: Gage RR results for Surface Roughness Measurements

	Surface Roughness
Tolerance Band	N/A
Units	Nanometers
Gage Variance	
Total	57.70
Repeatability	13.68
Reproducibility	44.03
Precision	39.12
Precision/Tolerance	N/A

9.6 Selecting a Quality Metric

Measurements of the initial rounds of hot embossing trials seem to indicate that the embossed parts replicate the channel depth and width dimensions of the mold accurately in a wide range of embossing parameters. In comparison, the ridge tends to be more sensitive to embossing parameters. This would indicate that the dimensions of the ridge would be a good indicator of embossed part quality.

Ideally, the quality of this ridge could be fully measured as its height, width, edge radii and draft. However, the results of the gage RR study for the radius and draft measurement procedures conclude that these measurement methods are not capable of characterizing the radius or draft with the desired precision. The two measurement methods with the highest precision to tolerance ratio were ridge width and ridge height. These two measurements should be used in conjunction to approximate the filling of the ridge.

The measured ridge width and ridge height of embossed parts can be directly compared to the measurements of these dimensions taken on the molding tool. A higher quality embossed part is defined as a part that has ridge height and width dimensions that closely match the dimensions of the embossing tool. A perfectly formed part would have ridge height and width measurements that are identical to these dimensions on the tool. For each embossed part, two ratios will be calculated. These are the ratio of the embossed part's ridge height to the tool's ridge height, and the ratio of the embossed part's ridge

width to the ridge width of the tool. These two ratios should then be multiplied together to get a single metric that estimates the total formation of the ridge.

This metric will underestimate the actual filling of the ridge. This is because the ridge width that is measured on embossed parts will be equal to only the width of the surface of the ridge that is perpendicular to the interferometer head. Regions that lie within the radiused portion of the ridge are not read by the interferometer and will appear as missing data on the resultant surface scan. Figure 56 depicts the interferometer contour scan and a microscope image of the cross-section of a part that had accurate ridge formation. On the microscope image, the boxed portion of the ridge is the area of the ridge that is perpendicular to the interferometer head and is the only portion of the ridge that will be picked up by the interferometer. On the interferometer contour scan the white band is the portion of data that corresponds to the top of this ridge and the black bands on either side are areas of missing data that correspond to the radiused portion of the ridge.

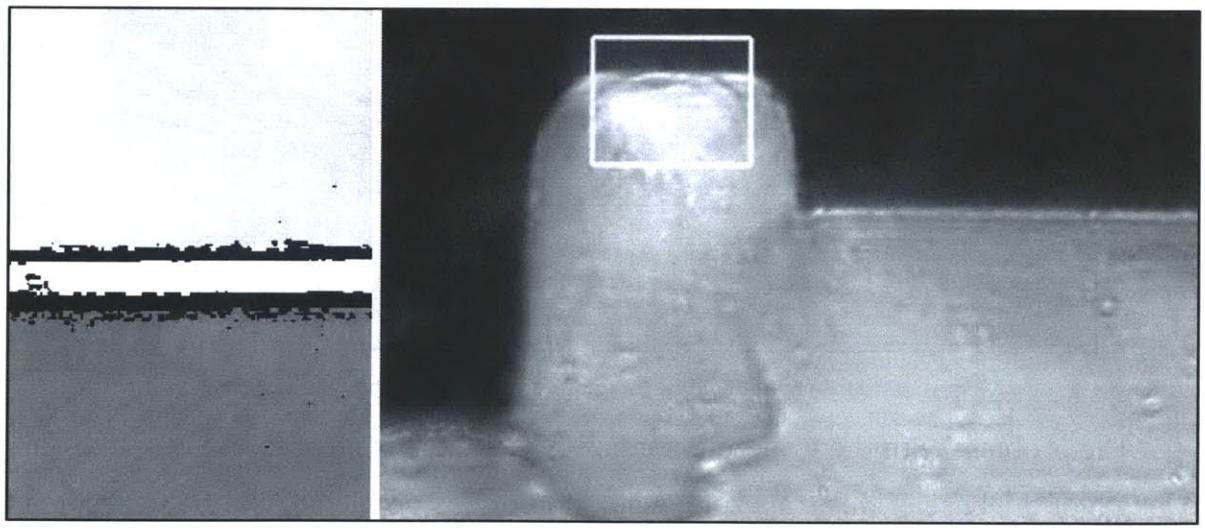

Figure 56: Ridge with Good Formation. Interferometer Scan and Microscope Image

Figure 57 depicts a part with poor ridge formation. The edge radii are much larger on this part and so the interferometer scan has a larger region of missing surface data. The corresponding ridge width for this part is small compared to the part shown in Figure 56.

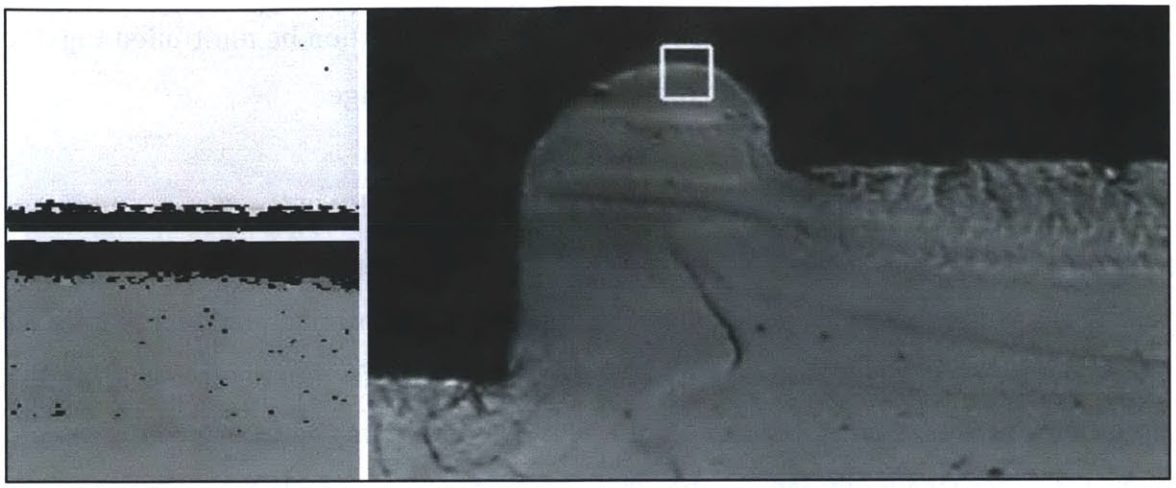

Figure 57: Ridge with Poor Formation. Interferometer Scan and Microscope Image

A method that could be used to more accurately estimate the total filling of the ridge would be to approximate the ridge as a trapezoid rather than a rectangle. Figure 58 depicts how each area approximation would represent that area of the ridge.

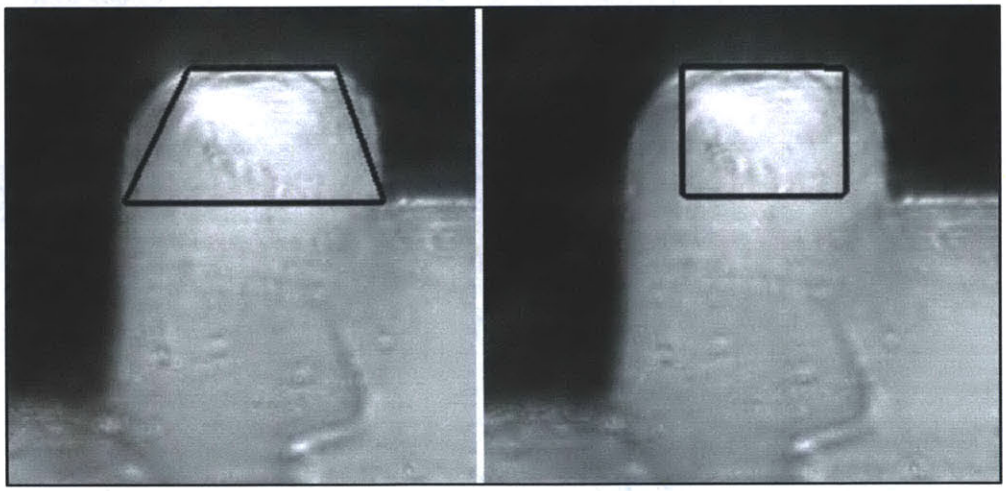

Figure 58: Trapezoidal and Rectangular approximations of Ridge Area

The problem with the trapezoid method is that there is no accurate way to estimate the length of the base of this trapezoid. A solution to this problem could be to assume the width of the base is constant for all embossed parts and that the only two dimensions that vary are the length of the top base and the height. This may not be such a bad assumption, as even partial filling of the ridge cavity of the mold will result in the base of the ridge having a width dimension that matches the tool. However, with this method the total fill ratio will weight the ridge width measurement less than the ridge height dimension. Ridge width should be weighted more heavily than ridge height, as it is the only dimension that

can be used to approximate the size of the edge radius. Edge radius is an important indicator of the functionality of an embossed part and so should at least be indirectly measured for determining the quality of a finished part.

10 Recommendations

It is recommended that embossed parts be evaluated by the accuracy of formation of the channel ridge. The width and height measurements of this ridge should be used to characterize this feature. These two dimensions should be converted into ratios of the corresponding dimensions on the embossing tool, one ratio for the percentage fill of ridge width, and one ratio for the percentage fill of ridge height. These two ratios should then be multiplied together to obtain a single metric that describes the quality of embossed parts. An ideal part will have a width fill ratio of 1, a height fill ratio of 1 and a total area ratio of 1. This would mean that both the ridge height and width perfectly match the dimensions of the tool.

Ridge height should be measured by scanning embossed parts with a Bruker Interferometer, and extracting surface data using the masking method described in section 8.3. Ridge width should be measured by processing cross-sectional data obtained from the Bruker Interferometer using the method and Matlab script described in section 8.4. The measurement error present with this proposed part evaluation scheme is roughly 800nm for the ridge height dimension and 3 microns for the ridge width measurement.

If more thorough characterization of parts is required, the other measurement methods discussed should be used with their respective errors kept in mind. Their precisions were: 6.6 microns for radius measurements, 10.6 degrees for draft measurements, 1.8 microns for channel depth measurements, 15.3 microns for channel width measurements and 40 microns for surface roughness measurements.

11 Conclusion and Future Work

This thesis is based on research conducted as part of the combined efforts of Viren Kalsekar [35], Khanh Nguyen [40] and myself to investigate the capabilities of hot embossing as a prototyping process for Daktari Diagnostics. This chapter will detail the conclusions drawn collectively from the team and present suggested next steps for Daktari.

11.1 Conclusion

The research concluded that hot embossing is a prototyping process capable of producing one of the critically toleranced features of Daktari's microfluidic backbone. When the process was optimized, fill rates of 98% and 91% were achieved for the height and width of the channel's smallest feature. To support this result the measurement system was validated using Gage R&R analysis. The precision-to-tolerance ratios of the critical measurements were between 0.30 and 0.50.

With optimal operating parameters, the 6σ process variation of this hot embossing system was within the specification limits of the assay channel. Surface roughness of the embossed part matched the surface roughness of the molding tool. In this work, micro-machined tools with surface roughness values of 150 nm and 350 nm were used. In summary, the quality of embossed parts is strongly dependent on the quality of the molding tool used.

The process is best suited for prototyping small (~10) to medium volume (~50) batches of parts. The tooling used for this study was purchased for roughly $1000 and took one week to machine. It is best to make this investment when multiple parts are necessary to evaluate a design. With the hot embossing machine detailed in this work, a cycle time of 20 minutes per part was achieved.

11.2 Future Work

This section overviews areas of work that could be pursued by Daktari to more fully understand the hot embossing process and increase the capability of the machine. First,

possible improvements to the existing machine will be outlined. Next, suggestions for further experimentation will be suggested.

11.2.1 Machine Improvements

The machine designed for this research was suitable as a proof of concept device; however there are several improvements that should be made if Daktari will actively pursue hot embossing as a prototyping process. In general, these are improvements that would give greater control over the process and improve the repeatability of its operation.

Alignment

The maximum positional error of this machine was found to be 43 microns, and parallelism was found to be 20 microns over the width of the assay channel. Daktari is interested in the possibility of simultaneously embossing microfluidic features on the front and back of a part. Higher precision in x y positional repeatability is required from the embossing machine for it to be possible to align features on two sides of a part.

Force Control

The current system used for the prototyping of the microfluidic part using the hot embossing process uses displacement-control and it does not have a feedback control on the applied force. When a part is loaded for embossing above the glass transition temperature, the material starts flowing and the load relaxes over time, which is undesirable. A force-controlled system will also allow for control over embossing velocity. Analysis of the effect of this variable was not possible with the current system.

Cooling system control

The cooling system currently used is a recirculating pump with lines passing through the cold plates, which are in contact with the heating platens. The purpose of using the cooling system in this research was to reduce the cycle time by decreasing the time to

cool down to the de-embossing temperature. A cooling system with control over the cooling rate would help in analyzing the effect of the cooling rate on the performance of the process.

Thermal insulation

Currently the machine uses an insulation material to isolate the force sensor and the air bladder from the heating platens. The middle plate and the top plate tend to heat up to 100 C after 4 cycles of heating and cooling the platens to around 150 C. In addition to the risk of damage to the load cell and air bladder, having a thermal path to the press frame drastically increases the thermal mass of the system and makes heating less efficient. A better insulation system using a more efficient insulator or using an air gap will be beneficial.

Tool alignment

If a better alignment system is integrated to make the embossing machine more precise with regards to the X and Y repeatability and parallelism, then a stage could be designed and integrated within the tool assembly to actively change the position of the tool for embossing. This may be a bigger issue when trying to emboss on both sides of the part or embossing on a part with pre-existing features.

Vacuum Control

The best width fill achieved by this system was 91%. The incomplete filling of width indicates that material is not flowing fully into the mold cavity. This results in a radius being left on edges of the channel. It may be possible to reduce the size of these edge radii by performing the embossing within a vacuum chamber. This would naturally complicate the embossing process and increase cycle time. Before this action is taken, the effect of larger edge radii on the end functionality of the part should be understood.

11.2.2 Further Experimentation

Further experimentation could be performed to better characterize the capabilities of hot embossing. These experiments could include studies to better understand variation in the process, to select optimal tooling options and to characterize the type of features that are well suited for the hot embossing process.

Robust Design

The current research focuses more upon the most significant factors and the main effects and interactions affecting the performance of the process. A further study using the Taguchi Array could be done to analyze the signal to noise ratio to characterize the robustness of the process. Another important future step would be to carry out a greater number of experiments with different optimal settings giving the same predicted response to find the most suitable set of parameters.

Feature Capability Tool

This work has demonstrated that the assay channel could be prototyped. More work could be done to catalogue the range of features that Daktari may have interest in prototyping and to study which of these features can be made with hot embossing. For example, a patterned tool could be designed such that it can be used to test hot embossing for a wide variety of features. Questions that could be answered by such a study are:

1. How closely can features be placed to one another?
2. What are the minimum and maximum feature sizes that can be embossed?
3. What aspect ratios of channels are achievable?
4. How can sharp and gradual changes in height be best prototyped?
5. Can features be placed on the edge of a part?

A further study of tool wear could be conducted with a higher quality tool so that measurement precision is not highly affected by defects on the tool. Characterizing the tool wear accurately is important to understanding the limits on tool use.

Experimentation with different Tools

Other tooling options should be considered and tested to compare the differences in their performance in terms of tooling accuracy, durability and feature transferring capability. For example, silicon tools may be able to provide a surface roughness below 100nm, but offer low durability. Titanium machined tools on the other hand can offer higher resistance to wear and complex feature geometries, but may have a higher surface roughness.

Future work on resin tools can be expanded to cover methods for combining qualities of different tools into an all-encompassing resin tool. The study in question could concern the methods and accuracy analysis of combining the low surface finishes of a silicon tools with complex geometries of a machined tools.

Appendix A

Engineering Drawings:

Assembly Drawing:

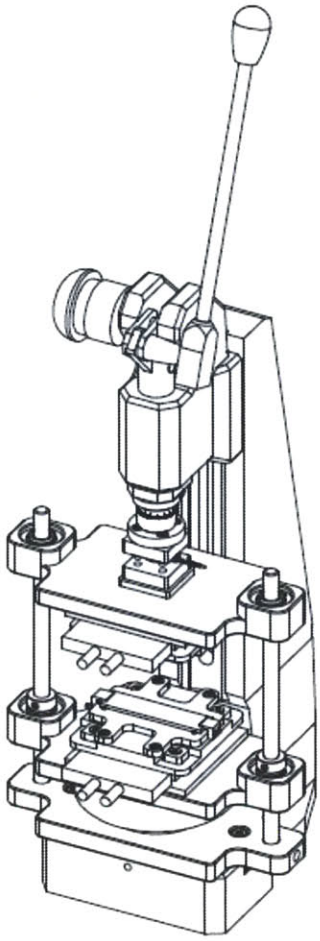

ITEM NO.	PART NUMBER	DESCRIPTION	QTY.
1	2-400105co	Schmidt Press Frame	1
2	92855A722	McMaster: M8—Pitch: 1.25 mm - 25mm	2
3	93615A510	McMaster: 3/8"-16 - 1/2"	4
4	AirSpring Valve - 9538K42	McMaster: AirSpring Valve	1
5	Rail Block		2
6	Half_in_rodx12in	SDP SI Rod	2
7	Bottom Heating plate		1
8	Corner Insulation Block		8
9	Cold Plate		2
10	MACOR		2
11	91253A251		8
12	Substrate plate ASMB		1
13	92220A161		4
14	heater		2
15	Sensor Block		2
16	Futek LCM200 Sensor		1
17	Sensor Insulator		1
18	Revised Top Heating plate		1
19	cuvette mold		1
20	91306A311		4
21	92855A522		5
22	Flange shaft		1
23	Small_Top		1
24	99642A229	McMaster: M12—Pitch: 1.5 mm - 12mm	2
25	94000A037		4
26	9414T11		2
27	Bottom ASMB		1
28	Airspring - 9539K41	McMaster: Airspring	1
29	Middle Plate		2
30	Bearing_S99LBC-050088	SDP SI Bearing	4
31	e clip_s73hw2-100-087	SDP SI e-clip for bearing	8
32	Top_Holder_New		1

Figure A 1: Full Hot Embossing Machine Assembly

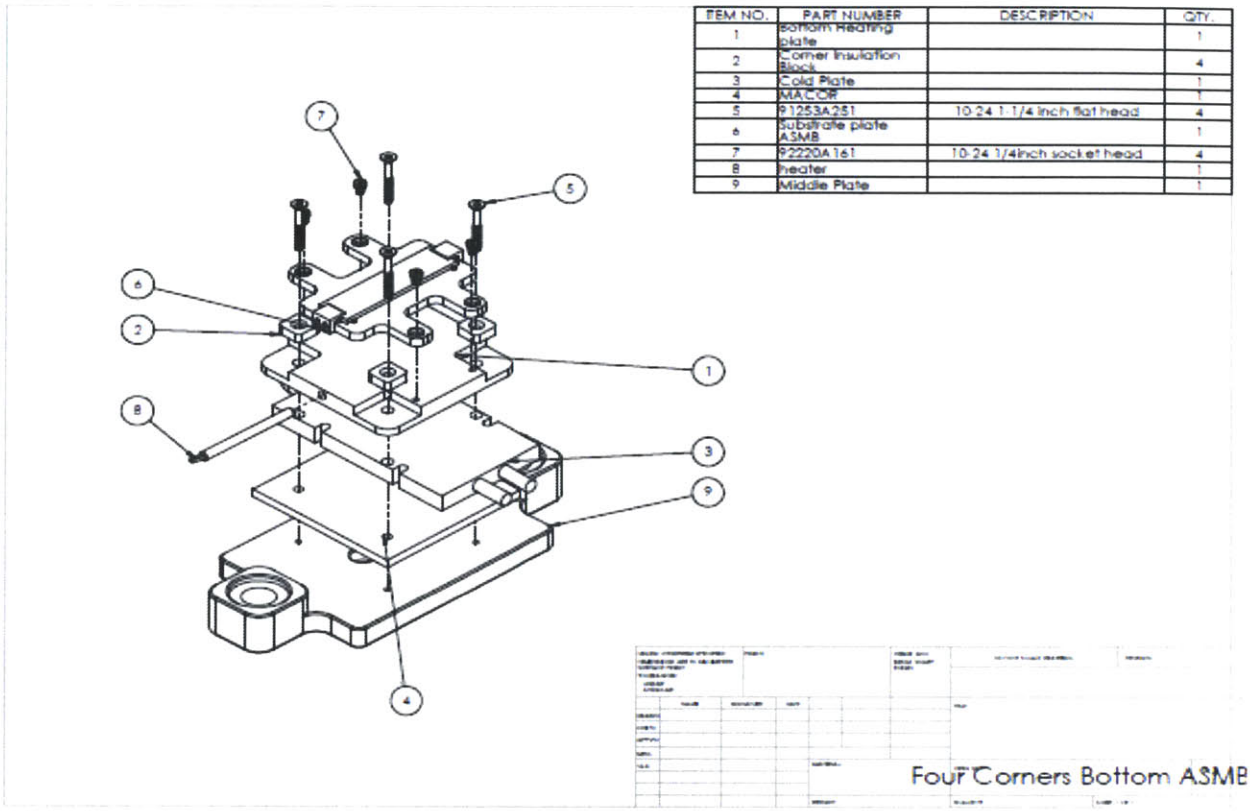

ITEM NO.	PART NUMBER	DESCRIPTION	QTY.
1	Bottom Heating plate		1
2	Corner Insulation Block		4
3	Cold Plate		1
4	MACOR		1
5	91253A251	10-24 1 1/4 inch flat head	4
6	Substrate plate ASMB		1
7	92220A161	10-24 1/4inch socket head	4
8	heater		1
9	Middle Plate		1

Figure A 2: Lower Heating Stack Assembly

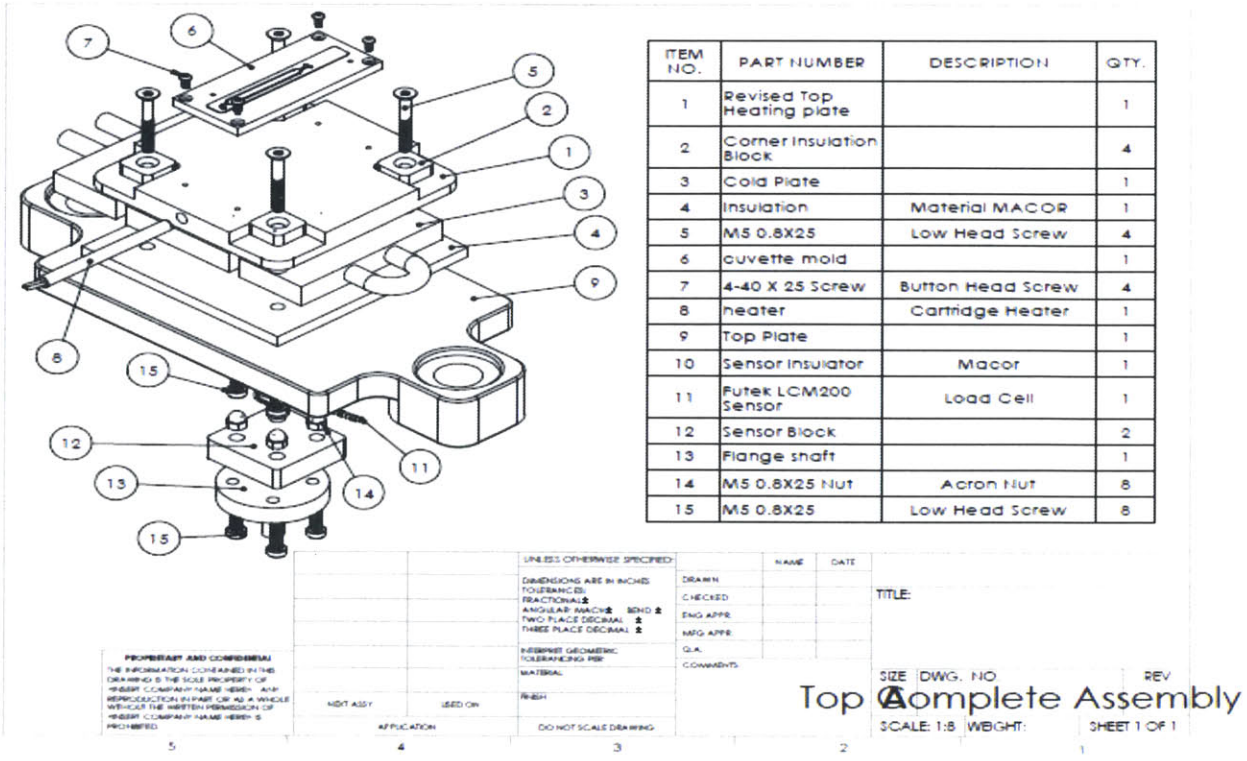

ITEM NO.	PART NUMBER	DESCRIPTION	QTY.
1	Revised Top Heating plate		1
2	Corner Insulation Block		4
3	Cold Plate		1
4	Insulation	Material MACOR	1
5	M5 0.8X25	Low Head Screw	4
6	cuvette mold		1
7	4-40 X 25 Screw	Button Head Screw	4
8	heater	Cartridge Heater	1
9	Top Plate		1
10	Sensor Insulator	Macor	1
11	Futek LCM200 Sensor	Load Cell	1
12	Sensor Block		2
13	Flange shaft		1
14	M5 0.8X25 Nut	Acron Nut	8
15	M5 0.8X25	Low Head Screw	8

Figure A 3: Top Heating Stack Assembly

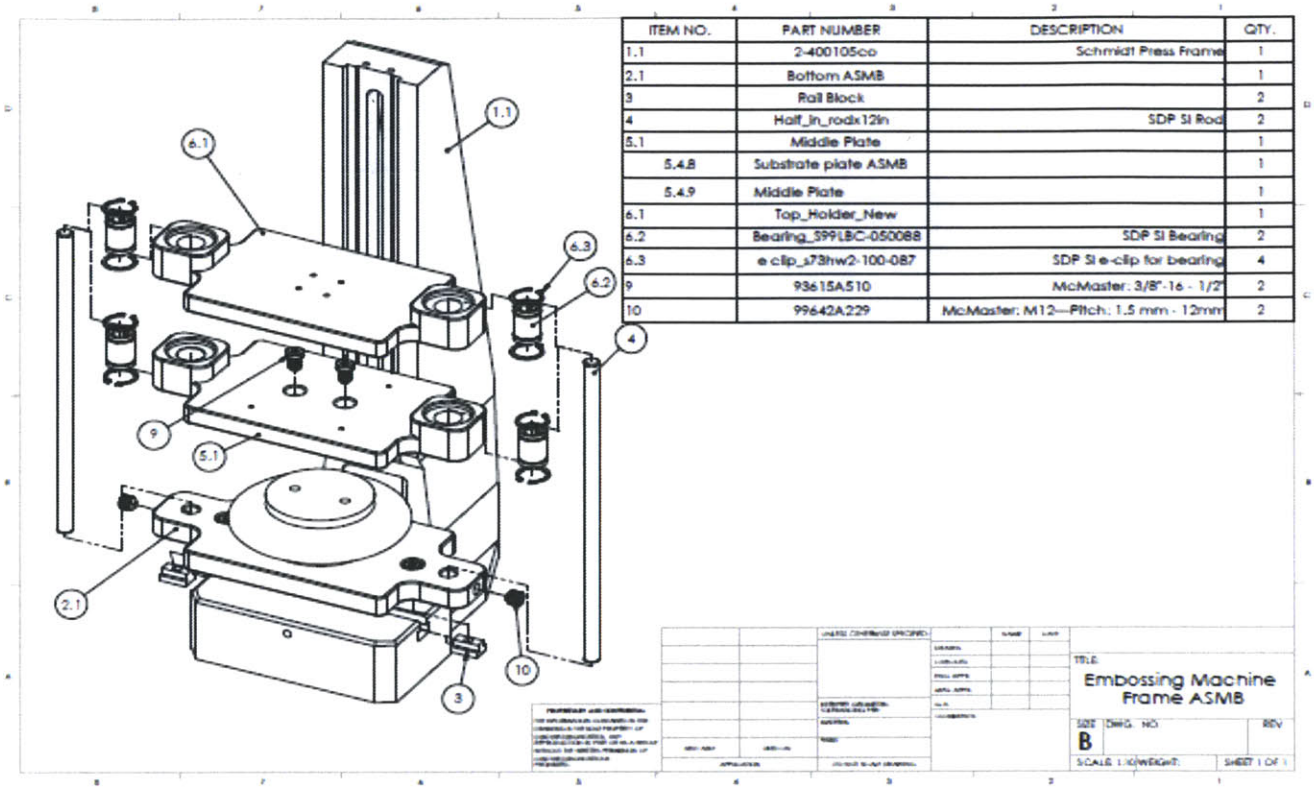

ITEM NO.	PART NUMBER	DESCRIPTION	QTY.
1.1	2-400105co	Schmidt Press Frame	1
2.1	Bottom ASMB		1
3	Rail Block		2
4	Half_in_rodx12in	SDP SI Rod	2
5.1	Middle Plate		1
5.4.8	Substrate plate ASMB		1
5.4.9	Middle Plate		1
6.1	Top_Holder_New		1
6.2	Bearing_S99LBC-050088	SDP SI Bearing	2
6.3	e clip_s73hw2-100-087	SDP SI e-clip for bearing	4
9	93615A510	McMaster: 3/8"-16 - 1/2"	2
10	99642A229	McMaster: M12—Pitch: 1.5 mm - 12mm	2

Figure A 4: Frame and Guide Rail Assembly

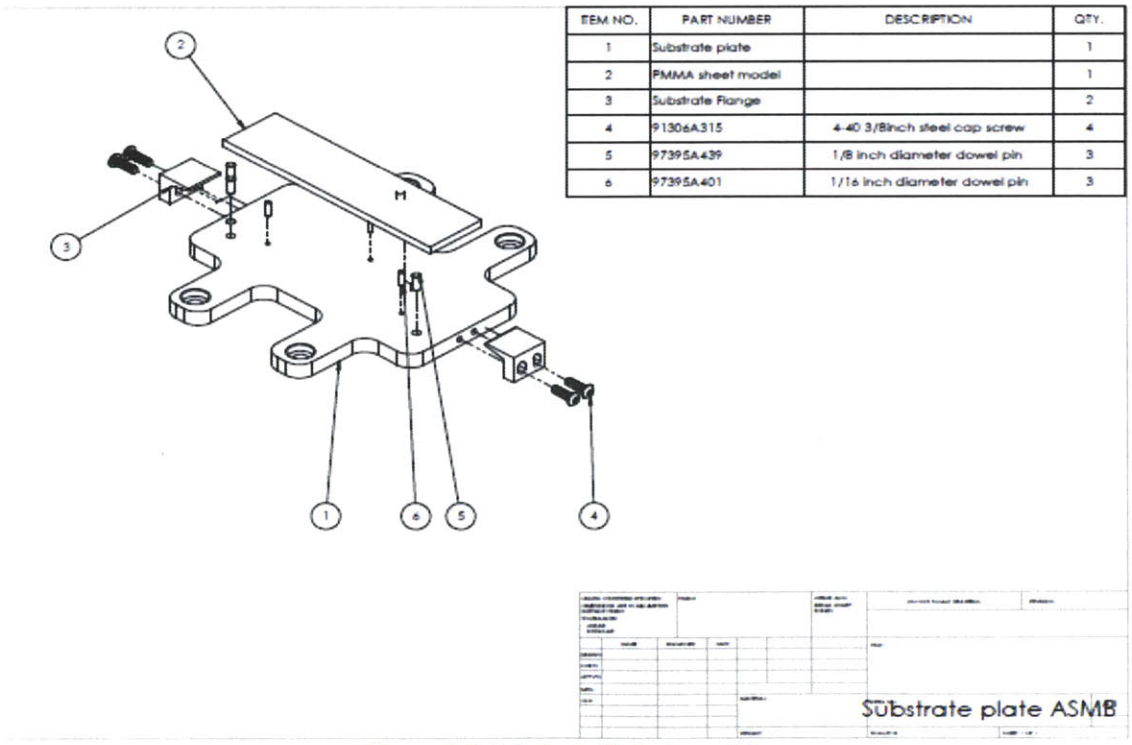

ITEM NO.	PART NUMBER	DESCRIPTION	QTY.
1	Substrate plate		1
2	PMMA sheet model		1
3	Substrate Flange		2
4	91306A315	4-40 3/8inch steel cap screw	4
5	97395A439	1/8 inch diameter dowel pin	3
6	97395A401	1/16 inch diameter dowel pin	3

Figure A 5: Substrate Plate Assembly

PARTS

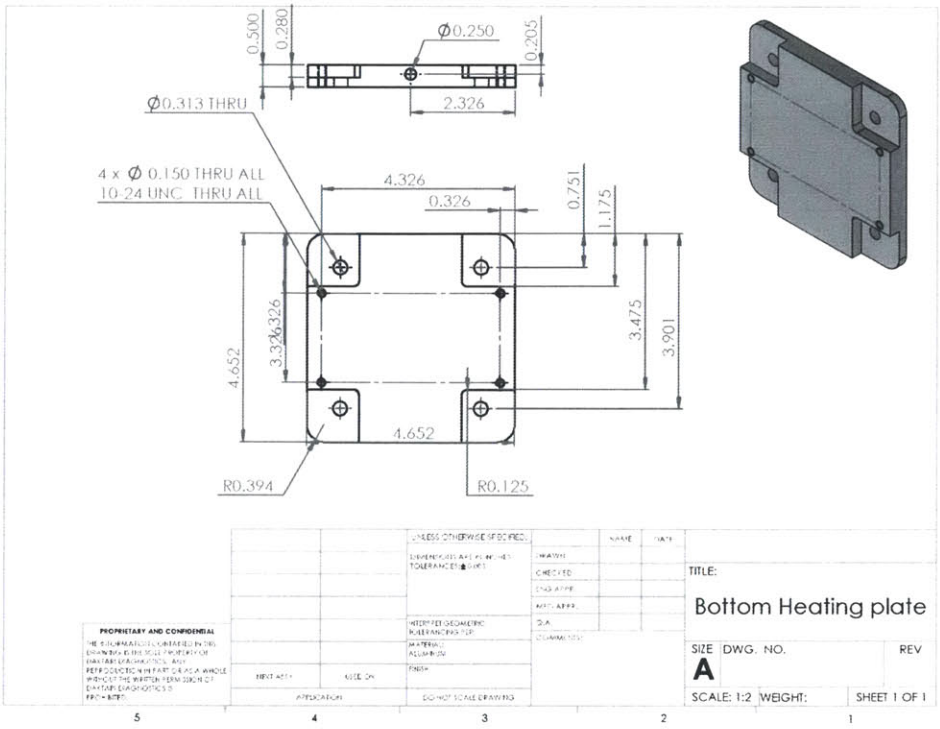

Figure A 6: Bottom Heating Plate

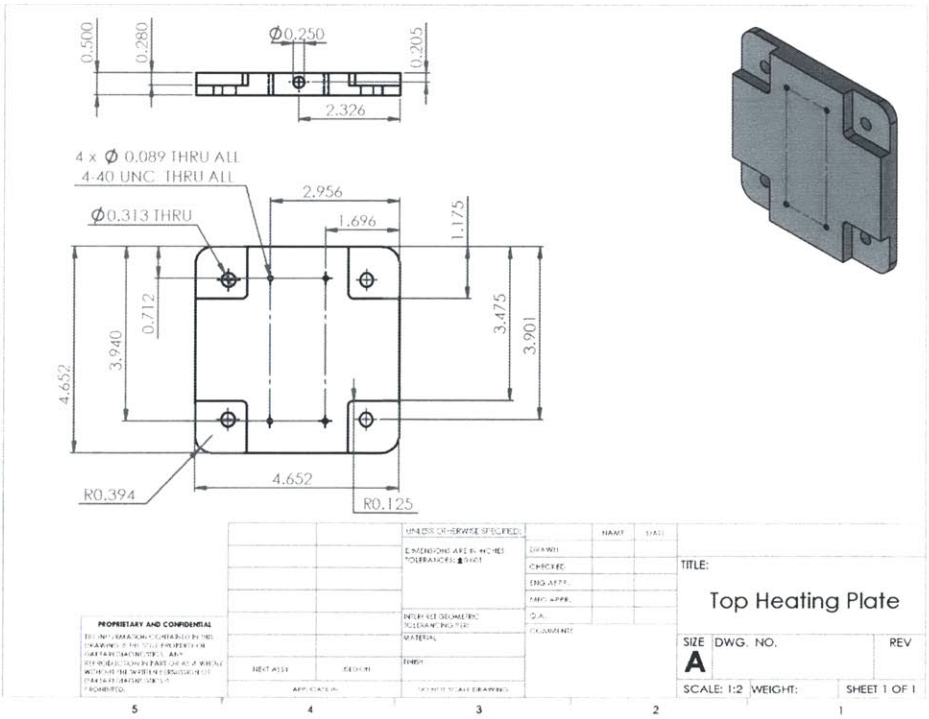

Figure A 7: Top Heating Plate

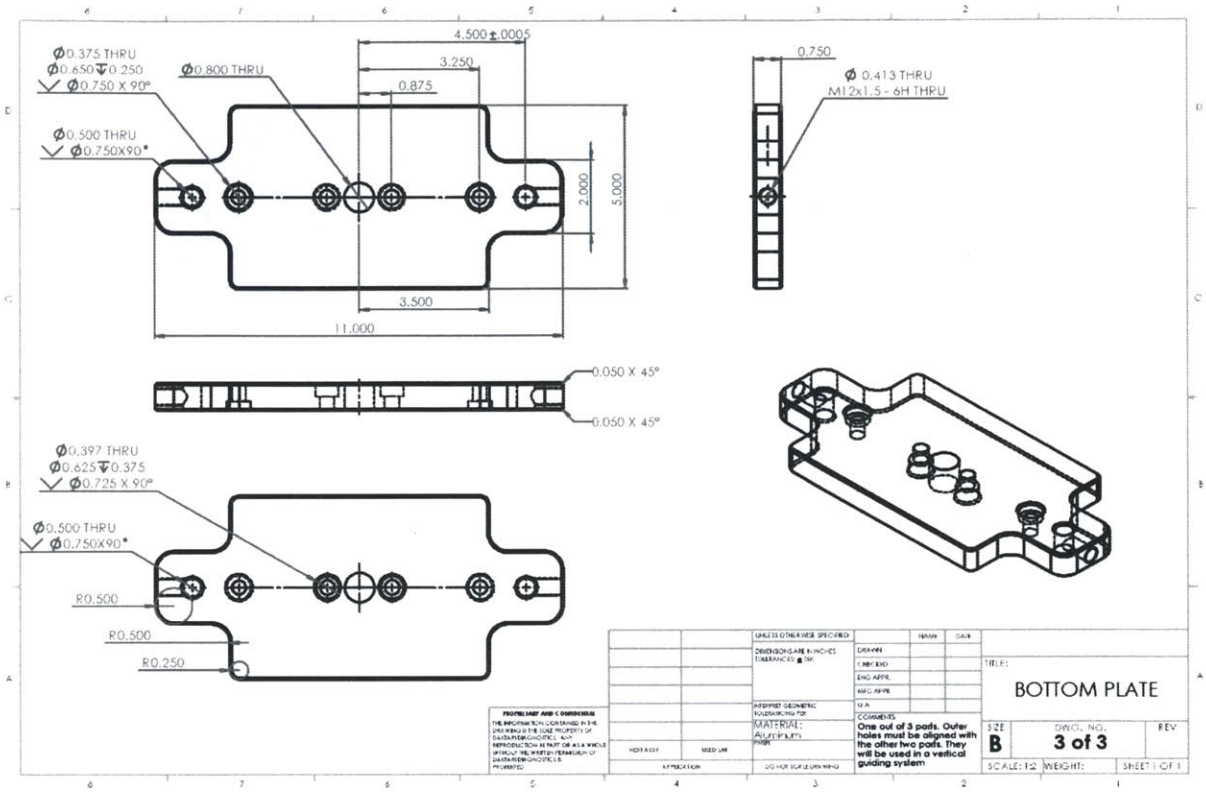

Figure A 8: Bottom Plate

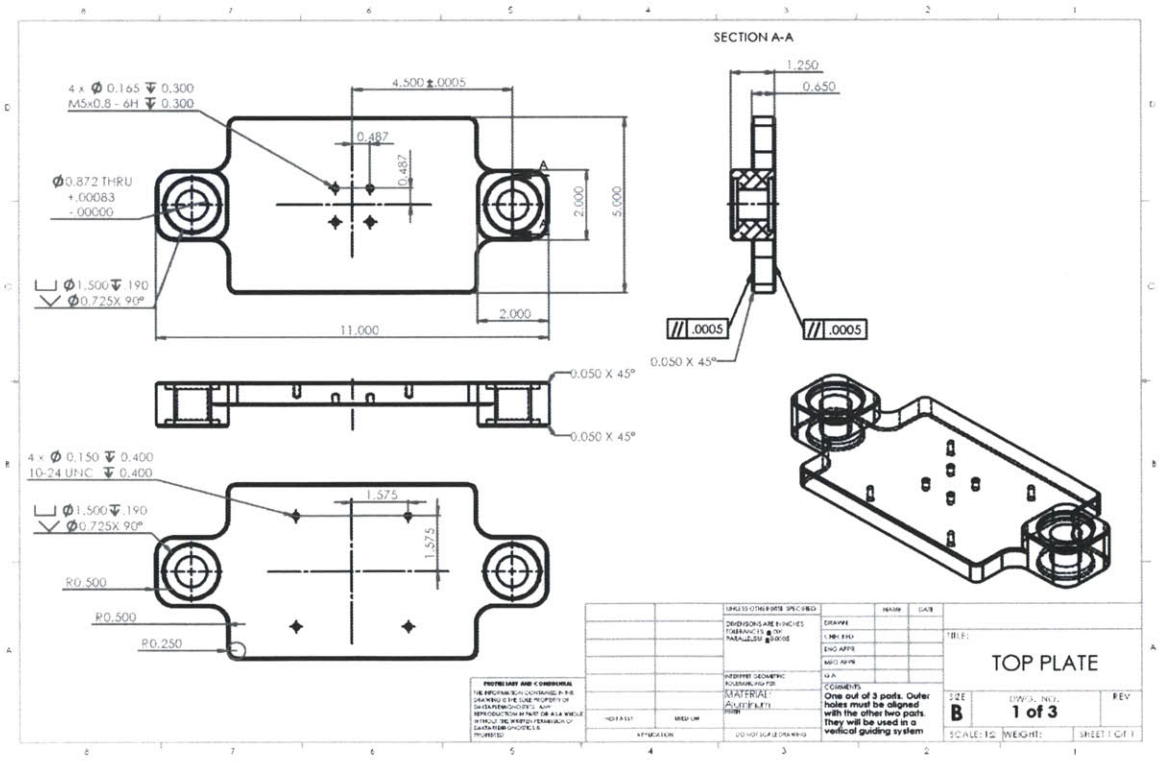

Figure A 9: Top Plate

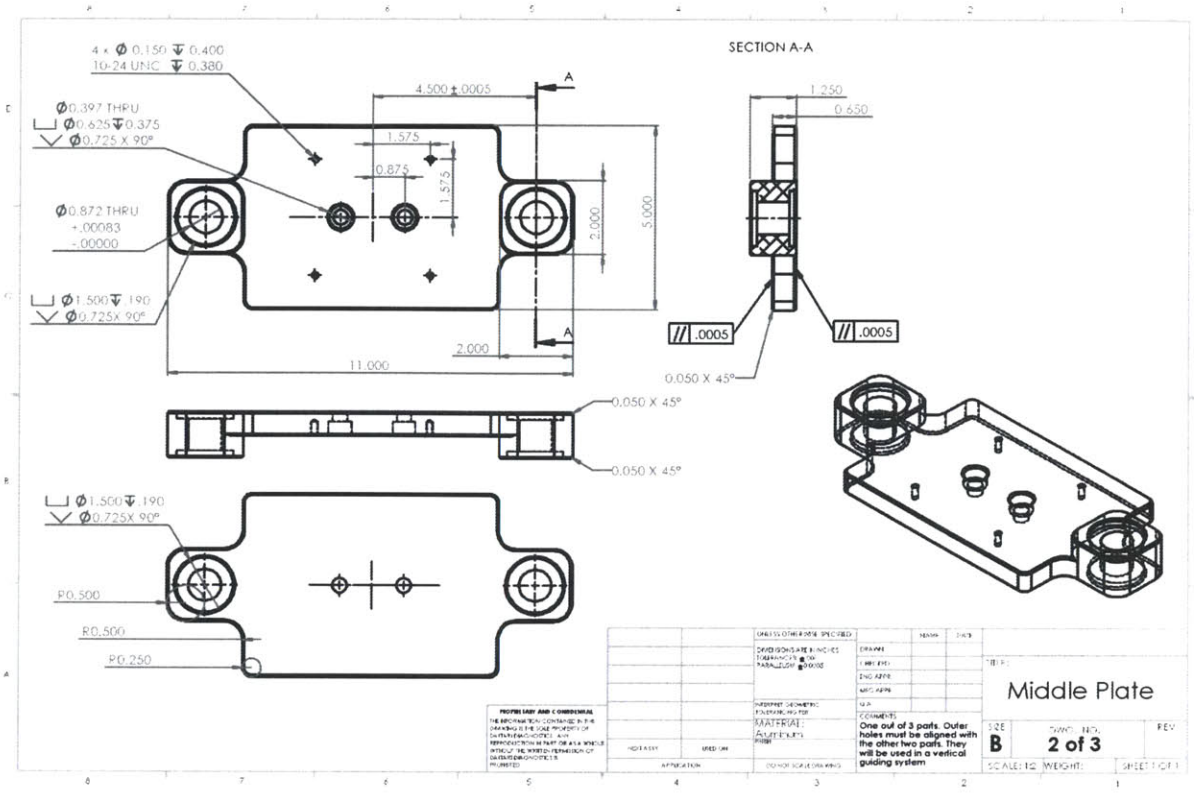

Figure A 10: Middle Plate

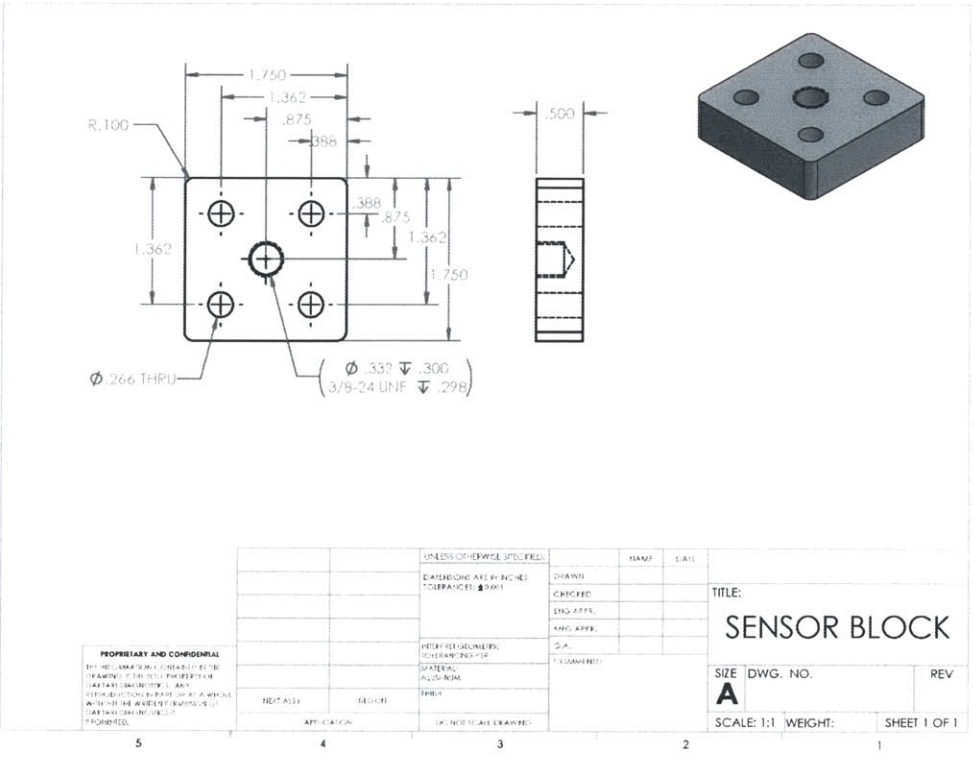

Figure A 11: Sensor Attachment Block

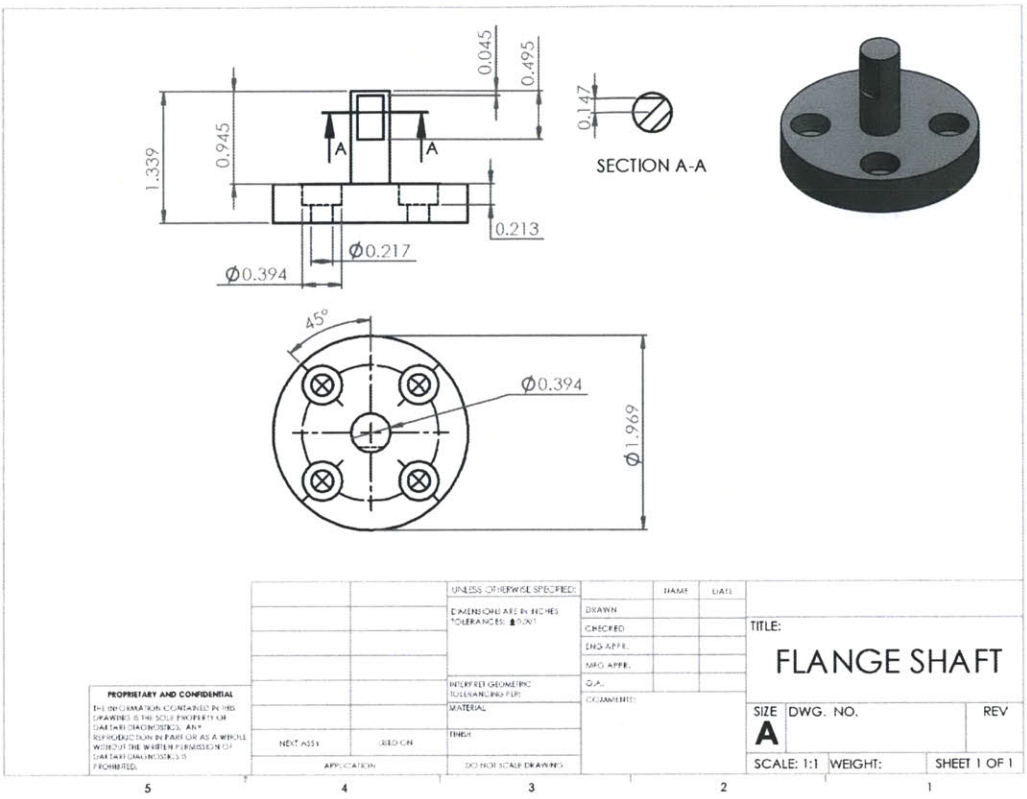

Figure A 12: Mounting Flange

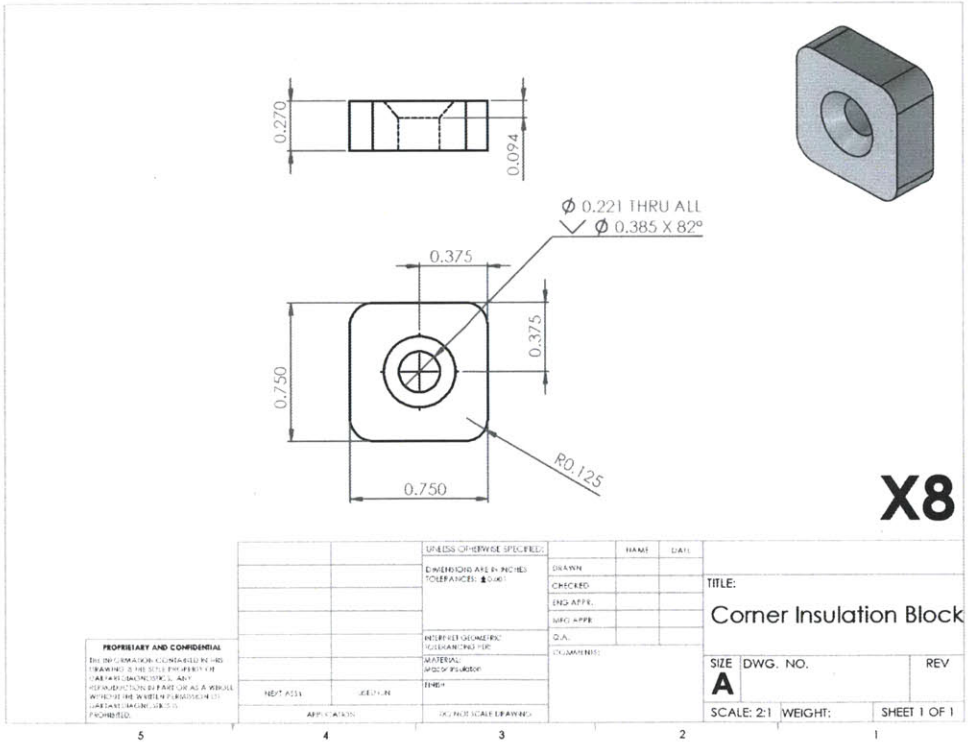

Figure A 13: Insulation Block

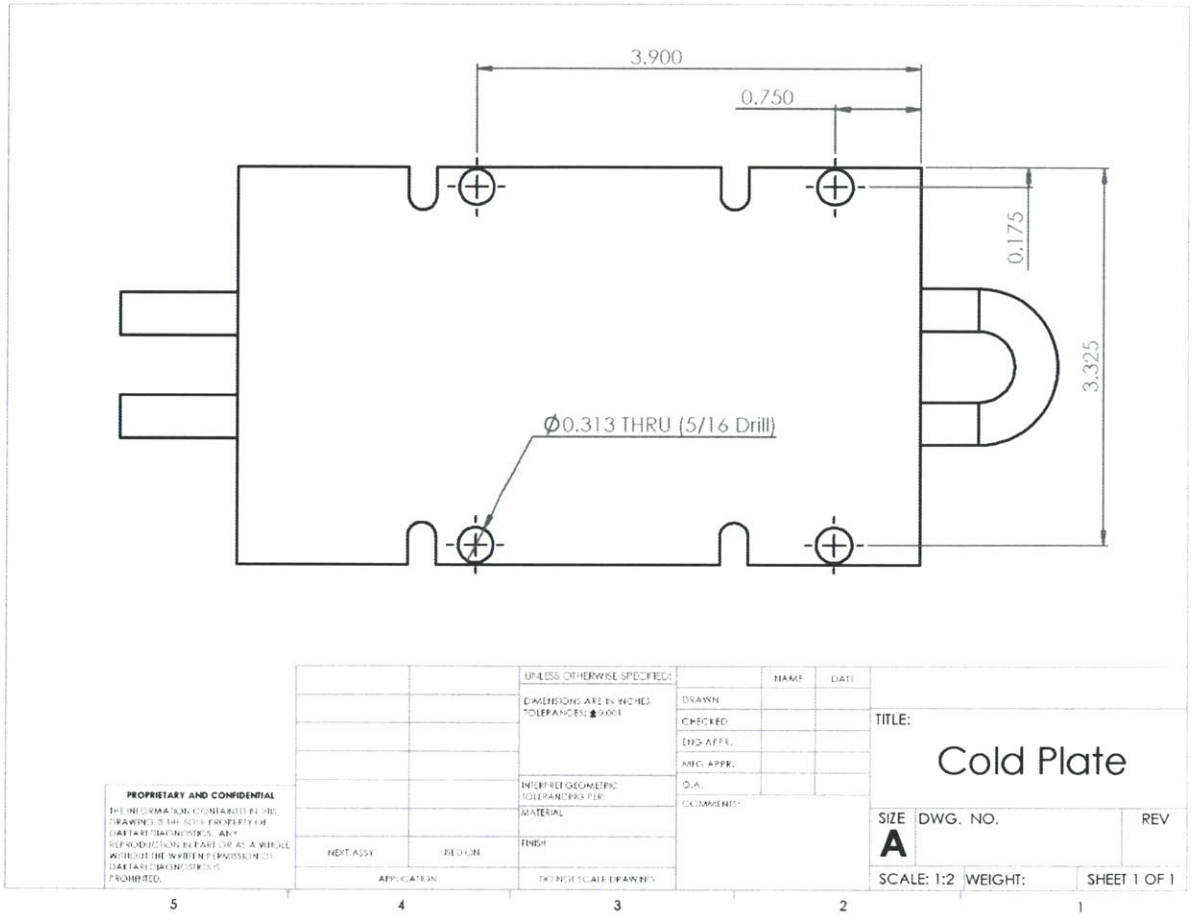

Figure A 14: Cold Plate

Bill of Materials

Table A 1: Complete Bill of Materials

Part	Vendor	Part No.	Material	Quantity	Unit Cost	Total
Top Assembly						
Flange	First Cut		Aluminum	1	$353.00	$353.00
Top Sensor Block	First Cut		Aluminum	1	$75.00	$75.00
Force Sensor	FUTEK			1	$575.00	$575.00
Ceramic Insulator	In house		Macor	1	$179.00	$179.00
Top Plate	Zero Hour Parts		Aluminum	1	$620.00	$620.00
Cold Plate	Mcmaster		Aluminum	1	$100.00	$100.00
Heating Plate	In house		Aluminum	1	$37.00	$37.00
Catridge Heaters	Mcmaster			1	$18.57	$18.57
Hose Pipes	Mcmaster			1	$29.00	$29.00
Tool	Atometric		Aluminum	2	$975.00	$1,950.00
Bearings	SDP-SI	S99LBC-050088		2	$17.12	$34.24
Shafts	SDP-SI	A 7X 1-1612A	Aluminum	2	$22.82	$45.64
Bottom Assembly						
Substrate Plate	First Cut		Aluminum	1	$198.00	$198.00
Substrate Flanges	First Cut		Aluminum	2	$42.00	$84.00
Heating Plate	In house		Aluminum	1	$0.00	$0.00
Cartridge Heater	Mcmaster			1	$18.57	$18.57
Cold Plate	Mcmaster		Aluminum	1	$100.00	$100.00
Ceramic Insulator	In House		Macor	1	$0.00	$0.00
Bottom Plate	Zero Hour Parts		Aluminum	1	$675.00	$675.00
Bearings	SDP-SI		Steel	2	$17.12	$34.24
Air Spring	Mcmaster	9539K41		1	$94.50	$94.50

Valve	Mcmaster	9538K42		1	$11.39	$11.39
Base Plate	Zero Hour Parts		Aluminum	1	$375.00	$375.00
Fasteners	Mcmaster					$0.00
Fasteners						
8mm hex bit	Mcmaster Carr	*7397A48*	Stainless Steel	1	$5.76	$5.76
M8-1.25 D5 Tap	Mcmaster Carr	*25235A43*	Stainless Steel	1	$27.86	$27.86
M8-1.25 rod	Mcmaster Carr	*94185A160*	Stainless Steel	1	$12.86	$12.86
Metric M8 Bolt 25mm	Mcmaster Carr	*92855A722*	Stainless Steel	1	$7.86	$7.86
M5 Size, 60 mm Length	Mcmaster Carr	*92855A543*	Stainless Steel	1	$9.51	$9.51
Hose Clamp for the piping of the cooling system for the hot embossing project	Mcmaster Carr	*45945K63*	Stainless Steel	8	$3.61	$28.88
M5x18 - Metric Class 12.9 Alloy Steel	Mcmaster Carr	*91290A238*	Stainless Steel	1	$11.66	$11.66
18-8 Stainless Steel Low Head Sckt Cap Screw 3/8"-16 Thread, 1/2" Length, packs of 5	Mcmaster Carr	*93615A510*	Stainless Steel	1	$7.72	$7.72
Alloy Steel Cup Point Set Screw M12 Size, 12mm Long, 1.5mm Pitch, packs of 5	Mcmaster Carr	*99642A229*	Stainless Steel	1	$12.18	$12.18
Alloy Steel Flat Head Socket Cap Screw 10-24 Thread, 1-1/2" Length, Black, packs of 25	Mcmaster Carr	*91253A251*	Stainless Steel	1	$10.36	$10.36
Alloy Steel Low Head Socket Cap Screw 10-24 Thread, 1/4" Length, packs of 25	Mcmaster Carr	*92220A161*	Stainless Steel	1	$7.31	$7.31
Zinc-Plated STL Button Head Socket Cap Screw 4-40 Thread, 1/4" Length, packs of 50	Mcmaster Carr	*91306A311*	Stainless Steel	1	$8.31	$8.31

Zinc-Plated STL Button Head Socket Cap Screw 4-40 Thread, 3/8" Length, packs of 50	Mcmaster Carr	*91306A315*	Stainless Steel	1	$8.63	$8.63
Corrosion Resistant Dowel Pin Type 316 SS, 1/8" Diameter, 5/16" Length, packs of 10	Mcmaster Carr	*97395A606*	Stainless Steel	1	$6.95	$6.95
Metric 18-8 Stainless Steel Acorn Nut M5 Size, .8mm Pitch, 8mm Width, 10mm Height, packs of 25	Mcmaster Carr	*94000A037*	Stainless Steel	1	$4.95	$4.95
Metric 18-8 SS Low Head Socket Cap Screw M5 Size, 25 mm Length, .8 mm Pitch, packs of 25	Mcmaster Carr	*92855A522*	Stainless Steel	1	$8.89	$8.89
E clips	Mcmaster Carr	*S73HW2-100-087*	Stainless Steel	8	$1.72	$13.76
Dowel Pins 1/8th dia 1/4 th length	Mcmaster Carr	*97395A439*	Stainless Steel	1	$6.14	$6.14
Corrosion Resistant Dowel Pin Type 316 SS, 1/16" Diameter, 1/4" Length, packs of 25	Mcmaster Carr	*97395A401*	Stainless Steel	1	$10.48	$10.48

Product Information

DOW CORNING

Encapsulants

Dow Corning® 184 Silicone Elastomer

Transparent encapsulant with good flame resistance

FEATURES

- Flowable
- RT and heat cure
- High tensile strength
- Same as Sylgard 182 but with RT cure capability
- UL and Mil Spec tested

BENEFITS

- Rapid, versatile cure processing controlled by temperature
- High transparency allows easy inspection of components
- Can be considered for uses requiring UL and Mil Spec requirements

COMPOSITION

- 2-part
- 10:1 mix ratio
- Polydimethylsiloxane elastomer

APPLICATION METHODS

- Automated metered mixing and dispensing
- Manual mixing

APPLICATIONS

- General potting applications
- Power supplies
- Connectors
- Sensors
- Industrial controls
- Transformers
- Amplifiers
- High voltage resistor packs
- Relays
- Adhesive/encapsulant for solar cells
- Adhesive handling beam lead integrated circuits during processing

TYPICAL PROPERTIES

Specification Writers: These values are not intended for use in preparing specifications. Please contact your local Dow Corning sales office or your Global Dow Corning Connection before writing specifications on this product.

Property	Unit	Value
Viscosity (Part A)	cP	5175
	mPa-sec	5175
	Pa-sec	5.2
Viscosity (Mixed)	cP	3500
	mPa-sec	3500
	Pa-sec	3.5
Specific Gravity (Uncured Base)	-	1.03
Specific Gravity (Cured)	-	1.04
Working Time at 25°C (Pot Life - hours)	hr	1.4
Cure Time at 25°C	hrs	48
Heat Cure Time @ 100°C	minutes	35
Heat Cure Time @ 125°C	minutes	20
Heat Cure Time @ 150°C	minutes	10

Figure A 15: PDMS

DESCRIPTION

Dow Corning® silicone encapsulants are supplied as two-part liquid component kits. When liquid components are thoroughly mixed, the mixture cures to a flexible elastomer, which is well suited for the protection of electrical/electronic applications. Dow Corning silicone encapsulants cure without exotherm at a constant rate regardless of sectional thickness or degree of confinement. Dow Corning silicone elastomers require no post cure and can be placed in service immediately following the completion of the cure schedule. Standard silicone encapsulants require a surface treatment with a primer in addition to good cleaning for adhesion while primerless silicone encapsulants require only good cleaning. Underwriters Laboratory (UL) 94 recognition is based on minimum thickness requirements. Please consult the UL Online Certifications Directory for the most accurate certification information.

MIXING AND DE-AIRING

The 10:1 mix ratio these products are supplied in gives one latitude to tune the modulus and hardness for specific application needs and production lines. In most cases de-airing is not required.

PREPARING SURFACES

In applications requiring adhesion, priming will be required for many of the silicone encapsulants. See the Primer Selection Guide for the correct primer to use with a given product. For best results, the primer should be applied in a very thin, uniform coating and then wiped off after application. After application, it should be thoroughly cured prior to application of the silicone elastomer. Additional instructions for primer usage can be found in the information sheets specific to the individual primers.

PROCESSING/CURING

Thoroughly mixed Dow Corning silicone encapsulant may be poured/dispensed directly into the container in which it is to be cured. Care should be taken to minimize air entrapment. When practical, pouring/dispensing should be done under vacuum, particularly if the component being potted or encapsulated has many small voids. If this technique cannot be used, the unit should be evacuated after the silicone encapsulant has been poured/dispensed. Dow Corning silicone encapsulants may be either room temperature (25°C/77°F) or heat cured. Room temperature cure encapsulants may also be heat accelerated for faster cure. Ideal cure conditions for each product are given in the product selection table. Two-part condensation cure encapsulants should not be heat accelerated above 60°C (140°F).

TYPICAL PROPERTIES, continued

Property	Unit	Value
Tensile Strength	psi MPa kg/cm2	1025 7.1 71
Elongation	%	120
Tear Strength (Die B)	ppi N/cm	5 2
Durometer Shore A	-	44
Dielectric Strength	volts/mil kV/mm	475 19
Volume Resistivity	ohm*cm	2.9E+14
Dielectric Constant at 100 Hz	-	2.72
Dielectric Constant at 100 kHz	-	2.68
Dissipation Factor at 100 hz	-	0.00257
Dissipation Factor at 100 kHz	-	0.00133
Mil Specification	NA	Mil Spec
Agency Listing	-	UL 94V-0
Shelf Life at 25°C	months	24
Refractive Index @ 589 nm	-	1.4118
Refractive Index @ 632.8 nm	-	1.4225
Refractive Index @ 1321 nm	-	1.4028
Refractive Index @ 1554 nm	-	1.3997

Figure A 16: PDMS Properties

CYTEC

TECHNICAL DATA SHEET CONAP®

CONAPOXY® FR-1080

CONAPOXY FR-1080 is a two-part high temperature epoxy potting system designed to meet Class H (180°C) operating requirements.

TYPICAL PRODUCT CHARACTERISTICS

	Resin Properties Part A	Curative Properties Part B
Viscosity @ 25°C	4,000 cps	300 cps
Specific Gravity @ 25°C	1.03	1.23
Color	Amber	Dark Brown

TYPICAL CURED PROPERTIES

Hardness, Shore D		90
Tensile Strength, psi		8200
Elongation, %		2
Tear Strength, pli		250
Shrinkage, %		1.42
	25°C	105°C
Volume Resistivity, ohm-cm	9.7×10^{16}	2.9×10^{14}
Surface Resistivity, ohms	5.5×10^{16}	5.7×10^{14}
Dielectric Constant @ 1 KHz	3.12	3.29
Dissipation Factor @ 1 KHz	0.004	0.004
Dielectric Strength, vpm	600	450
Flexural Strength, psi		12,789
Flexural Modulus, psi		388,650
Compressive Strength, psi		4230

RECOMMENDED PROCESSING PARAMETERS

Mix Ratio by Weight, Resin/Curative	100/83
Mix Ratio by Volume, Resin/Curative	100/67
Initial Mixed Viscosity @ 25°C	2500 cps
Work Life @ 25°C	>2 hours
Gel Time @ 100°C	1-2 hours
Cure @ 120°C	4-16 hours
Post Cure @ 180°C (for maximum properties)	2 hours

STORAGE AND HANDLING

The shelf life of CONAPOXY FR-1080 resin and hardeners is 18 months from date of manufacture when stored in the original unopened containers.

Some settling of fillers may occur in the resin. Mix resin thoroughly before each use.

CAUTION: FOR INDUSTRIAL USE ONLY!

Epoxy resins and hardeners can cause skin rashes, dermatitis, and eye irritation. Use only in well ventilated areas. The use of appropriate clothing and safety glasses is recommended. Avoid breathing of vapors and protect skin and eyes from contact with material. Should skin contact occur, immediately clean with suitable hand cleaner, then scrub with soap and water. For eye contact, immediately flush with water for at least 15 minutes and obtain medical attention.

FOR COMPLETE SAFETY AND HEALTH INFORMATION, REFER TO THE MATERIAL SAFETY DATA SHEET (MSDS) FOR THIS PRODUCT.

AVAILABILITY

CONAPOXY FR-1080 is available in gallon, 5-gallon, and 55-gallon containers. An evaluation kit of CONAPOXY FR-1080 is available for a nominal fee.

CAUTION

Responsible handling of Cytec products requires a thorough preview of safety, health, and environmental issues prior to use. Review the Material Safety Data Sheets(s) for the specific Cytec product(s) and container label information before opening containers. Ensure that employee exposure issues are understood, communicated to all workers, and controls are in place to prevent exposures above Permissible Exposure Limits (P.E.L.'s). Review safety and environmental issues to be certain controls are in place to prevent injury to employees, the community, or the environment, and ensure compliance with all applicable Federal, State, and Local laws and regulations. For assistance in this review process, please call your Cytec representative or our office noted below.

www.cytec.com/conap

• Email: custinfo@cytec.com Worldwide Contact Info: www.cytec.com/conap Tel: 716.372.9650 Fax: 716.372.1594 •

UPT-P-206C

Figure A 17: Epoxy

FUTEK MODEL LCM200

ULTRA LIGHT MINIATURE UNIVERSAL THREADED LOAD CELL

Drawing Number: FI1064-B

INCH [mm] | R.O.= Rated Output

WIRING CODE (WC1)			
+Excitation	-Excitation	+Signal	-Signal
RED	BLACK	GREEN	WHITE
Shield			
FLOATING			

+OUTPUT
(TENSION)
-OUTPUT
(COMPRESSION)

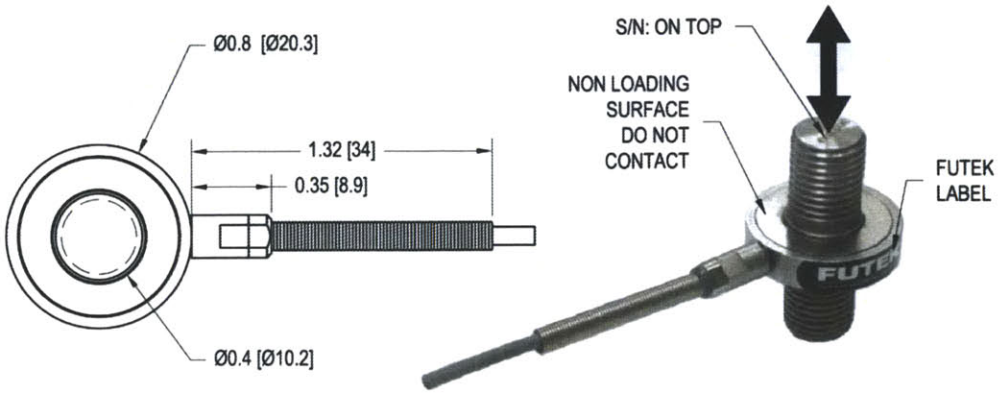

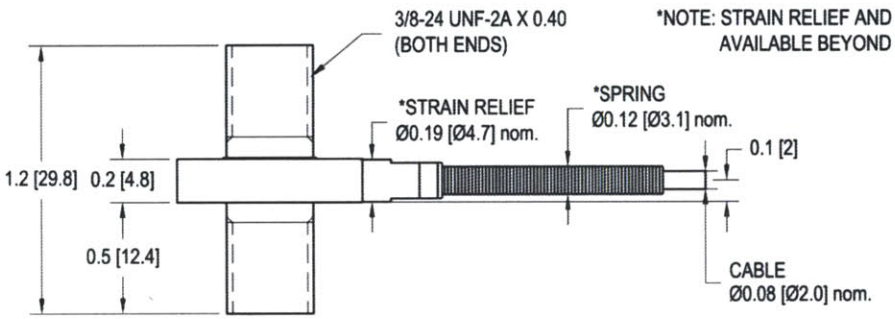

*NOTE: STRAIN RELIEF AND SPRING ONLY AVAILABLE BEYOND S/N: 305196

ITEM #	CAPACITIES lb	N
FSH01934	250	1112
FSH01933	500	2224
FSH01932	1000	4448

SPECIFICATIONS:

RATED OUTPUT	1 mV/V nom (250 lb); 2 mV/V nom.
SAFE OVERLOAD	150% of R.O.
ZERO BALANCE	±3% of R.O.
EXCITATION (VDC OR VAC)	15 MAX
BRIDGE RESISTANCE	350 Ω nom.
NONLINEARITY	±0.5% of R.O.
HYSTERESIS	±0.5% of R.O.
NONREPEATABILITY	±0.1% of R.O.
TEMP. SHIFT ZERO	±0.01% of R.O./°F [0.018% of R.O./°C]
TEMP. SHIFT SPAN	±0.02% of LOAD/°F [0.036% of LOAD/°C]
COMPENSATED TEMP.	60 to 250°F [15 to 121°C]
OPERATING TEMP.	-60 to 285°F [-50 to 140°C]
WEIGHT	0.6 oz [17 g]
MATERIAL	17-4PH S.S.**
DEFLECTION	0.002 [0.05] nom.
CABLE: #29 AWG, 4 Conductor, Spiral Shielded Teflon Cable 10 ft [3 m] Long	
ACCESSORIES AND RELATED INSTRUMENTS AVAILABLE	
CALIBRATION (STD)	5 pt. TENSION; 60.4 KΩ SHUNT CAL. VALUE 100 KΩ FOR 250 lb SHUNT CAL. VALUE
CALIBRATION (AVAILABLE)	COMPRESSION
CALIBRATION TEST EXCITATION	10 VDC

FUTEK
ADVANCED SENSOR TECHNOLOGY, INC.

10 THOMAS
IRVINE, CA 92618 USA
1-800-23-FUTEK (38835)

INTERNET:
http://www.futek.com

Figure A 18: Load Cell

1/32 DIN Ramp/Soak Controllers

CN7500 Series

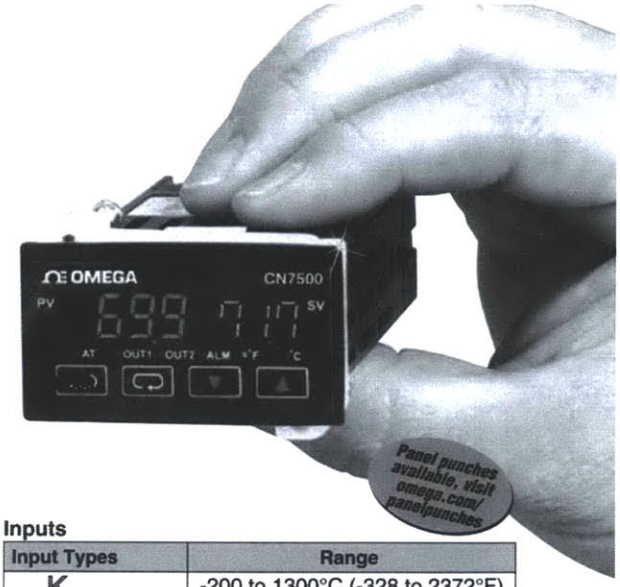

- **Dual 4-Digit LED Display**
- **8 Ramp/Soak Programs, 8 Segments Each**
- **Universal Inputs**
- **Autotune**
- **Dual Control Outputs**
- **RS485 Communications Standard**
- **Alarm Functions**
- **Free Software**

The CN7500 Series temperature/process controller's advanced control features can handle the most demanding temperature or process applications. Enclosed in a compact 1/32 DIN housing, the CN7500 has dual, 4-digit LED displays for local indication of process value and setpoint. Control methods include on/off, PID, autotune, and manual tune. PID control is supported with 64 temperature and time (ramp/soak) control actions. The dual-loop output control allows simultaneous heating and cooling. The second output can be configured as an alarm mode using one of the 13 built-in alarm functions.

RS485 communications is standard. Up to 247 communication addresses are available, with transmission speeds of 2400 to 38,400 bps. Other features include universal inputs, selectable temperature units (°C/°F), selectable resolution, quick sampling rate, and security protection.

Specifications

Inputs: Thermocouple, RTD, DC voltage or DC current
Display: Two 4-digit, 7 segment 6.35 mm H (25") LEDs;
PV: red
SV: green
Accuracy: ±0.25% span, ±1 least significant digit
Supply Voltage: 100 to 240 Vac, 50/60 Hz
Power Consumption: 5 VA max
Operating Temperature: 0 to 50°C (32 to 122°F)
Memory Backup: Non-volatile memory
Control Output Ratings:
Relay: SPST, 5A @ 250 Vac resistive
Voltage Pulse: 14 V, 10 to -20% (max 40 mA)
Current: 4 to 20 mA
Communication: RS485 MODBUS® A-5-11/RTU communication protocol
Weight: 114 g (4 oz)
Panel Cut-Out: 45 x 22.5 mm (1.772 x 0.886")
Maximum Panel Thickness: 3.40 mm (0.14")
Panel Depth: 99.80 mm (3.86")

Inputs

Input Types	Range
K	-200 to 1300°C (-328 to 2372°F)
J	-100 to 1200°C (-148 to 2192°F)
T	-200 to 400°C (-328 to 752°F)
E	0 to 600°C (32 to 1112°F)
N	-200 to 1300°C (-328 to 2372°F)
R	0 to 1700°C (32 to 3092°F)
S	0 to 1700°C (32 to 3092°F)
B	100 to 1800°C (212 to 3272°F)
L	-200 to 850°C (-328 to 1562°F)
U	-200 to 500°C (-328 to 932°F)
Pt100 RTD	-200 to 600°C (-328 to 1112°F)
0 to 50 mV	-999 to 9999
0 to 5 V	-999 to 9999
0 to 10 V	-999 to 9999
0 to 20 mA*	-999 to 9999
4 to 20 mA*	-999 to 9999

** Requires external 250 Ω precision shunt resistor,* ***OMX-R250*** *(sold separately).*

To Order *Visit omega.com/cn7500 for Pricing and Details*

Model No.	Description
CN7523	Dual output, DC pulse/relay, RS485*
CN7533	Dual output, relay/relay, RS485*
CN7553	Dual output, 4 to 20 mA/relay, RS485*

Accessories (Field Installable)

Model No.	Description
CNQUENCHARC	Noise suppression RC snubber (2 leads),110 to 230 Vac
OMX-R250	250 Ω precision resistor
CN7-485-USB-1	RS485 to USB mini-node converter

Comes complete with operator's manual.
** Free CN7-A software download available at* ***omega.com/cn7500***
Ordering Example: CN7523, *dual-output controller, DC pulse and a mechanical relay output, RS485 communications.*

P-23

Figure A 19: Omega Temperature Controller

NEW

Inch Inch Inch Inch Inch Inch Inch

SDP/SI

Linear Ball Bearings – Closed Type

Stock Drive Products/Sterling Instrument ■ Phone: 516-328-3300 ■ Fax: 516-326-8827

■ LOW FRICTION COEFFICIENT ■ HIGH POSITIONING ACCURACY
■ HIGH LOAD CAPACITY ■ QUIET MOVEMENT ■ LONG TRAVEL LIFE

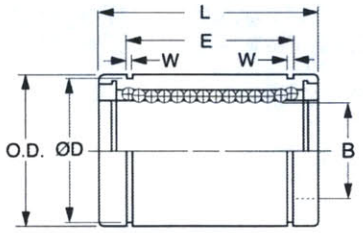

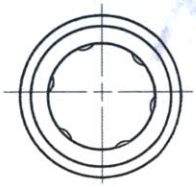

MATERIAL: **Sleeve and Balls** – AISI 52100 Steel
Retainer – Duracon M90

Catalog Number	Ball Circuit	B* Bore	O.D.□	L△ Length	E§ Groove Distance	W Groove Width	D Groove	Load Capacity	
								Dynamic lbf	Static lbf
S99LBC-025075□	4	.2500	.5000	.750	.511	.0390	.4687	46	60
S99LBC-038063□		.3750	.6250	.875	.636		.5880	51	71
S99LBC-050088□	4	.5000	.8750	1.250	.963	.0459	.8209	115	176
S99LBC-063113□		.6250	1.1250	1.500	1.104	.0559	1.0590	174	265
S99LBC-075125□	5	.7500	1.2500	1.625	1.166	.0559	1.1760	194	308
S99LBC-100156□	6	1.0000	1.5625	2.250	1.755	.0679	1.4687	220	353
S99LBC-125200□	6	1.2500	2.0000	2.625	2.005	.0679	1.8859	353	616
S99LBC-150238□		1.5000	2.3750	3.000	2.412	.0859	2.2389	490	904

NOTE: To order bearings with no seals, use catalog numbers as they are. To order bearings with seals at both ends, add **"S"** to the end of catalog number.

BEARING TOLERANCES

* B Tolerance:	.2500, .3750, .5000 & .6250	+.0000 / -.00025
	.7500 & 1.0000	+.0000 / -.00030
	1.2500 & 1.5000	+.0000 / -.00035
□O.D. Tolerance:	.5000	+.0000 / -.00045
	.6250, .8750 & 1.1250	+.0000 / -.00050
	1.2500 & 1.5625	+.0000 / -.00065
	2.0000 & 2.3750	+.0000 / -.00075
△L Tolerance:	.750, .875, 1.250, 1.500 & 1.625	+.000 / -.008
	2.250, 2.625 & 3.000	+.000 / -.012
§ E Tolerance:	.511, .636, .963, 1.104 & 1.166	+.000 / -.008
	1.755, 2.005 & 2.412	+.000 / -.012

72

Figure A 20: Bearings Used

PRECISION GROUND SHAFTING

SDP/SI

UNDERSIZE, NOMINAL AND OVERSIZE DIAMETERS

PHONE: 516.328.3300 • FAX: 516.326.8827 • WWW.SDP-SI.COM

Inch
0 1

Precision Component

› MATERIAL:
303 Stainless Steel

Other lengths and diameters available on special order.

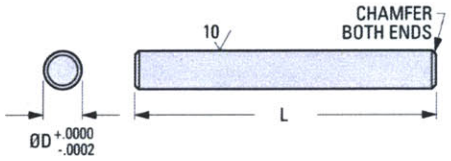

INCH COMPONENT

Catalog Number	D Diameter +.0000 -.0002	L Length ± .125 in.
A 7X 1-0112B	.0311	12
A 7X 1-0112	.0313	12
A 7X 1-0112A	.0317	12
A 7X 1-0212	.0622	12
A 7X 1-0212A	.0626	12
A 7X 1-0212B	.0630	12
A 7X 1-0312	.0778	12
A 7X 1-0312A	.0781	12
A 7X 1-0312B	.0786	12
A 7X 1-0312C	.0934	12
A 7X 1-0312F	.0935	12
A 7X 1-0312D	.0938	12
A 7X 1-0312E	.0942	12
A 7X 1-0424	.1247	24
A 7X 1-0424A	.1250	24
A 7X 1-0424B	.1252	24
A 7X 1-0424C	.1255	24
A 7X 1-0524	.1560	24
A 7X 1-0524A	.1562	24
A 7X 1-0524B	.1567	24
A 7X 1-0624	.1872	24
A 7X 1-0624A	.1875	24
A 7X 1-0624B	.1877	24
A 7X 1-0724	.2184	24
A 7X 1-0724A	.2187	24
A 7X 1-0724B	.2192	24

Catalog Number	D Diameter +.0000 -.0002	L Length ± .125 in.
A 7X 1-0824	.2497	24
A 7X 1-0836	.2497	36
A 7X 1-0824A	.2500	24
A 7X 1-0836A	.2500	36
A 7X 1-0824B	.2502	24
A 7X 1-0836B	.2505	36
A 7X 1-1024	.3122	24
A 7X 1-1016	.3123	16
A 7X 1-1016A	.3125	16
A 7X 1-1024A	.3125	24
A 7X 1-1016B	.3127	16
A 7X 1-1024B	.3130	24
A 7X 1-1216	.3747	16
A 7X 1-1236	.3747	36
A 7X 1-1216A	.3750	16
A 7X 1-1236A	.3750	36
A 7X 1-1216B	.3752	16
A 7X 1-1236B	.3755	36
A 7X 1-1616	.4997	16
A 7X 1-1636	.4997	36
A 7X 1-1612A	.5000	12
A 7X 1-1616A	.5000	16
A 7X 1-1636A	.5000	36
A 7X 1-1616B	.5002	16
A 7X 1-1636B	.5005	36
A 7X 1-2412A	.7500	12

Figure A 21: Cartridge Heater

Appendix B

Matlab:

Readall.m:

This function reads the raw cross-sectional data and removes points that contain missing scan data.

```
function cleaneddata = readall(filename)

format short

cd('Profiles/')

fid = fopen(filename);

c = textscan(fid,'%s','HeaderLines',2,'delimiter',',');

% finds all missing data points donated b 1.#QNAN entries and replaces
% them with a numerical value of 999999

idx = find(strcmp([c{1}], '1.#QNAN'));

nmissing = length(idx);

data = c{1};

fclose('all');

for i = 1:nmissing

    data(idx(i),1) = {'999999'};

end

rawdata = str2double(data);

% columnates string data into x and y coordinates

npoints = length(rawdata)/2;

columnated=zeros(npoints,2);


for i = 1:npoints

    columnated(i,1) = rawdata(2*i - 1);
    columnated(i,2) = rawdata(2*i);

end
```

```
% Rotates data so that left and right side of channel scans can be compared
if columnated(1,2) > columnated(end,2)
    columnated(:,2) = flipud(columnated(:,2));
end
% remove rows with missing data (given by 999999)
remove=find(columnated(:,2)==999999);
nremove = length(remove);
if nremove == 0
    cleaneddata = columnated;
end
for i = 1:nremove+1

    if i==1
        cleaneddata=columnated(1:remove(i)-1,:);
    elseif i == nremove+1
        cleaneddata=[cleaneddata; columnated(remove(i-1)+1:end,:)];
    else
        cleaneddata=[cleaneddata; columnated(remove(i-1)+1:remove(i)-1,:)];
    end

end
% makes first data point at 0 height
cleaneddata(:,2) = cleaneddata(:,2) - cleaneddata(1,2);
cleaneddata(:,2) = cleaneddata(:,2)/1000;
% determines if scale is mm or micron and scales to microns if necessary
if cleaneddata(2,1)-cleaneddata(1,1) < 0.1
    cleaneddata(:,1) = cleaneddata(:,1)*1000;
end
cd ..

end
```

Depthmeasure.m:

This script looks at cross-sectional data files and looks for edge locations. It then divides the data into regions based on these edge locations and calculates the average height of each region. Finally the width of the regions are computed.

```
function [filelist, ridgewidth, regionheight] = depthmeasure

clear all
close all

burwidth = 5; %data not to average if seen a burth with this width
burheight = 3;

% set region finding sensitivity

files=dir(fullfile('Profiles/*.CSV'));

cd('Profiles/')

nfiles = length(files);

steplocation = zeros(nfiles,2);
regionheight = zeros(nfiles,3);
basewidth = zeros(nfiles,1);

cd ..

for i = 1:nfiles

    % Read in cross sectinal data
    currentfile = (files(i).name);
    readfile = readall(currentfile);

    ndatapoints = length(readfile);

    %% Look for Edges
    differences = zeros(ndatapoints,1);

    for j = 2:ndatapoints

        differences(j) = abs(readfile(j,2) - readfile(j-1,2));

    end


    edge1 = find(differences == max(differences));

    edge2 = find(differences == max(max(differences(1:edge1-burwidth)),...
        max(differences(edge1+burwidth:end))));

    differences(edge2) = 0;

    edges=[edge1,edge2];
    edges=[min(edges),max(edges)];
```

```
    %% Look for Burs

    edge1zone = differences(edges(1)-burwidth:edges(1)+burwidth);
    edge2zone = differences(edges(2)-burwidth:edges(2)+burwidth);

    if max(edge1zone) > burheight

        burs = find(edge1zone > burheight) - burwidth - 1;

        if max(burs) > 0

            edges(1) = edges(1) + max(burs);

        end

    end

    if max(edge2zone) > burheight

        burs = find(edge2zone > burheight) - burwidth - 1;

        if min(burs) < 0

            edges(2) = edges(2) + min(burs) - 1;

        else

            edges(2) = edges(2) - 1;

        end

    else

        edges(2) = edges(2) - 1;

    end

% edges(2) = edges(2) - 1;
    % store edge locations

    steplocation(i,1) = readfile(edges(1),1);
    steplocation(i,2) = readfile(edges(2),1);


    % calculate region heights (ignoring region around edge that is assumed
to be a burr

    regionheight(i,1) = mean(readfile(1:edges(1)-burwidth,2));
    regionheight(i,2) = mean(readfile(edges(1):edges(2),2));
    regionheight(i,3) = mean(readfile(edges(2)+burwidth:end,2));


    %% Plot Cross Sectional Data
    % moves data so 0 is location of first step
    readfile(:,1)=readfile(:,1)-readfile(edges(2)+1,1);
```

```
    plot(readfile(:,1),readfile(:,2),'g')
    hold on
    axis equal
    axis([-100,50,-25,100])

    %% Plot Edge Locations

    plot(readfile(edges(1),1),readfile(edges(1),2),'* r')
    hold on

    plot(readfile(edges(2),1),readfile(edges(2),2),'* r')
    hold on

    %% Function to Plot Averaged Cross Section

    % plotaverage(edges, ndatapoints, regionheight, readfile, i);

end


ridgewidth = (steplocation(:,2)-steplocation(:,1));
regionheight = regionheight - kron(regionheight(:,3),ones(1,3));

%cuvette depth

regionheight(:,2)-regionheight(:,1);

%ridge height

regionheight(:,2);

filelist = {files.name};

[averageridge, averageheights] = averagemultiple(ridgewidth, regionheight);

averageridge
averageheights(:,2) - averageheights(:,1)
averageheights(:,2)

end


% optional functions

function [averageridge, averageheights] = averagemultiple(ridgewidth,
regionheight)

ncross = 5; %number of files to average over

n = length(ridgewidth)/ncross;
averageridge = zeros(n,1);
averageheights = zeros(n,2);

for i = 0:n-1
```

```
    nstart = ncross*i +1;
    nend = ncross*i + ncross;

    averageridge(i+1) = mean(ridgewidth(nstart:nend));

    averageheights(i+1,1) = mean(regionheight(nstart:nend,1));
    averageheights(i+1,2) = mean(regionheight(nstart:nend,2));
end
end


function plotaverage(edges, ndatapoints, regionheight, readfile, i)

    averagedcontour = zeros(ndatapoints,2);

    averagedcontour(1:edges(1)-1,2) = regionheight(i,1);
    averagedcontour(edges(1):edges(2),2) = regionheight(i,2);
    averagedcontour(edges(2)+1:end,2) = regionheight(i,3);
    averagedcontour(:,1)=readfile(:,1);

    plot(averagedcontour(:,1),averagedcontour(:,2))

end
```

Order of Measurements:

Below is the order of measurements performed. This order was generated using Minitab.

Run Order	Part Number	Operator
1	8	Operator 2
2	9	Operator 1
3	5	Operator 1
4	9	Operator 2
5	2	Operator 1
6	6	Operator 2
7	1	Operator 1
8	3	Operator 1
9	10	Operator 1
10	7	Operator 2
11	6	Operator 1
12	8	Operator 1
13	4	Operator 1
14	2	Operator 1
15	4	Operator 2
16	1	Operator 2
17	1	Operator 2

18	2	Operator 2
19	7	Operator 2
20	1	Operator 1
21	10	Operator 1
22	9	Operator 2
23	3	Operator 1
24	6	Operator 1
25	5	Operator 2
26	2	Operator 2
27	4	Operator 2
28	7	Operator 1
29	4	Operator 1
30	3	Operator 2
31	5	Operator 2
32	10	Operator 2
33	10	Operator 2
34	8	Operator 1
35	5	Operator 1
36	3	Operator 2
37	9	Operator 1
38	8	Operator 2
39	7	Operator 1
40	6	Operator 2

References

[1] WHO, 2006, AIDS Epidemic Update.

[2] Cheng X., Irimia D., Dixon M., Ziperstein J. C., Demirci U., Zamir L., Tompkins R. G., Toner M., and Rodriguez W. R., 2007, "A Microchip Approach for Practical Label-Free CD4+T-Cell Counting of HIV-Infected Subjects in Resource-Poor Settings," Basic Science, **45**(3), pp. 257–261.

[3] Peter T., Badrichani A., Wu E., Freeman R., Ncube B., Ariki F., Daily J., Shimada Y., and Murtagh M., 2008, "Challenges in implementing CD4 testing in resource-limited settings.," Cytometry. Part B, Clinical cytometry, **74 Suppl 1**(January), pp. S123–30.

[4] Pratt E. D., Huang C., Hawkins B. G., Gleghorn J. P., and Kirby B. J., 2011, "Rare Cell Capture in Microfluidic Devices.," Chemical engineering science, **66**(7), pp. 1508–1522.

[5] Dirckx M. E., and Hardt D. E., 2011, "Analysis and characterization of demolding of hot embossed polymer microstructures," Journal of Micromechanics and Microengineering, **21**(8), p. 085024.

[6] Lin M., Yeh J., Chen S., Chien R., Hsu C., and Chuck B., 2013, "Study on the replication accuracy of polymer hot embossed microchannels G̃ Baffle," **42**, pp. 55–61.

[7] Becker H., and Heim U., 2000, "Hot embossing as a method for the fabrication of polymer high aspect ratio structures," Sensors and Actuators A: Physical, **83**(1-3), pp. 130–135.

[8] Tran N. K., Lam Y. C., Yue C. Y., and Tan M. J., 2010, "Manufacturing of an aluminum alloy mold for micro-hot embossing of polymeric micro-devices," Journal of Micromechanics and Microengineering, **20**(5), p. 055020.

[9] Hale M., 2009, "Development of a Low Cost, Rapid-Cycle Hot Embossing System for Microscale Parts."

[10] Koerner T., Brown L., Xie R., and Oleschuk R. D., 2005, "Epoxy resins as stamps for hot embossing of microstructures and microfluidic channels," Sensors and Actuators B: Chemical, **107**(2), pp. 632–639.

[11] Figeys D., and Pinto D., 2004, Lab-on-a-Chip : A Revolution in Biological and Medical Sciences A look at some of the basic concepts and.

[12] Beebe D. J., Mensing G. a, and Walker G. M., 2002, "Physics and applications of microfluidics in biology.," Annual review of biomedical engineering, **4**, pp. 261–86.

[13] Schudel B. R., Choi C. J., Cunningham B. T., and Kenis P. J. a, 2009, "Microfluidic chip for combinatorial mixing and screening of assays.," Lab on a chip, **9**(12), pp. 1676–80.

[14] Leu T.-S., and Chang P.-Y., 2004, "Pressure barrier of capillary stop valves in micro sample separators," Sensors and Actuators A: Physical, **115**(2-3), pp. 508–515.

[15] Love J. C., Wolfe D. B., Jacobs H. O., and Whitesides G. M., 2001, "Microscope Projection Photolithography for Rapid Prototyping of Masters with Micron-Scale Features for Use in Soft Lithography," Langmuir, **17**(19), pp. 6005–6012.

[16] Sia S. K., and Whitesides G. M., 2003, Microfluidic devices fabricated in poly(dimethylsiloxane) for biological studies.

[17] Singleton L., 2003, "Manufacturing Aspects of LIGA Technologies," Journal of Photopolymer Science and Technology, **16**(3), pp. 413–422.

[18] Berkeley U. C., and David A., 2004, "A Study of Surface Roughness in the Micro-End-Milling Process," Consortium on Deburring and Edge Finishing,.

[19] Lee K. S., and Kim K., 2010, "Analysis of unavoidable geometric errors in the side wall of end-milled parts for corner surface," Journal of Mechanical Science and Technology, **23**(2), pp. 525–535.

[20] Attia U. M., Marson S., and Alcock J. R., 2009, "Micro-injection moulding of polymer microfluidic devices," Microfluidics and Nanofluidics, **7**(1), pp. 1–28.

[21] Niggemann M., Ehrfeld W., and Weber L., "Fabrication of miniaturized biotechnical devices," SPIE - The International Society for Optical Engineering, Santa Clara, CA, pp. 204–213.

[22] Pirskanen, Immonen, Kalima, Pietarinen, Siitonen, Kuittinen, Mönkkönen, Pakkanen, Suvanto, Pääkkönen E. J. ., 2005, "Replication of sub-micrometre features using microsystems technology," Plastics, Rubber and Composites, **34**(5-6), pp. 222–226.

[23] Lorenz H., Despont M., Vettiger P., and Renaud P., 1998, "Fabrication of photoplastic high-aspect ratio microparts and micromolds using SU-8 UV resist," Microsystem Technologies, **4**(3), pp. 143–146.

[24] Wang Q., 2006, "Process Window Characterization and Process Variation Identification of Micro Embossing Process."

[25] Tran N. K., Lam Y. C., Yue C. Y., and Tan M. J., 2010, "Manufacturing of an aluminum alloy mold for micro-hot embossing of polymeric micro-devices," Journal of Micromechanics and Microengineering, **20**(5), p. 055020.

[26] Chien R.-D., 2006, "Hot embossing of microfluidic platform," International Communications in Heat and Mass Transfer, **33**(5), pp. 645–653.

[27] Mekaru H., Yamada T., Yan S., and Hattori T., 2004, "Microfabrication by hot embossing and injection molding at LASTI," Microsystem Technologies, **10**(10), pp. 682–688.

[28] Hale M., 2009, "Development of a Low Cost, Rapid-Cycle Hot Embossing System for Microscale Parts."

[29] Sun H. L., Liu C., Li M. M., Liang J. S., and Chen H. H., 2009, "Study on Replication of Densely Patterned, High-Depth Channels on a Polymer Substrate Using Hot Embossing Techniques," Materials Science Forum, **628-629**, pp. 411–416.

[30] Leveder T., Landis S., Davoust L., Soulan S., and Chaix N., 2007, "Demolding strategy to improve the hot embossing throughput," **6517**, p. 65170N–65170N–8.

[31] Guo Y., Liu G., Xiong Y., and Tian Y., 2007, "Study of the demolding process—implications for thermal stress, adhesion and friction control," Journal of Micromechanics and Microengineering, **17**(1), pp. 9–19.

[32] Dirckx M. E., and Hardt D. E., 2011, "Analysis and characterization of demolding of hot embossed polymer microstructures," Journal of Micromechanics and Microengineering, **21**(8), p. 085024.

[33] Guo Y., Liu G., Xiong Y., and Tian Y., 2007, "Study of the demolding process—implications for thermal stress, adhesion and friction control," Journal of Micromechanics and Microengineering, **17**(1), pp. 9–19.

[34] Liu C., Li J. M., Liu J. S., and Wang L. D., 2010, "Deformation behavior of solid polymer during hot embossing process," Microelectronic Engineering, **87**(2), pp. 200–207.

[35] Kalsekar V., 2013, "Design and Process Optimization of a Hot Embossing Machine for Microfluidics with High Aspect Ratios," MIT.

[36] Kalsekar V., 2013, "Design and Process Optimization of Hot Embossing System for High Aspect Ratio Microfluidics," Massachusetts Institute of Technology.

[37] Senn T., Esquivel J. P., Lörgen M., Sabaté N., and Löchel B., 2010, "Replica molding for multilevel micro-/nanostructure replication," Journal of Micromechanics and Microengineering, **20**(12), p. 129804.

[38] Ye X., Liu H., Ding Y., Li H., and Lu B., 2009, "Research on the cast molding process for high quality PDMS molds," Microelectronic Engineering, **86**(3), pp. 310–313.

[39] Brune D., Hellborg R., Whitlow H. J., and Hunderi O., 1997, Surface Characterization: A User's Sourcebook, Wiley-Vch Verlag GmbH., Weinheim.

[40] Nguyen K., 2013, "Design of a Hot Embossing Machine and Tool Design for micro-features with High Aspect Ratios."